AD-A140 400 DEVELOPMENT AND APPLICATION OF LOW ENERGY X-RAY AND ELECTRON PHYSICS(U) HAWAII UNIV HONOLULU DEPT OF PHYSICS AND ASTRONOMY B L HENKE 14 MAR 84 1/1

UNCLASSIFIED AFOSR-TR-84-0252 AFOSR-79-0027 F/G 14/2 NL

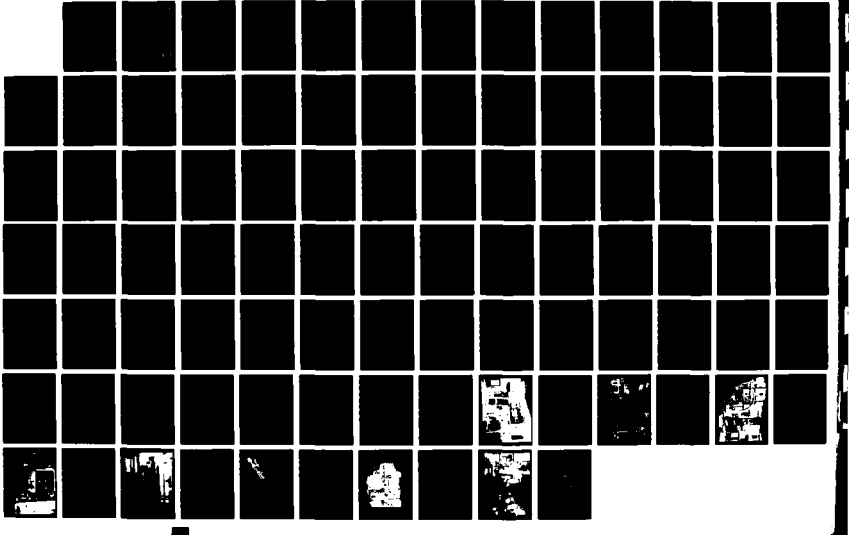

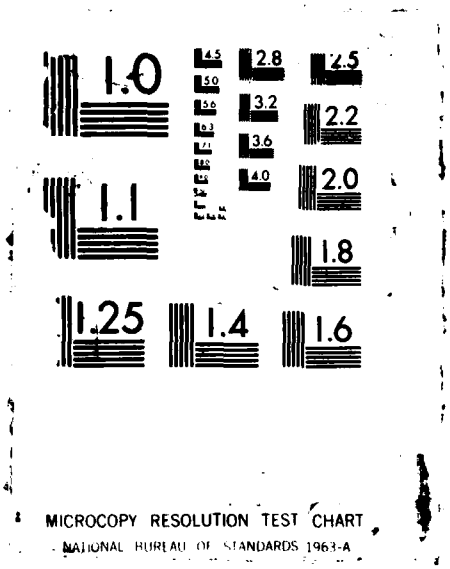
1.0
1.1
1.25
1.4
1.6
2.8
3.2
3.6
4.0
2.5
2.2
2.0
1.8
MICROCOPY RESOLUTION TEST CHART
NATIONAL BUREAU OF STANDARDS 1963-A

DEVELOPMENT AND APPLICATION OF LOW ENERGY X-RAY AND ELECTRON PHYSICS

Final
Scientific Report
for the period

01 October 1978 through 30 September 1983

AFOSR Grant 79-0027[redacted]

BURTON L. HENKE
Principal Investigator

Department of Physics and Astronomy
University of Hawaii
Honolulu, Hawaii 96822

Prepared for the

Air Force Office of Scientific Research
Directorate of Physics
Building 410, Bolling Air Force Base
Washington, D. C. 20332

March 1984

CONTENTS

page

REPORT DOCUMENTATION PAGE i

I. PROGRAM OBJECTIVES 1

II. RESEARCH RESULTS 2

A. Basic Interaction Physics 2

B. Molecular and Solid State Spectroscopy; Radiation Damage..... 3

C. Pulsed X-Ray Source Spectroscopy 100-10,000 eV ($\Delta t > 10$ picoseconds)..... 4

D. X-Ray Optics 5

1. Analyzers and Monochromators..... 5

2. Position Sensitive Detection 6

a. Photographic Films..... 6

b. X-Ray Streak Cameras 6

3. X-Ray Lithography..... 7

E. High Temperature Plasma Diagnostics 8

F. Student Training in X-Ray Physics Research.... 9

G. Collaborative Efforts 10

III. FIRST-PAGE ABSTRACTS OF RESEARCH PUBLICATIONS FOR THE 1978-1983 PERIOD 13

- Research Publications by the Principal Investigator and Co-Workers on this Research Program (1973-1983).....63

- Research Publications by the Principal Investigator Listed in the Science Citation Index 67

IV. INVITED AND CONTRIBUTED RESEARCH PAPERS PRESENTED BY THE PRINCIPAL INVESTIGATOR (1978-1983).....69

V. SOME OF THE LABORATORY FACILITIES OF THIS PROGRAM 73

Unclassified

SECURITY CLASSIFICATION OF THIS PAGE (When Data Entered)

REPORT DOCUMENTATION PAGE		READ INSTRUCTIONS BEFORE COMPLETING FORM
1. REPORT NUMBER AFOSR-TR- 84-0252	2. GOVT ACCESSION NO. AD-A140 484	3. RECIPIENT'S CATALOG NUMBER
4. TITLE (and Subtitle) DEVELOPMENT AND APPLICATION OF LOW ENERGY X-RAY AND ELECTRON PHYSICS		5. TYPE OF REPORT & PERIOD COVERED Final 10/01/78 through 09/30/83
		6. PERFORMING ORG. REPORT NUMBER
7. AUTHOR(s) Burton L. Henke, Principal Investigator		8. CONTRACT OR GRANT NUMBER(s) AFOSR-79-0027
9. PERFORMING ORGANIZATION NAME AND ADDRESS Department of Physics and Astronomy University of Hawaii 2505 Correa Road, Watanabe 210 Honolulu, Hawaii 96822		10. PROGRAM ELEMENT, PROJECT, TASK AREA & WORK UNIT NUMBERS 2301/A8 61102F
11. CONTROLLING OFFICE NAME AND ADDRESS Directorate of Physics Air Force Office of Scientific Research/NP Building 410, Bolling Air Force Base Washington, D.C. 20332		12. REPORT DATE 03/14/84
		13. NUMBER OF PAGES 91
14. MONITORING AGENCY NAME & ADDRESS (if different from Controlling Office)		15. SECURITY CLASS. (of this report) unclassified
		15a. DECLASSIFICATION/DOWNGRADING SCHEDULE

16. DISTRIBUTION STATEMENT (of this Report)

Approved for public release; distribution unlimited

17. DISTRIBUTION STATEMENT (of the abstract entered in Block 20, if different from Report)

18. SUPPLEMENTARY NOTES

19. KEY WORDS (Continue on reverse side if necessary and identify by block number)

20. ABSTRACT (Continue on reverse side if necessary and identify by block number)

The objectives and results of this on-going AFOSR program in low-energy x-ray physics are reviewed for the five-year period, 1978-1983. Its thirty major research publications for this period are abstracted. The following applications of this research are discussed: measurement, compilation and calculation of low-energy x-ray interaction coefficients; molecular and solid state spectroscopy; pulsed x-ray source spectrometry; instruments, methods and techniques for low-energy x-ray optics; high temperature plasma diagnostics. The role of this program in the training of students for x-ray physics and in participating in collaborative research efforts with other laboratories is described.

DD FORM 1 JAN 73 1473 EDITION OF 1 NOV 65 IS OBSOLETE

Unclassified

SECURITY CLASSIFICATION OF THIS PAGE (When Data Entered)

SCIENTIFIC REPORT

AFOSR GRANT 79-0027A-E

DEVELOPMENT AND APPLICATION OF
LOW ENERGY X-RAY AND ELECTRON PHYSICS

01 October 1978 through 30 September 1983

I. PROGRAM OBJECTIVES

The objectives of this on-going program have been (a) the development of the basic physics of the low-energy x-ray and associated electron interactions and (b) the application of this physics to problems of immediate need and importance.

In recent years the particular application areas to which this program has been addressed are:

1. Molecular and solid state spectroscopy; radiation damage.

2. Pulsed x-ray source spectroscopy ($\Delta t \geq 10$ picoseconds).

3. X-ray optics

   a. Analyzers (crystals and multilayers)

   b. Focussing, primary monochromators for x-ray microscopes, telescopes and for synchrotron radiation light sources.

   c. Position sensitive detectors: time integrating and time resolving.

   d. X-ray lithography for microelectronics fabrication.

4. High temperature plasma diagnostics

   a. Fusion energy

   b. X-ray lasers

   c. X-ray astronomy

II. RESEARCH RESULTS*

A. Basic Interaction Physics

We are pleased to report that an entire issue of the journal, Atomic Data and Nuclear Data Tables [77], was published during this contract period upon our recent work on Low-Energy X-Ray Interaction Coefficients: Photoabsorption, Scattering and Reflection, E = 100-2000 eV, Z = 1-94. This 144-page monograph includes a summary of the methods for using these atomic scattering factor tables for the characterization of reflection by x-ray mirrors, multilayers and crystals as applied in low-energy x-ray spectrometry. These tables, for the 94 elements, have also been made available on data disks for efficient computational analysis [75]. The data disks have been supplied to groups at all of the National Laboratories involved in x-ray research. And we have arranged (cost supported by this University) to send four-hundred reprint copies of this monograph to requestors throughout the scientific community.

In order to apply these data for absorption and scattering of the low-energy x-rays, we have reviewed the old programs and have developed new ones for the calculation of the reflection characteristics of crystals multilayers and mirrors. These have been applied for the detailed characterization of monochromator and analyzer systems of current interest for the 100-2000 eV region. These results have been important in guiding the development of new systems for spectroscopic analysis and their calibration [73,82].

A sensitive test and measure of the low-energy x-ray atomic scattering factors has been the experimental characterization of crystal and multilayer analyzers and of mirror monochromators. (Their reflectivities are strongly dependent upon both the real and the imaginary parts of the scattering factors.) A comprehensive work is now nearly completed on the Model Calculations and Measurement of Low-Energy X-Ray Reflecting Systems [82,83].

The basic, associated electron interactions which we have been investigating have been involved with the conversion of photons to photoelectrons. The electronic

---

*Numbers refer to first-page abstracts presented in Sec. III.

photoemission characteristics are of particular practical importance in the design and optimization of x-ray detectors as the x-ray diodes and the x-ray streak cameras (see below). In the research program period reviewed here, we have been making the very needed measurements of the absolute quantum yields and of the photon counting efficiencies of practical photocathode materials, cesium iodide in particular. The ratio of the quantum yield to the photon counting efficiency is the average number of electrons generated per signal pulse and is an important basic electron generation statistic that is needed for the optimum design of photocathodes for x-ray detection and imaging devices.

Another fundamental characteristic of photocathode emission is the secondary electron energy distribution associated with photoemission. The width of the energy distribution curve (EDC) ultimately determines the limit of the time resolution for the x-ray streak camera. We have carried out on this program a comprehensive series of EDC measurements of metal and insulator type photocathodes. [56,57,61,63,68,71,72,78,82]

B. Molecular and Solid State Spectroscopy; Radiation Damage

The chemical physics of thin films and surfaces and of radiation damage phenomena can be effectively studied through low-energy x-ray fluorescence spectroscopy. This is because the electronic transitions from the outermost electron levels to the first, sharp inner core holes involve subsequent fluorescent x-ray emission in the low-energy region (less than a few hundred eV). The rich structural detail of these spectra accurately reflect energies and symmetries of the outer electronic levels that identify molecular and/or crystalline states. A series of exploratory investigations were conducted in order to define the important problems involved in such measurement and analysis. [58,59,62,64,65,67,69,70]

A very significant result of these studies has been the demonstration that for molecular/solid state spectroscopy of many thin film systems, the x-radiation excitation of the material that is required for the fluorescence analysis is also sufficient to seriously change the sample's surface chemical state. An important conclusion has been that for this very useful analysis technique, more intense excitation light sources are not needed. Rather there is a strong indicated need for more efficient, "faster" low-energy x-ray spectroscopy. It has been for this reason that an important effort of this

program has been directed to the development of optimized, high efficiency spectrographic systems. For this part of our program we have been fortunate to receive added development funding through a DOD-University Instrumentation Grant for the development of a "state of the art" fast spectrograph for high resolution, low-energy x-ray spectroscopy. This system, currently under development, utilizes close coupled curved crystal focussing optics and position sensitive detection along the Johann circle (for simultaneous spectral band measurement). Along with the basic low-energy spectroscopy, this instrumentation will be applied to sensitive and precise studies of the radiation damage growth process in thin films. [89]

C. Pulsed X-Ray Source Spectroscopy 100-10,000 eV ($\Delta t \geq 10$ picoseconds)

In order to accomplish the diagnostics of the intense pulsed x-ray sources that are now available, an important need has developed for well calibrated, absolute pulsed source spectrometry. A spectrograph with time integrating and time resolving recording is required for x-ray pulse measurement in the picosecond to millisecond range and for the 100-10,000 eV region. Typical pulsed sources include those produced by focussed laser or particle beams, by magnetic confinement machines such as the Tokomaks, by the Z-pinch, exploding wire and imploding liner plasmas. The spectrograhic design requirements for this type of spectroscopy are very different from those for the high-sensitivity scanning spectrograph described above.

We have developed a spectrometer based upon an elliptically curved Bragg reflecting analyzer, placing the intense, small source of pulsed x-rays at one focal point and a small scatter aperture at the second focal point through which all Bragg reflected wavelengths will proceed to a detection circle (with this second focal point as its center). A detailed geometrical and physical optics analysis of this fixed analyzer spectrometer for pulsed sources has just been published and is appended here at the end of Sec. III [79]. Also presented in this report are notes on the construction of elliptical analyzers for the 100-10,000 eV region, on analysis methods for absolute line and continuum spectral analysis, and on some initial measurements made with a laser-produced plasma source. We have applied this type of spectrograph in collaboration with the diagnostics group at the Sandia National Laboratories. Similar instruments are now under development at the Lawrence Livermore National Laboratory and at the Los Alamos National Laboratory.

We were invited in 1982 to develop a special elliptical analyzer spectrograph system for x-ray diagnostics applications on the 24-laser-beam OMEGA facility at the Laboratory for Laser Energetics, University of Rochester. This instrument has been designed and constructed in this laboratory in the 1982-83 period and is now undergoing its initial testing on OMEGA at the University of Rochester. Additional construction funds and the support of a post-doctoral research associate for this part of our program were provided by the DOE through the LLE, University of Rochester.

Detailed reports on this spectrograph system are now in preparation [84,85,86]. A photograph and drawing of this instrument are presented in Sec. IV. As will be noted, it incorporates matched, elliptical analyzer spectrometers, one with a time-integrating photographic camera and the other with a specially designed streak camera.

D. X-Ray Optics

1. Analyzers and Monochromators

Along with our theoretical model calculations for the reflectivity characteristics of crystals, multilayers and mirrors, as described earlier, we have maintained an experimental program on the characterization of these x-ray optical elements. Our on-going program on the development of the Langmuir-Blodgett molecular multilayers is unique in its long standing achievements, particularly in the perfection of molecular multilayers as low-energy x-ray analyzers. A special laboratory has been established for this project. Many workers from other institutions have trained in this laboratory on fabrication techniques. And this program has freely supplied other research laboratories with multilayer analyzers constructed of lead salts of the straight-chain fatty acids with 2d-spacings in the 70-160 A range for their low-energy x-ray spectroscopy programs.

We have been able to routinely construct multilayers such as lead myristate, lead stearate and lead behenate (2d-spacings of 80, 100 and 120 A, respectively) that have reached the theoretically predicted values for peak, integrated reflectivities and for the reflectivity curve widths.

The Langmuir-Blodgett multilayers may be deposited upon surfaces of any curvature and consequently can be developed as focussing analyzers and as fixed analyzers

(as the elliptical analyzers described above).

Another on-going investigation of this program, as noted earlier, has been upon the systematic measurement of the reflectivity of grazing incidence mirror monochromators versus photon energy and angle of incidence [74,88]. Again, for mirrors of good quality, we have been able to demonstrate reflection efficiencies that are as predicted by the Fresnel theory using our calculated scattering factors (except very near critical absorption edge energies).

Described in a photograph presented in Sec. IV is a special calibration facility that has been established in this laboratory for the characterization of mirrors, multilayers and crystals in the 100-10,000 eV region with which many focussing geometries may also be evaluated.

2. Position Sensitive Detection

In the development in this laboratory of the spectrograph for pulsed source spectrometry, described above, the Streak and Photographic Elliptical Analyzer X-Ray Spectrograph (SPEAXS system), some new approaches were taken to obtain absolute time integrated and time resolved recording of the Bragg reflected spectra. Essentially no adequate film calibration data were available for absolute measurements in the low-energy x-ray region. And no x-ray streak cameras were available with entrance slit lengths sufficiently large to accomodate other than a very small section of a Bragg reflected spectrum. The following important programs on position sensitive detection were completed this past year.

a. Photographic Films--New mathematical models and new methods for absolute characterization for photographic film response in the 100-10,000 eV region have been developed in order to meet a serious present need for better understanding and implementation of absolute photographic measurement. As examples of application of this new approach, five films of current importance in x-ray diagnostic measurement have been characterized. These are Kodak's 101-07, SB-392, the RAR 2492, 2495 and 2497 films. Abstracts of a two-part report on this work are presented in Sec. III [80,81].

b. X-Ray Streak Cameras--Beginning this last year we have been fortunate to have working with us a post-

doctoral research associate, Dr. Paul Jaanimagi, on the construction of a new x-ray streak camera specially designed for our SPEAXS system [86,87].

We have appreciably modified the RCA 73435 Streak Tube. Increasing the photocathode length to access more resolution elements required demagnified electron optical imaging; spherical and other aberrations degrade the off-axis image. Also the image size gets unwieldy. Very strict mechanical and electrical tolerances were maintained to achieve good spatial resolution over a large area photocathode. Large (20 kV/cm) accelerating fields at the photocathode were required to obtain 10 ps time resolution in the x-ray region. This was achieved by using a slot aperture rather than a mesh in proximity to the cathode. The diverging lens properties of the slot resulted in a net demagnification (6:1) for the photocathode slit width, permitting 1 mm wide input slits for high sensitivity. An accurate electron optics ray trace code proved very useful in the preliminary design work.

Dr. Jaanimagi is now characterizing this new x-ray streak camera on a 50 picosecond laser-produced x-ray source at the Laboratory for Laser Energetics, University of Rochester. We plan next to evaluate the dynamic response of transmission photocathodes of gold, low and high density cesium iodide which have been characterized as to their quantum yield and photon counting efficiency in this laboratory.

With this calibrated streak camera on one channel and with a photographic camera on the other matched channel of the SPEAXS system, we plan to effectively test the dynamic response of the photographic film in the picosecond region (e.g., to gain a test of the reciprocity law for picosecond x-ray bursts).

3. X-Ray Lithography

We would like to note here the potential importance of the low-energy x-ray physics and technology described here to the semiconductor research programs.

By "contact printing" through electron-beam fabricated, high resolution integrated circuit templates onto suitable resists with low-energy x-rays rather than with light, the diffraction-limited resolution of the resulting IC's might be improved by an order of magnitude or more. Intense, pulsed, soft x-ray sources would be required. Focussing x-ray mirrors for concentrating the required high intensity of x-rays onto the templates are

needed. Efficient mirror monochromators for such x-ray lithography could be large aperture, near-normal incidence optical mirrors coated with multilayers to enhance their reflectivity at the desired low-energy x-ray wavelengths.

The optimum choice and the characterization of appropriate resist materials for x-ray lithography might be very effectively guided by the type of molecular state spectroscopy and measurement of radiation damage that has been established on this research program.

Finally, it has already been proposed that Langmuir-Blodgett films of the type that are fabricated in this laboratory might well constitute the basic thin film material for superior, high resolution electron and x-ray resists. See, for example, A. Barraud et al., "Monomolecular Resists: A New Class of High Resolution Resists for Electron Beam Microlithography," Solid State Technology (August 1979) and M. C. Petty, "Langmuir-Blodgett Films," Endeavour, New Series, Vol. 7, No. 2 (Pergamon, 1983).

E. High Temperature Plasma Diagnostics

The work of this program on achieving well-calibrated absolute low-energy x-ray spectroscopy has been inspired by and directed to collaborative efforts with the large programs involved with high temperature plasma diagnostics. The pulsed source spectrometry described here is being applied at several laboratories including the Lawrence Livermore National Laboratory, Los Alamos National Laboratory and the Laboratory for Laser Energetics at the University of Rochester for fusion energy reearch involving very intense, pulsed x-ray sources. Also, alongside this ICF research is that on the development of x-ray lasers which requires the large pulsed x-ray sources and similar x-ray spectroscopic diagnostics.

We are also collaborating with several x-ray astronomy groups on low-energy x-ray imaging and spectroscopy of astrophysical, high-temperature plasmas. Our significant contributions for advancing x-ray astronomical research has been, for example, our work on interaction cross sections [77], low-energy x-ray focussing multilayer and mirror systems [87,88] and the absolute yield measurements and photon counting efficiency of optimized, high yield CsI photocathodes for position sensitive imaging [82].

F. Student Training in X-Ray Physics Research

There is a serious shortage in the U.S. at this time of graduates experienced in radiation physics generally and particularly in the x-ray physics. The training of young x-ray physicists has continued to be an important part of this University grant research program.

Rupert C. C. Perera conducted his PhD program in x-ray physics on this project and is now in the x-ray optics group at the National Bureau of Standards. The title of his thesis is "Low-Energy X-Ray Emission Spectroscopy in the 100-500 eV Region: Molecular Orbital Interpretation," He has just been appointed to a Staff Scientist position at the new Center for XUV Optics, Lawrence Berkeley Laboratory.

Kandategе Premaratne has completed his PhD program and is now teaching university physics and has worked on this project as a post-doctorate. The title of his thesis is "X-Ray Photoemission Theory and Experiment: Characterization of X-Ray Photocathodes."

Tina J. Tanaka completed her PhD program in May 1983. The title of her thesis is "X-Ray Diagnostics of Laser Plasmas with a Calibrated Elliptical Analyzer Spectrograph." She has accepted a Staff Scientist position at the Sandia National Laboratories, Albuquerque in x-ray physics.

Since its beginning, this program has very successfully involved the participation of research assistants of undergraduate physics students, usually through their Junior and Senior years. They have contributed significantly to the program and often as co-authors on research papers, and graduate as motivated and experienced applied physicists. Those who have had their high school and BS programs in Hawaii are strongly encouraged to proceed on to their graduate work at major Universities on the U.S. mainland. During the summer after graduation and before graduate school, we have been able to arrange for many of these students to work as summer researchers at the National Laboratories. Listed below are students who have recently trained as undergraduate assistants on this program and are now completing their graduate work at other Universities.

Ronald Ono completed his PhD this year at the State University of New York at Stony Brook. He is now a post-doctorate at the University of Colorado. Christophe Berg has completed his MS in X-Ray Astronomy at the Massachusetts Institute of Technology and Mark Schattenburg plans to complete his PhD in X-ray Physics

also at MIT within the next year. Eric Gullikson will be completing his PhD by mid-summer at the University of California-San Diego. Brian Fujikawa is finishing the third year of his Physics PhD program at the California Institute of Technology as is Bruce Young at the University of California-Davis in a Physics PhD program supported by the Lawrence Livermore National Laboratory. Randy Shimabukuro has just completed his MS in Physics at the University of California-San Diego and plans to complete his PhD program at UCSD as part of a work/study program with the Naval Electronics Laboratory there. Grace Lim has completed her first year's graduate studies in Physics at the San Jose State University supported through her position in the x-ray analysis laboratory at IBM-San Jose. Mary Pottenger Hockaday is gaining her PhD in X-ray Physics at the University of New Mexico-Las Cruces. Robert Hockaday has joined Mary there and is now completing his MS thesis for an Engineering degree at UNM. (Bob and Mary continue to be part-time staff members as x-ray physicists at the Los Alamos National Laboratory.) Finally, Hubert Yamada was appointed to a summer research position in x-ray plasma diagnostics at the Lawrence Livermore National Laboratory and proceeded this year with a fellowship for his PhD program at the California Institute of Technology.

G. Collaborative Efforts

As has already been indicated, this program continues to involve close collaborations with groups working particularly in the low-energy x-ray diagnostics at major government, university and industrial laboratories. These efforts include work sessions of a few days or more at this laboratory and also visits by this principal investigator at the other laboratories (see Sec. IV). These collaborations are of considerable importance to this program, not only in gaining an efficient exchange of new information but also in having the opportunity to learn about the specific important current needs of the U.S. scientific community in the area of low-energy x-ray physics.

This principal investigator was the co-organizer with Dr. David T. Attwood of the Lawrence Berkeley Laboratory for a special Topical Conference on Low-Energy X-Ray Diagnostics sponsored through the American Physical Society. It was held in Monterey, California, June 8-10, 1981. This three-day meeting included invited, tutorial-type papers by scientists from major laboratories throughout the world addressing most of the topics which have been discussed here. In 1981 the American Institute

of Physics published a complete bound volume on the Proceedings of the meeting (*AIP Conference Proceedings No. 75 on Low-Energy X-Ray Diagnostics*, 1981, D. T. Attwood and B. L. Henke, Editors). [73,74,75] We believe that the very enthusiastic reception of this conference by all of the 250 participants has clearly and strongly expressed the considerable growing importance and needs for development of the XUV physics and associated optical techniques.

III. FIRST-PAGE ABSTRACTS OF RESEARCH PUBLICATIONS FOR THE 1978-83 PERIOD

AND

A REPRINT OF THE RECENTLY PUBLISHED REPORT,

"Pulsed Source Spectrometry in the 80-8000 eV Region"

B. L. Henke, H. T. Yamada, and T. J. Tanaka

Rev. Sci. Instrum. 54 (10), October 1983

(57)

0.1–10-keV x-ray-induced electron emissions from solids—Models and secondary electron measurements

Burton L. Henke and Jerel A. Smith

University of Hawaii, Honolulu, Hawaii 96822

David T. Attwood

Lawrence Livermore Laboratory, Livermore, California 94550
(Received 15 September 1976; accepted for publication 14 December 1976)

Analytical models are presented describing the x-ray-excited emission of "no-loss" photoelectrons and Auger electrons and the energy distribution of emitted secondary electrons. The secondary electron energy distribution is given in terms of the electron kinetic energy E_K, work function W, photon energy E_o, and mass photoionization coefficient $\mu(E_o)$, as proportional to $E_o\mu(E_o)E_K(E_K+W)^{-4}$. Techniques of electron spectral measurements utilizing uniform field preacceleration and limited acceptance angle spectrometers are discussed. Secondary electron energy distributions are measured at about 10^{-6} Torr from thick evaporated films of gold and aluminum at photon energies 277, 1487, and 8050 eV. The shapes of these distributions do not depend significantly upon photon energy. The full width at half-maximum (FWHM) of these distributions are 3.9, 6.7, and 4.4 eV for Au and ion-cleaned Au and Al photocathodes, respectively. The data agree well with the model predictions.

PACS numbers: 79.60.Cn, 73.30.+y, 72.10.Bg

I. INTRODUCTION

This work is in sequel to and in support of a recent presentation by the authors of some measurements on the secondary electron energy distributions from gold as excited by C-K_α (277 eV) and Al-K_α (1487 eV) x-ray photons.[1] It is an attempt to present the basic physics for the measurement and for the interpretation of the x-ray-induced electron emissions from uniform isotropic solids.

In Fig. 1 are shown the typical characteristics of an electron spectrum induced by an x-ray beam incident upon a solid. Illustrated here are the sharp photoelectron and Auger electron "no-loss" lines with their characteristic energy loss tail structure, along with the low-energy secondary electron distribution. In contrast to uv-excited electron spectra, here the photoelectrons and the principal sharp Auger electron emissions are well outside the low-energy secondary electron energy region. The secondary electron spectrum peaks at about 1 to 2 eV and has a full width at half-maximum (FWHM) that is usually below 10 eV. In this 0–30 eV interval are typically from 50 to 90% of the total number of electrons emitted for photon excitation in the 100–10 000-eV region.

The x-ray-excited electron spectra constitute a unique "window" into the solid and its electron excitation, transport, and escape processes. When a thorough understanding of the physics of these processes is gained, electron spectroscopy can provide an important quantitative basis for the physical and chemical analysis of solids. The electron spectroscopy for chemical analysis (referred to as ESCA or XPS) has become a well-recognized research area within the last ten years.[2]

The photoelectric conversion of x-ray intensity into electron emission can provide an important practical basis for x-ray intensity measurement. X-ray photoelectric detectors are vacuum devices and, unlike gas ionization detectors, can be windowless. A unique advantage of the photoelectric detector is that it can be applied effectively over a wide band of photon energies.[3,4]

A very recent application of secondary electron detectors has been in the development of streak and framing cameras for the diagnostics of x-ray bursts from laser-produced plasmas. The time spread in the photoconverted secondary electron emission per photon is probably of the order of 10^{-14} sec, and the energy spread is of the order of 10 eV. An x-ray source can be imaged and photoconverted to an electron source which may then be reimaged down a streak or framing camera tube with an accelerating electron lens system. The time history of an x-ray event can be obtained by a fast transverse deflection of this image, e.g., to form a "streak" pattern with a time resolution in the picosecond range.[1,3–6]

In order to support research and application in x-ray photoemission, considerably more theoretical and experimental work should be done on the development of a quantitative relationship between the electron emission spectrum, the incident photon energy, and the characteristics of the photocathode. There is no complete theory of x-ray photoemission that is available

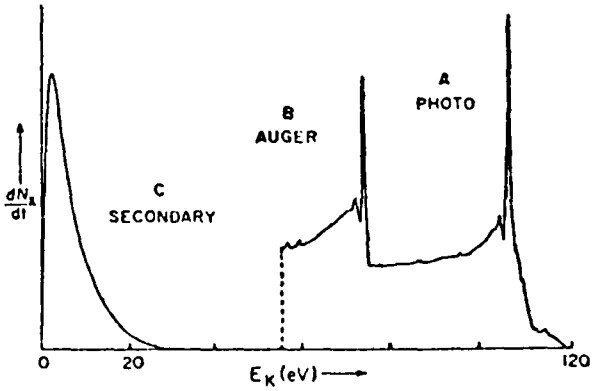

FIG. 1. A typical x-ray-excited photoemission spectrum.

High-efficiency low-energy x-ray spectroscopy in the 100–500-eV region

Burton L. Henke, Rupert C. C. Perera, Eric M. Gullikson, and Mark L. Schattenburg

University of Hawaii, Honolulu, Hawaii 96822
(Received 21 July 1977; accepted for publication 1 September 1977)

The lead myristate multilayer analyzer has provided a basis for a relatively simple and efficient spectroscopy for the low-energy x-ray emissions in the 20–80-Å region (where conventional crystal spectroscopy and grazing incidence grating spectroscopy are generally inefficient). The percent reflectivity, the integrated coefficient of reflection, and the Bragg diffraction width of the lead myristate analyzer have been measured and found to be consistent with the predictions of a simple theoretical model for multilayer diffraction. This multilayer spectroscopy at large Bragg angles has a high efficiency (high instrument transmission) as compared to grazing incidence grating spectroscopy in this 20–80-Å region. However, the resolution is limited to that set by the diffraction width of the lead myristate analyzer of about 1 eV. Because the collimator-crystal broadening function can be precisely defined, a simple and effective deconvolution procedure can be applied with this multilayer spectroscopy to bring the resolution into the sub-electron-volt region. To demonstrate the efficiency of lead myristate spectroscopy in the 20–80-Å region, spectra were measured and analyzed from x-ray excited fluorescent sources which are characteristically of low intensity. (X-ray excitation yields a minimum of background spectra and of radiation damage.) These include the $L_{2,3}$ atomic spectrum of argon and the C-K molecular spectrum of CO_2, both in the gas phase, and the Cl-$L_{2,3}$ and O-K spectra from solid lithium perchlorate. Many samples undergo appreciable radiation-induced chemical change during the exposure time that is required for measurement—even with an optimally fast spectrograph and with fluorescent excitation. A method has been developed to evaluate and to correct for radiation damage by distributing the exposure over an effectively large sample volume either by gas flow or by rotating through multiple samples during measurement. Several spectral scans were made on the $LiClO_4$ using six samples. The total exposure time for each data point in each scan was recorded which permitted an extrapolation into a "zero" exposure spectrum. Finally, Fe-$L_{2,3}$/O-K spectrum (from Fe_2O_3) in the 17–25-Å region is presented to illustrate the effectiveness of the lead myristate analyzer in third-order diffraction. For this multilayer, the third-order diffraction efficiency is one-third that of the first order and is nearly twice that of the second order for this wavelength region.

PACS numbers: 07.85.+n, 32.30.Rj, 52.70.Kz, 33.20.Rm

I. INTRODUCTION

There are two areas in which low-energy x-ray spectroscopy is of particular importance at this time—the diagnostics of high-temperature plasmas[1] and the determination of the chemical and solid-state electronic structure of atomic systems.[2]

In the controlled thermonuclear fusion research, a critical temperature region of current interest is in the (1–10) × 10^6 °C range. The plasmas involved emit radiations most characteristically in the low-energy x-ray region (100–1000 eV/10–100 Å). The detailed spectroscopy of these plasma radiations can yield information as to the plasma density, temperature, and the identity and amount of contaminating elements. The low-energy x radiation from pulsed plasma sources (as produced by lasers or exploding wires) can be very efficiently converted to relatively sharp distributions in energy of secondary electrons[3] that are amenable, with streak camera techniques, to time-history measurements approaching psec resolutions.

Often, the energy and the symmetry of the outer electronic states of atomic systems can be sensitively revealed through the spectra associated with the transitions from these states into a nearby relatively sharp core level. Such spectra can yield valuable data complementary to that which are available from photoelectron Auger electron spectroscopy on the structure of valence bands, solid-state bands, and molecular orbitals.[4] These sensitive first transitions into the core levels typically result in low-energy x-ray spectra at a few hundred eV or less.

Using, for example, the acid phthallate crystals (2d value of about 26.6 Å), the conventional x-ray crystal spectroscopy has been very effectively extended down to about 500 eV.[5] Extreme ultraviolet diffraction grating spectroscopy has been extended with high efficiency (with relatively large angles of grazing incidence) up to about 100 eV.[6] We have found that a very efficient spectroscopy in the gap region of 100–500 eV is by using the multilayer analyzers as the lead stearate and lead myristate of 2d values equal to 100 and 80 Å, respectively. We have recently presented the detailed characteristics and application of the lead stearate analyzer.[7,8] In this paper, we extend the presentation of the methods and techniques of low-energy x-ray spectroscopy as specially applied with the lead myristate analyzer.

In Secs. II–V, we present an analysis and measurements of the x-ray optical characteristics of this multilayer analyzer, an optimized spectroscopic and data analysis procedure for gaining maximum overall efficiency and resolution, and, finally, we present some examples of applications to atomic and molecular low-energy x-ray spectroscopy.

II. REFLECTION PARAMETERS FOR THE LEAD MYRISTATE MULTILAYER

Lead salts of the fatty acids deposited as Langmuir-Blodgett multilayers have been demonstrated to be highly efficient

 0021-8979/78/4902-0480$01.10

59

Cl-$L_{II, III}$ fluorescent x-ray spectra measurement and analysis for the molecular orbital structure of ClO_4^-, ClO_3^-, and ClO_2^-

Burton L. Henke, Rupert C. C. Perera, and David S. Urch[a)]

University of Hawaii, Honolulu, Hawaii 96822
(Received 28 September 1977)

The chlorine $L_{II, III}$ low energy x-ray spectra from sodium perchlorate, chlorate and chlorite have been obtained using carbon K_α (277 eV) photon excitation and a lead myristate analyzing "crystal" ($2d = 80$ Å). X-ray induced decomposition was observed for each of these compounds. By taking repeated spectral scans, systematically distributed over six samples, it was possible to extrapolate to "zero-dose" Cl-$L_{II, III}$ spectra. A specially developed least-squares fitting program was applied to precisely determine the energy and strength of each spectral component which utilized the known collimation and crystal broadening functions and yielded energy resolutions of less than 1 eV. Broad low-energy satellite structures were observed for all the oxy-anions and for chloride (NaCl) and have been compared to similar satellites as measured in the Ar-$L_{II, III}$ spectrum. These structures were thus identified as resulting from multielectron processes. The other peaks in the Cl-$L_{II, III}$ spectra of the oxy-anions could be understood as corresponding to transitions from molecular orbitals with Cl $3s$ or $3d$ character. These results have demonstrated that $3d$ orbitals do play a definite role in the formation of chemical bonds in the oxy-anions of chlorine and that the importance of this role increases with the oxidation state of the chlorine. Satisfactory correlations have been obtained with the complementary K_β x-ray emission and photoelectron spectra and with molecular orbital theory for the same anions.

I. INTRODUCTION

Transitions between the molecular orbital states and the nearby and relatively sharp core level states result in low energy x-ray spectra that typically lie in the 100–300 eV (40–100 Å) region. Such spectra can sensitively portray the orbital structure of the molecule (or, in many cases, of an ionic group). For the second-row elements, the nearest core levels are the $2p_{1/2}$–$2p_{3/2}$ spin-orbit split states. The atomic binding energies of these $L_{II, III}$ levels, for example, for 15 P, 16 S, 17 Cl, and 18 Ar are 136–135, 165–164, 202–200, and 247–245 electron volts, respectively. In a particular chemical environment, these core levels of a given atom may shift as much as 10 eV. Such core level chemical shifts can be measured by x-ray photoelectron spectroscopy (XPS). The molecular orbital energies are of the order of 10 eV and can also be measured directly by ultraviolet photoelectron spectroscopy (UPS). The x-ray emission spectra directly yield the difference in the energy of the molecular orbitals and the core level states. However, unlike the photoelectron spectra, the x-ray emission spectra reveal appreciable information about the symmetries of the molecular orbital states. The $L_{II, III}$ spectral intensities are determined mostly by the s and d character of the orbitals and the K_β spectral intensities are determined mostly by the p character of the orbitals. If the $L_{II, III}$ or K_β spectrum originates from an atom of a molecule or of a strongly ionic group that contains only one such atom, it is then relatively easy to approximately calculate the energy and the relative intensity of the x-ray spectral components. Such theoretical predictions can simply be based upon one-electron integrals with the molecular orbital states described as linear combinations of the s, p, and d atomic orbital functions (LCAO approximation). The calculated eigenvectors are used to obtain the dipole transition probabilities. From such MO calculations the relative amounts of s, p, and d contribution can readily be estimated.

In an earlier work, Henke and Smith[1] were able to demonstrate the feasibility of obtaining the $L_{II, III}$ spectra of phosphorous, sulfur, and chlorine in different chemical states by applying spectrographic techniques of such efficiency as to minimize the effects of radiation decomposition. Recently, the S-$L_{II, III}$ spectra have been more precisely measured and analyzed by Henke and Taniguchi[2,3] for the SO_3^{-2} and SO_4^{-2} ions for polycrystalline samples and for the molecules containing single sulfur atoms and in the gas or vapor states—H_2S, SO_2, SF_6, C_4H_4S. The molecular orbital information derived from these spectra were compared to that obtained from the complementary photoelectron and K_β spectroscopy and to the predictions of molecular orbital theory. In this present work, the Cl-$L_{II, III}$ spectra for the ClO_4^-, ClO_3^-, and ClO_2^- ions for polycrystalline samples are measured, analyzed and compared to the photoelectron, K_β and MO calculated[4] data for the same ionic systems. Also, important comparisons with the measured atomic $L_{II, III}$ spectra for Ar and NaCl are presented.

A striking difference in the experimental determinations of the $L_{II, III}$ spectra of the sulfur and the chlorine compounds has been that the latter undergo considerably greater chemical change as induced by the excitation radiation that is required for the spectral measurement. That radiation decomposition might be important in the soft x-ray spectra of chloro-anions had been discussed by Best[5] in the electron excitation of Cl K_β spectra and had also been suggested by Urch[6] in attempting to interpret the early spectra of Henke and Smith.[1] Subsequently, both Prins[7] in x-ray photoelectron experiments and Sadovskii *et al.*[8] in measuring Cl-$L_{II, III}$ emission

---

[a)] Permanent address: Department of Chemistry, Queen Mary College, Mile End Road, London, E1 4NS, England.

 0021 9606/78/6808 3692$01.00

LOW ENERGY X-RAY EMISSION SPECTROSCOPY IN THE 100-500 eV REGION: MOLECULAR ORBITAL INTERPRETATION

By

Rupert C. C. Perera
Department of Physics and Astronomy

A Dissertation Submitted to the Graduate Division
of the University of Hawaii in Partial Fulfillment of
the Requirements for the Degree of
Doctor of Philosophy
in Physics

ABSTRACT

Low energy x-ray spectroscopy in the 100-500 eV region has been applied here to molecular orbital analysis. The available spectroscopic techniques have been extended for very high efficiency in this low energy x-ray region in order to minimize radiation-induced changes in the samples. The lead stearate and lead myristate multilayer analyzers have been employed which set the energy resolution at about 1 eV. The resolution of these multilayer analyzers has been brought into the sub-electron volt region by a simple and accurate deconvolution method for which the collimation-crystal broadening function has been precisely defined. A critical review of the underlying assumptions of the CNDO/2 and MINDO/3 approximate molecular orbital methods is presented and their predictions have been compared with the experimental radiative yield values and orbital binding energies. C-K and O-K spectra from CO and CO_2 in the gas and solid

Proceedings of the International Conference on X-Ray and XUV Spectroscopy, Sendai, 1978;
Japanese Journal of Applied Physics, Volume 17 (1978) Supplement 17-2, pp. 477–482

The Secondary Electron Emission Photocathode Characteristics for Time Resolved X-Ray Spectroscopy

Burton L. HENKE and Kandatege PREMARATNE

Department of Physics and Astronomy
University of Hawaii, Honolulu, Hawaii 96822, U.S.A.

Recently the secondary electron energy distributions and the relative secondary electron yields for the 0.1 to 10 keV photon excitation region have been measured for gold, aluminum and for sixteen representative semiconductors and insulators (alkali halides), and a simple phenomenological model for X-ray photoemission has been developed. This work is discussed here as it might be applied to the application of streak cameras for time resolved X-ray spectroscopy.

§1. Introduction

Time resolved X-ray spectroscopy has recently become of considerable value in studies of high temperature plasmas in the one second range (magnetically confined fusion) to the picosecond range (laser produced fusion). Mode-locked laser systems are available that can generate high intensity pulses of X-radiation from matter in the picosecond region. Ultra-fast spectroscopy is needed for the characterization of such X-ray sources and of the effects of their radiation bursts upon materials. Pico second X-ray spectroscopy may be a valuable tool for the measurement of the lifetimes of metastable atomic and molecular states and of certain photochemical processes.[1–3]

A proven method for accomplishing time resolved X-ray spectroscopy is that with the X-ray streak tube.[4–6] An X-ray beam is dispersed according to its photon energy along a slit-defined photocathode using a non-focusing crystal or a diffraction grating (or by a series of absorption filter and/or total-reflection monochromator channels). The secondary electrons from this slit source are used to form a line image at an image intensifier (needed particularly for ultra-fast spectroscopy). This line image is "streaked" to establish a time base using a pair of deflecting plates. The optical output of the image intensifier is recorded photographically. A schematic of such an X-ray streak tube is shown in Fig. 1. As indicated here, two types of imaging can be used, either an electron lens system[7,8] or a simple, proximity-focusing microchannel plate system.[9,10]

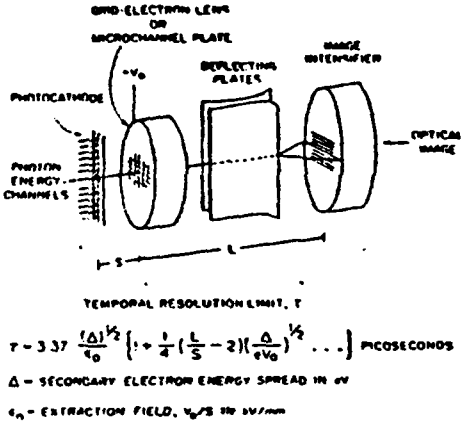

Fig. 1. Schematic of an X-ray streak tube as applied for time resolved X-ray spectroscopy. The temporal resolution limit, τ, is the difference in arrival time at the image intensifier for axially emitted electrons from the photocathode of initial velocities equal to zero and to v_0. The corresponding energy spread, Δ, of the secondary electron emission is $1/2 \cdot mv_0^2$.

The intensity-and-photon-energy response and the temporal resolution of the streak camera are ultimately determined by the characteristics of the photocathode. In the sections that follow, we have attempted to review (1) the basic relationship between the photoemission and the electron-optical characteristics of the X-ray streak tube, and (2) the experimental and theoretical determination of the relevant photoemission properties of metal and dielectric X-ray photocathodes as have been recently investigated in this laboratory.[11–13]

Proceedings of the International Conference on X-Ray and XUV Spectroscopy, Sendai, 1978;
Japanese Journal of Applied Physics, Volume 17 (1978) Supplement 17-2, pp. 112–115

C-K and Cl-L Emission Spectra and Molecular Orbital Analysis of CCl_4

Rupert C. C. PERERA*,** and Burton L. HENKE

Department of Physics and Astronomy,
University of Hawaii, Honolulu, Hawaii 96822

The C-K and Cl-$L_{II,III}$ low energy X-ray spectra from solid CCl_4 have been obtained using monoenergetic X-ray excitation and a lead myristate multilayer analyzing crystal. The Cl-L spectra was also measured in the vapor phase and compared with that measured in the solid phase. The deconvolved C-K and Cl-$L_{II,III}$ spectra are compared with the available Cl-Kβ and UPS spectra and with the results of CNDO/2, MINDO/3 and extended Hückel MO calculations.

§1. Introduction

The X-ray emission spectra from gaseous chlorinated methane derivatives have been previously reported by many authors. LaVilla and Deslattes[1] studied the chlorine-Kβ emission spectra and Ehlert and Mattson[2] reported the carbon-K and chlorine-L spectra from four chlorinated derivatives of methane. The photoelectron spectra of chloromethanes were measured by Potts *et al.*[3] using 21 eV and 40 eV excitations and by Turner *et al.*[4] using 21 eV excitation. The experimental photoelectron spectra are in good agreement. Hopfgarten and Manne[5] provided a molecular orbital interpretation of available photoelectron and X-ray emission spectra of chloromethanes on the basis of the extended Hückel molecular orbital calculations.

In this laboratory,[6,7] the C-K and Cl-L emission spectra of CCl_4 and $CHCl_3$ and the C-K emission spectra of CH_4 were measured in the solid phase. The C-K emission spectra of methane and the Cl-L emission spectra of chloromethanes were also measured in the gas phase. Molecular orbital analysis of these chloromethanes were based upon the CNDO/2 and MINDO/3 SCF-MO calculations and upon results of available extended Hückel MO calculations.[5] As an example, the spectra and molecular orbital analysis of CCl_4 will be presented here.

*In partial fulfillment of PhD, University of Hawaii, May 1978.

**Present address: Department of Physics, University of Sri Lanka, Peradeniya, Sri Lanka.

§2. Experimental

Basic details of the experimental approach have been given elsewhere.[7,8] For high efficiency, an oxidized copper excitation source was used to create the C-1s hole and a carbon excitation source was used to create the Cl-2p hole. The X-ray tube was operated at 8 kV and 150 mA. A lead myristate multilayer[8] was used as the analyzer. A "pressure tuned"[9] constant flow proportional counter filled with propane at subatmospheric pressure was used as the detector.

In measuring the chlorine-$L_{II,III}$ spectra in the vapor phase, the sample pressure in the gas cell was maintained at one Torr for maximum intensity.[10] The chlorine-$L_{II,III}$ spectra of CCl_4 in the solid and vapor phases were measured under the same excitation and are presented in Fig. 1. As seen from Fig. 1, there are no substantial differences between the gas phase and solid phase spectra. Since the fluorescent intensity from the solid phase was about ten times higher than in the gas phase, the spectra from the solid samples were used in the detailed analysis presented here.

Reagent grade CCl_4 was obtained commerically with better than 99% purity. All of the spectra presented in this work are the sum of at least three repeated runs and the individual runs reproduced within statistical deviations. Over 10^4 counts were collected at the peak in all spectra and the spectrometer was calibrated using Rh, Mo and Nb Mζ lines.[7,8] In all of the spectra, the peak intensities were normalized and background was not subtracted from the data because it was negligibly small.

A step-scanned spectrum thus obtained was

65

A Soft X-Ray Spectrometer for the Study of Plutonium and Plutonium-based Materials†

P.L. Wallace, W.L. Haugen, E.M. Gullikson and B.L. Henke
Lawrence Livermore Laboratory, University of California, Livermore, California 94550, USA

A low-energy spectrometer for the X-ray analysis of plutonium and plutonium-containing materials has been built. We use an ultra-thin window to maintain different pressures and contamination levels in the spectrometer's sample and crystal chambers. Ultra-thin windows are also used on the X-ray tube and detector. Methods have been developed by which the spectrometer can analyze both metal and loose-powder samples. Representative calibration spectra are presented for the fluorine band in polyfluoroethylene, the oxygen band in α-Al_2O_3, and the carbon band in graphite. Experimental spectra are presented for the fluorine band in PuF_3 and PuF_4 and for the oxygen band in PuO_2.

INTRODUCTION

The surface chemistry of metals is important to the understanding of their behavior and to their application. This is just as true for radioactive metals as for others. One way to study the surface chemistry of metals is by low-energy X-ray spectrometry. This technique[1,2] uses the low-energy X-ray region (defined here as below 2 keV) to analyze for light elements (Mg through Be). Often the technique can also produce valence-band or orbital-energy information that helps us learn more about the energy and symmetry of the outer electronic states in atomic systems.

The information produced complements that obtained in either photoelectron or Auger electron spectrometry. However, experimentally the low-energy X-ray technique has the advantage of not requiring the very-high-vacuum environments of the electron-spectrometry techniques. This lower vacuum requirement is very important in our plutonium studies. Our system has to be connected to a glove box because of plutonium's toxicity,[3] and very-high-vacuum systems attached to glove boxes have proven difficult to build and keep clean.

A prior low-energy X-ray study of plutonium used an electron microprobe.[4] The aim of that work was to document the low-energy X-ray spectrum of plutonium rather than to study its surface chemistry.

APPARATUS

Our system is similar to that first reported by Henke[5] and marketed by Philips Electronic Instruments.‡ However, we had to substantially alter our Philips system to accommodate alpha-emitting materials and to produce a clean environment in the sample chamber. Figure 1 is a schematic of our system.

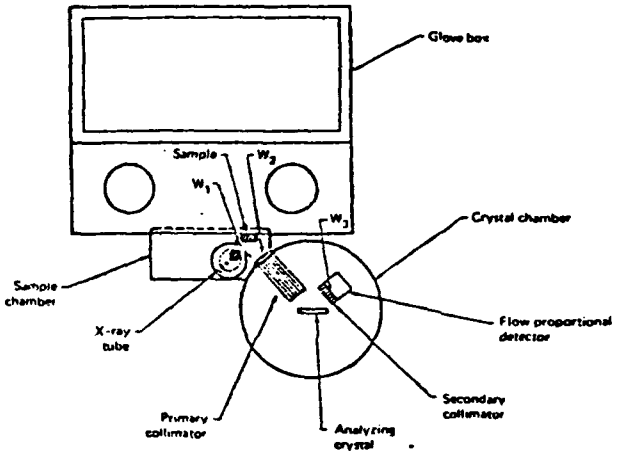

Figure 1. Schematic of the low-energy X-ray spectrometer designed for plutonium-materials studies. Of particular importance are the ultra-thin windows W_1, W_2 and W_3, which permit operation with very different pressures in the X-ray tube, sample chamber, crystal chamber and the X-ray detector. The window compositions are: W_1, 0.42 g m^{-2} carbon; W_2 and W_3, 0.72 g m^{-2} Formvar.

Vacuum systems

The X-ray tube, the sample chamber, the crystal chamber, and the flow proportional detector are each kept at a different pressure during analytical runs. These different pressures are maintained by the use of ultra-thin isolation windows. The X-ray tube has a 0.42 g m^{-2} (area density) pure carbon window (W_1) that has been coated with a dilute Formvar (polyvinyl formal) solution to fill pinholes. The window between the two chambers and the detector window are both 0.72 g m^{-2} Formvar film and were produced at this laboratory.[6]

† Work performed under the auspices of the US Department of Energy by the Lawrence Livermore Laboratory, under contract number W-7405-ENG-48.

‡ Reference to a company or product name does not imply approval or recommendation of the product by the University of California or the US Department of Energy to the exclusion of others that may be suitable.

0049-8246/78/0007-0160 $02.00

PHYSICAL REVIEW B VOLUME 19, NUMBER 6 15 MARCH 1979
pp. 3004-3021

Soft-x-ray-induced secondary-electron emission from semiconductors and insulators: Models and measurements

Burton L. Henke, John Liesegang,* and Steven D. Smith
University of Hawaii, Department of Physics and Astronomy, Honolulu, Hawaii 96822
(Received 27 July 1978)

Secondary-electron energy distribution curves (EDC's) and the total secondary-electron yields relative to such for gold have been measured for seven semiconductors for which electron-electron scattering losses within the emitter were considered dominant and for nine insulators (alkali halides) for which electron-phonon scattering losses were expected to be dominant in the transport process. The secondary-electron spectra were excited by Al-$K\alpha$ (1487 eV) photons and were measured from evaporated dielectric films (of about 0.3 μ thickness) on conducting substrates with an electrostatic hemispherical analyzer of about 0.03-eV resolution. Some of the dielectric photoemitters have appreciably narrower energy distributions and higher yields than has gold; CuI and CsI have EDC widths at half-maximum of about one-third of that for gold, and yield values of 11 and 30 times greater. The FWHM and secondary-electron yield for gold were measured to be about 4 eV and 0.50 electrons per normally incident photon, respectively. The shapes of the EDC's were found to be essentially unchanged for photon excitation in the 0.1–10-keV region. Strong structural features appear only in the alkali halide EDC's, and it is proposed that these are mainly the result of single-electron promotion of secondaries from the valence band by plasmon deexcitation. A relatively simple model for x-ray photoemission has been developed which assumes that direct excitation of secondaries by photoelectron and Auger-electron "primaries" is the dominant excitation mechanism, and accounts for both electron-electron and electron-phonon scattering in the transport process. Free-electron conduction-band descriptions are assumed. The theoretical and experimental curves are in satisfactory agreement.

I. INTRODUCTION

There has been a considerable amount of effort on the theory and application of secondary-electron emissions using electron excitation in the kilovolt region (as applied, for example, in scanning microscopy) and using extreme ultraviolet excitation (as applied in band-structure analysis). There has been relatively little theoretical or experimental work reported on the generation of the secondary electrons using x-ray excitation (which is of considerable current interest as applied to the measurement of the intensity and the temporal history into the picosecond region of pulsed x-ray sources with the diode detector, the streak, and the framing cameras in high-temperature plasma diagnostics).

With electron and extreme ultraviolet generation of the secondary-electron distribution, the effective escape depths of the electrons can be very dependent upon the attenuation mechanism of the exciting radiation. With x-ray excitation of the photoelectron and subsequent emission of the associated Auger-electron "primaries" which in turn generate the internal secondary-electron distribution, the electron escape depths are usually independent of the x-ray attenuation process. This is because the x-ray penetration is very large as compared to the effective electron escape length. Thus with x-ray excitation, often a more direct and precise interpretation of the secondary-electron energy distribution can be made in terms of models for the excitation, transport, and escape processes.

In an earlier work,[1] the electron energy dependence of the secondary-electron energy distribution from metals as excited by x-rays in the 0.1–10-keV region was measured and found to be consistent and predictable by applying currently available theoretical descriptions for the excitation, mean free paths, and escape for secondaries in metals. In this present work, we have measured the energy dependence and relative yields of the secondary electrons as excited by soft x rays (principally at 1487-eV photon energy) for a representative series of semiconductors and insulators. For these systems, the secondary-electron generation processes are more complex, particularly for the insulators for which multiple scattering has an appreciable role in the transport process. In order to test available theoretical expressions for the secondary-electron excitation and for the mean free paths for pair production and for electron-phonon interactions for the energy region below 10 eV, we have used the relatively simple rate equation developed by Kane[2] for a description of the multiple scattering transport process. We believe this approach will be helpful at this time in guiding the application of more exact transport theories, analytical and numerical, in later studies.

In Sec. II, we present the "semiclassical," simple case for x-ray excited secondary- electron generation for the "no-loss" transport (no multi-

67

Low energy x-ray emission spectra and molecular orbital analysis of CH_4, CCl_4, and $CHCl_3$

Rupert C. C. Perera[a] and Burton L. Henke

University of Hawaii, Department of Physics and Astronomy, Honolulu, Hawaii 96822
(Received 11 January 1979)

The C-K and Cl-$L_{II,III}$ low-energy x-ray spectra from solid CCl_4, $CHCl_3$, and the C-K x-ray spectrum from solid CH_4 have been obtained using monoenergetic x-ray excitation and a lead myristate multilayer analyzing crystal. The C-K spectrum of methane and Cl-$L_{II,III}$ spectra of the chloromethanes were also measured in the gas/vapor phase and compared with those measured in the solid phase. The deconvolved spectral components are aligned on a common energy scale with the complementary x-ray emission and photoelectron spectra by identifying the same molecular orbital in all spectra. Such an alignment procedure yields a C-1*s* ionization energy of gaseous CH_4, and solid CCl_4 and $CHCl_3$ as 290.0 293.5 and 293.1 eV, respectively; and the Cl-$2p_{3/2}$ ionization energy of solid CCl_4 and $CHCl_3$ as 206.5 and 204.8 eV. Results of the CNDO/2 and MINDO/3 MO calculations have been presented and compared with the available results of the extended Hückel MO method and with the deconvolved spectral components. From the geometry program in the MINDO/3 MO calculation, the C–H bond length in CH_4 is 1.102 Å, the C–Cl bond length in CCl_4 is 1.751 Å, and the C–H and C–Cl bond lengths in $CHCl_3$ are 1.100 and 1.744 Å, respectively. Comparison with the vapor/gas phase spectra shows essentially the same energies for spectral components in the C-K and Cl-L spectra from CH_4 and CCl_4, whereas the spectral components in the Cl-L spectra of $CHCl_3$ have energies in the gas phase that are significantly higher than those for the solid phase.

I. INTRODUCTION

The x-ray emission spectra from gaseous methane and chlorinated methane derivatives have been previously reported by many authors. LaVilla and Deslattes[1] studied the Cl-Kβ emission spectra and Ehlert and Mattson[2] reported the C-K and Cl-L spectra from four chlorinated derivatives of methane. G'ilberg[3] also studied the Kα and Kβ spectra of chlorine in CH_3Cl and compared them with the HCl and Cl_2 chlorine spectra. The ultraviolet-excited photoelectron (UPS) of chloromethanes were measured by Potts *et al.*[4] and by Turner *et al.*[5] using 21 eV photon excitation. The 21 eV excited spectrum of CH_3Cl has been studied by Ragle *et al.*[6] The x-ray excited photoelectron spectrum (XPS) of methane was measured by Hamrin *et al.*[7] The experimental photoelectron spectra are in good agreement. Hopfgarten and Manne[8] provided a molecular orbital (MO) interpretation of available photoelectron and x-ray emission spectra of methane and the chloromethanes on the basis of the extended Hückel molecular orbital calculations and confirmed the symmetry assignments of CH_3Cl and CCl_4. However, revisions of previous assignments were suggested by them for CH_2Cl_2 and $CHCl_3$.

In this present work, the C-K emission spectra of CH_4 were measured for the solid and gas phases, the C-K and Cl-L emission spectra of CCl_4 and $CHCl_3$ were studied in the solid phase, and the Cl-L spectra in the solid phase were compared with the vapor phase spectra. Molecular orbital analysis of these chloromethanes were based upon the CNDO/2 (Complete Neglect of Differential Overlap) and MINDO/3 (Modified Intermediate Neglect of Differential Overlap) SCF-MO calculations and upon results of available extended Hückel MO calculations.

II. EXPERIMENTAL

Basic details of the experimental approach have been given elsewhere.[9,10] For high excitation efficiency, an oxidized copper excitation source was used to create the C-1*s* hole and a carbon excitation source was used to create the Cl-2*p* hole. The x-ray tube was operated at 8 kV and 150 mA. A lead myristate multilayer[9] was used as the analyzer. A "pressure tuned"[11] constant flow proportional counter filled with propane at subatmospheric pressure was used as the detector.

Gaseous methane, and CCl_4 and $CHCl_3$ were obtained commercially with purities over 99%. For the gas/vapor phase, the sample pressure in the gas cell was adjusted for maximum fluorescent intensity.[12] Solid methane and chloromethanes were obtained using a closed cycle refrigeration system capable of reducing the sample temperature to as low as 10 °K. The temperature at the cold head was maintained not lower than necessary to freeze the samples[13] and a small constant deposition rate was maintained to avoid any possible surface contamination. All of the spectra presented in this work are the sum of at least three repeated runs with the individual runs reproducible to within statistical deviations. Over 10^4 counts were collected at the peak intensity in all spectra. The spectrometer was calibrated[10] using Rh, Mo, and Nb Mζ lines which include the C-K and Cl-L wavelength regions. In all of the spectra, the peak intensities were normalized and background was not subtracted from the data because it was negligibly small. Corrections were made for window transmission, crystal and counter efficiencies after the data was deconvolved.

A step-scanned spectrum thus obtained was deconvolved into Voigt spectral components using a computer analysis program developed for low energy x-ray spec-

[a] Present address: Department of Physics, University of Sri Lanka, Peradeniya Campus, Peradeniya, Sri Lanka. This work has been in partial fulfillment of the University of Hawaii requirements for the Ph. D. in Physics.

 0021-9606/79/125398-09$01.00

Multilayer X-Ray Spectrometry in the 20—80 Region: A Molecular Orbital Analysis of CO and CO_2 in the Gas and Solid States

R.C.C. Perera† and B.L. Henke
University of Hawaii, Honolulu, Hawaii 96822, USA

Optimized multilayer X-ray spectrometry, using lead myristate and lead stearate analyzers (2*d* values of 80 and 100 Å) has been applied to the measurement of the O–Kα and the C– Kα spectral bands from CO and CO_2 in the gas and solid phases. The $L_{II,III}$ spectra were also measured for argon in the gas and solid states under similar conditions in order to identify and to minimize any non-molecular components in the CO and CO_2 spectra. These molecular orbital data have been related to those obtained with X-ray and ultraviolet photoelectron spectroscopy and grating X-ray spectroscopy. The consistency of the results of these complementary measurements is excellent. The ionization energies for the C and O 1s levels have been determined to be 295.4 and 542.0 eV for CO and 296.8 and 540.3 eV for CO_2. The MO data have also been compared with that predicted from the symmetry, strength and binding energy of the molecular orbital spectral components as calculated using the currently available computational models, CNDO/2, MINDO/3, MNDO, extended Hückel and *ab initio*. The molecular orbital calculated results for these organic compounds, CO and CO_2, are not in as good agreement with the experimental data as previously demonstrated for molecular orbital spectra measured for C–Kα and the $L_{II,III}$ bands of Cl, S and P for both organic and inorganic compounds.

INTRODUCTION

A molecular group of atoms is chemically characterized by the symmetries, strengths and binding energies of the molecular orbitals that are generated from the valence electrons of the atoms involved. In recent years, with the increased availability of large computers, more accurate programs have been developed for calculating these molecular orbital characteristics.[1] Because the more efficient of these programs are semi-empirical at this time, it is of considerable value to have precise experimental molecular orbital data on a selected series of molecular systems as can be obtained with photoelectron and X-ray spectroscopy. The molecular orbital binding energies can usually be measured within 1 eV or better by ultraviolet (UPS) or X-ray (XPS) photoelectron spectroscopy. The X-ray spectrometry of the fluorescent radiation resulting from single electron transitions from the molecular orbitals into single ionization vacancies in the nearby, relatively sharp core levels can provide data on the symmetries and the relative strengths of the molecular orbital components as well. For example, the Kα bands of the first-row elements reflect the p-character of the orbitals that are most strongly associated with the particular atom with the initial 1s vacancy. For the second-row elements, in a similar way, the Kβ bands and the $L_{II,III}$ bands measure the p-character and the s- and d-character, respectively, of the associated molecular orbitals. These Kβ and $L_{II,III}$ radiations are mostly in the 20–100 Å wavelength region. X-ray spectrometry in this long wavelength region requires either grazing *incidence diffraction gratings* or large *d*-spacing *multilayer* analyzers.

† Present address: Department of Physics, University of Sri Lanka, Peradeniya Campus, Peradeniya, Sri Lanka.

In order to generate the 'cleanest' spectra possible that are characteristic of the simple, single-electron transitions (and therefore which can be directly and quantitatively related to the calculated molecular orbital symmetries, populations and binding energies), it is necessary to minimize and to identify extraneous spectral features. For example, effects resulting from multiple ionization, high-order diffraction and radiation damage must be minimized. This can be accomplished by using photon excitation so as to selectively excite the desired initial core level vacancy. But even with such selective deposition of the excitation energy, the total spectral energy that is allowed for measurement is often seriously limited by the requirement that the excitation dosage should not cause significant radiation-induced changes in the sample. In order to meet the requirement for 'fast' X-ray spectroscopy, an optimized, high-efficiency spectroscopy has been developed[2,3] which utilizes multilayer analyzers such as the lead myristate, lead stearate and lead lignocerate systems with 2*d*-spacings of about 80, 100 and 130 Å, respectively. Because the transmission functions of the multilayer spectrograph can be accurately measured, the attainable energy resolution can be in the sub-electron-volt region through simple spectral devolution procedures.

Multilayer measurements of the $L_{II,III}$ spectral bands for the second-row elements, Cl, S and P, have been reported from this laboratory[4–6] as applied to the molecular orbital analyses of a selected series of chlorine, sulfur and phosphorus compounds. The samples were polycrystalline and it was established that the molecular orbital spectra for the central atoms of the anions were not affected significantly by crystal field effects (different cations). More recently, C–Kα and Cl–$L_{II,III}$ spectral band measurements by multilayer X-ray spectrometry have been applied to the

(70)

Nuclear Instruments and Methods 177 (1980) 161–171

X-RAY SPECTROSCOPY IN THE 100–1000 eV REGION

Burton L. HENKE

University of Hawaii, Department of Physics and Astronomy, 2505 Correa Road, Watanabe Hall, Honolulu, Hawaii 96822, USA

Some current methods for achieving low energy X-ray spectroscopy in the 10–100 Å region are reviewed. Gratings, crystals and multilayers can be used as monochromators or dispersive analyzers. Some of the important characteristics are noted here which can help to determine their applicability to a given spectroscopic analysis situation. The "trade-off" between resolution and spectrographic speed (gratings versus multilayers) may be an important consideration when the number of photons available for measurement is limited, as, for example, by the excitation dosage allowed for a given sample. For pulsed X-ray sources and for time-resolved spectroscopy, special fixed-crystal spectrographs have been developed. These may be applied with X-ray diodes and fast oscilloscopes or with X-ray streak cameras for detection. The optimum design and characterization of the photocathode systems for such detection have been studied in detail and some of the results of this work are briefly reviewed.

1. Introduction

The new synchrotron radiation and laser-produced plasma sources can provide pulsed, broad-band radiation in the UV and X-ray region of such high intensity as to present a new dimension for spectroscopic analysis. This may be of particular importance for low energy X-ray spectroscopy in the 10–100 Å region for which high intensity, selective excitation has generally not been available.

X-ray absorption and emission spectroscopy in this low energy region is of considerable interest for the measurement of the spectra that originate from transitions between the outermost electronic levels and the relatively sharp, first core levels. Such valence band spectroscopy can sensitively reflect the chemical, optical and electronic properties of matter.

The importance of having continuous selectivity of the excitation for absorption spectrometry is well known, particularly for extended absorption fine structure measurements. Selective, narrow-band excitation can also present a critical advantage in emission spectrometry by providing "clean" meaningful spectra with a minimum of background radiation, and by minimizing possible effects of radiation-induced changes in the sample.

An illustration of the critical role of radiation damage in molecular orbital spectroscopy is presented in fig. 1. The chlorine-LII,III spectra in the 150–250 eV region were measured in order to determine the relative molecular orbital strengths of s and d symmetries for various oxidation states in chlorine

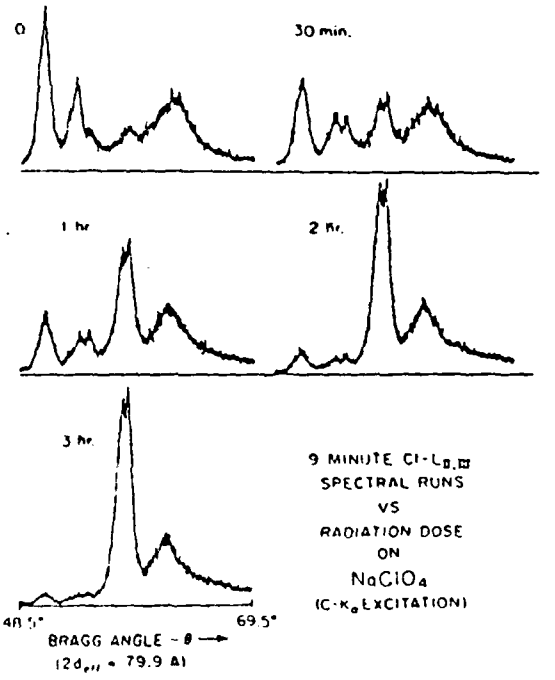

Fig. 1. Radiation-induced decomposition of polycrystalline $NaClO_4$. The excitation intensity was similar to that employed for the Cl-$L_{II,III}$ spectroscopy [1.75×10^{13} C-Kα (277 eV) photons/s cm^2 at the sample surface]. The quick scans reveal spectral changes corresponding to the appearance of reduction products such as $NaClO_3$ and $NaClO_2$. After three hours, the spectra correspond to that for NaCl

Reprinted from Applied Optics, Vol. 19, page 749, March 1, 1980

71

Evaluation of high efficiency CsI and CuI photocathodes for soft x-ray diagnostics

E. B. Saloman, J. S Pearlman, and B. L. Henke

The photoefficiency of CsI and CuI photocathodes was measured for photons in the 22–240-eV (50–560-Å) energy range. The within-batch and batch-to-batch variation in photoefficiency were studied as was the sensitivity of the samples to storage under dry nitrogen. The effect of exposure to air was investigated. The shape of the photoefficiency curves was found to agree quite well with that expected from the photoabsorption cross sections of the materials. CsI in particular appears useful as a detector in soft x-ray diagnostics, especially as a narrowband detector in the 100-eV photon energy range where peak measured efficiencies can exceed 300%.

There has been increased interest recently in time-resolved measurements of UV and soft x-ray emission for the study of picosecond processes in fusion plasmas, biological systems, atomic collisions, and photochemical reactions. High sensitivity x-ray photocathodes for use in diodes or streak cameras could enhance the capability of existing diagnostic equipment used in these research areas. Two high-sensitivity photocathode surfaces, CsI and CuI,[1] were evaluated and compared with an evaporated aluminum surface. Their efficiences are substantially higher than aluminum (factors of 5–50 near 100-eV photon energy).

Several characteristics are important for a photocathode surface to be useful for ultrafast temporal diagnostics. These include good efficiency, reproducibility from batch to batch or good exposure and shelf-life characteristics, and a narrow secondary electron emission spectrum. In the results reported here, these characteristics are evaluated for CuI and CsI.

The electron emission of a photocathode involves several processes. Absorption of incident radiation leads to the generation of primary electrons. If the material thickness is larger than the primary electron range, a number of lower energy secondary electrons are created by each primary. In addition, the atoms excited by the incident radiation decay through fluorescence and Auger processes creating additional electrons. A certain number of the secondary electrons reach the photocathode surface with enough energy to escape. These electrons are measurable as a photoemission current.

The photoemission is proportional to the incident photon energy, the photon absorption characteristics, and the material's electron properties. From a simple phenomenological model, the photoemission is proportional to[2] $I\rho E\mu(E)f(E)$, where I is the incident x-ray intensity (photons/cm^2 sec), ρ is the mass density, E is the photon energy, $\mu(E)$ is the mass photoionization cross section, and $f(E)$ is the fraction of total energy deposited that is effective in secondary electron emission. This efficiency factor $f(E)$ is strongly material dependent. In metals, the predominant secondary electron generation mechanism is electron-electron collisions, while for semiconductors and insulators, where the number of free conduction electrons is lower, processes other than electron-electron collisions can be important. For example, in semiconductors (CuI), hole pair formation plays an important role in creating low-energy electrons, while in insulators (CsI), electron-phonon processes (lattice vibration) can be significant. The dominance of different generation processes leads to widely varying values of secondary electron production efficiency, as will be seen.

The secondary electron generation process not only affects the emission efficiency but also the photoelectron energy distribution. Presented in Fig. 1 are the photoelectron energy distributions for the gold, aluminum (effectively Al_2O_3), copper iodide, and cesium

E. B. Saloman is with U.S. National Bureau of Standards, Center for Radiation Research, Synchrotron UV Radiation Facility, Washington, D.C. 20234. J. S. Pearlman was with U.S. Department of Energy's Office of Laser Fusion; he is now with Maxwell Laboratories, Inc., San Diego, California 92123. B. L. Henke is with University of Hawaii, Department of Physics & Astronomy, Honolulu, Hawaii 96822.

Received 9 October 1979.
0003-6935/80/050749-05$00.50/0.

(72)

The characterization of x-ray photocathodes in the 0.1–10-keV photon energy region

B.L. Henke, J. P. Knauer,[a] and K. Premaratne
University of Hawaii, Honolulu, Hawaii 96822

J.Appl.Phys.
pp. 1509-1520

(Received 25 September 1980; accepted for publication 2 December 1980)

A method and an instrument are described for the measurement of the absolute quantum yield for front-surface and transmission photocathodes in the 0.1–10-keV photon energy region. The total and the secondary electron photoemission yields have been measured for the Al, Au, CuI, and CsI photocathodes as required for the absolute calibration of the x-ray diode detectors and for the x-ray streak cameras. The relative secondary electron yields have also been measured for the same photocathodes by high resolution electron spectroscopy of the secondary electron energy distributions, which are in good agreement with the absolute yield measurements. The secondary electron yield of CsI is ten to one-hundred times higher than that for Au in the 0.1–10-keV region and with a secondary energy distribution that is appreciably sharper. For these reasons, CsI should be an effective photocathode for sensitive, time-resolved spectroscopy into the picosecond region. It is verified experimentally that the secondary electron quantum yield varies approximately as $E\mu(E)$, with E as the photon energy and $\mu(E)$ as the photoionization cross section, and that the primary (fast) electron quantum yield is a small fraction of the total yield and varies approximately as $E^2\mu(E)$. A simple model for x-ray photoemission is described which leads to semiempirical equations for front- and back-surface secondary electron photoemission as based upon an escape depth parameter that may be obtained from yield-versus-photocathode thickness data. The model predictions are in good agreement with experiment.

PACS numbers: 79.60.Cn, 79.60.Eq, 72.10. – d

I. INTRODUCTION

Time-resolved x-ray spectroscopy has become of considerable importance in the temperature density composition diagnostics of high-temperature plasmas involved in controlled thermonuclear fusion studies which utilize laser, particle beam, or magnetic compression-confinement production. The time duration of the associated x-ray emission ranges from picoseconds to seconds. Time-resolved x-ray spectroscopy is also important in the development of superradiant, pulsed x-ray sources, their application to studies of the radiation effects of x-ray bursts upon materials, and the x-ray analysis of atomic, molecular, and solid-state time-resolved processes into the picosecond region.

The electron currents that are emitted by photocathodes under x-ray excitation can be a very effective basis for time resolved spectroscopic measurement using x-ray diode or streak camera detection.[1-5] In the latter, an x-ray spectrum can be established along a slit-defined transmission photocathode of the streak camera by using focussing filter-total-reflection monochromator, crystal/multilayer arrays, or nonfocussing, Bragg reflecting crystal/multilayer analyzer systems.

In time-resolved x-ray spectroscopy, the ultimate limit on the achievable time resolution is the quantum conversion efficiency of the photocathode (which determines signal statistics) and the energy spread of the emitted electrons as is noted in Fig. 1 (which determines the time resolution).[6] The relatively small fraction of fast electrons that is photoemitted is effectively blocked by the electron optical apertures of the typical streak camera. In Fig. 2 the difference in the arrival time at the output end of the streak camera is given as a function of the energy width Δ of the secondary electron energy distribution, the extraction field ϵ_0, and of the geometry of the camera. In addition to the absolute yield-versus-photon energy and the shape of the secondary electron distribution curves, other important characteristics of the x-ray photocathode are its stability, reproducibility, simplicity of spectral response, and the linearity of its time response. Described here is a method and an instrument for the measurement of the absolute total and secondary electron yields

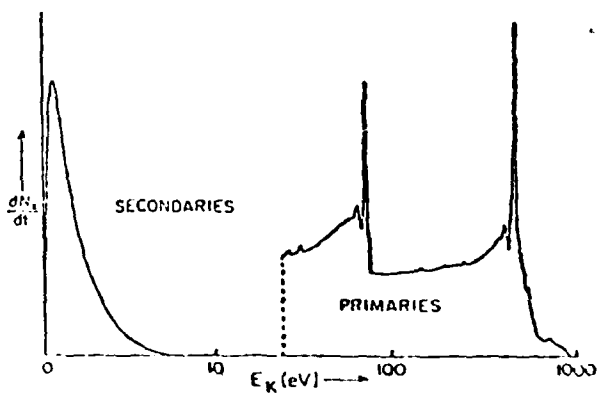

FIG. 1. In the 0.1-10 keV photon energy region the larger fraction of the electrons that are emitted are the secondary electrons, typically as a narrow distribution below 10 eV. The higher energy, fast electron photoemission consists of relatively sharp elastically scattered photoelectrons and Auger electron "lines" along with a much larger number of inelastically scattered electrons in their low-energy tail region

[a]Present address: Lockheed, LMSC Palo Alto Research Laboratory, Org. 52-11, Building 203, 3251 Hanover Street, Palo Alto, California 94304

 0021-8979/81/1509-12$01.10

Published in the Conference Proceedings No. 75, Low Energy X-Ray Diagnostics 1981, Monterey (American Institute of Physics, New York, 1981) pp. 146-155.

73

Low Energy X-Ray Interactions: Photoionization, Scattering, Specular and Bragg Reflection

B. L. Henke

University of Hawaii, Department of Physics and Astronomy, Honolulu, Hawaii 96822

ABSTRACT

For the low energy x-ray region of 100-2000 eV, the complete atomic interaction, coherent scattering and photoelectric absorption can be described by a complex scattering amplitude which may be given through the atomic scattering factor, $f_1 + if_2$. For this low photon energy region, it is shown by the relativistic quantum dispersion theory that the atomic scattering factors can be uniquely determined from simple relations involving only the atomic photoionization cross section dependence upon photon energy. We have compiled "state of the art" tables for the photoionization cross sections for 94 elements and for the photon energy region of 30- 10,000 eV. With this compilation, we have established atomic scattering factor tables for the 100-2000 eV region. By a summing of the complex, atomic scattering amplitudes, a low energy x-ray interaction can be determined. Even for atoms in the molecular or solid state the scattering cross sections remain atomic-like except for photon energies very near the thresholds. Using practical examples, the methods of calculation, with the atomic scattering factors, are reviewed here for the following: 1) x-ray energy deposition within materials (energy response of x-ray photocathodes); 2) transmission through a homogeneous medium: refraction; 3) transmission through a random collection of uniform spheres: low angle scattering in an inhomogeneous medium; 4) specular, Fresnel reflection (total and large angle reflection) at smooth boundary; and 5) Bragg reflection from a periodic, layered system--(reflection by crystals and multilayers).

I. INTRODUCTION--THE ATOMIC SCATTERING FACTORS

In this review, we would like to discuss, for the low energy x-ray region (100-2000 eV region), how the interactions of absorption, scattering and reflection can be well described by using the atomic scattering factors as the primary parameters for the material system. In the Appendix of these proceedings we present tables for the atomic scattering factors as directly derived from a recent work [1] on a "state of the art" compilation of the photoionization cross sections for 94 elements for the 30-10,000 eV region, along with the calculated atomic scattering factors for the 100-2000 eV photon energy region. We present here, as applied to selected examples of relevance in low energy x-ray diagnostics, some basic procedures for predicting low energy x-ray interactions.

The interaction physics for the conventional x-ray region (for photon energies above 1000 eV) has been presented by many excellent texts including that of Compton and Allison [2] and R. W. James [3]. What is summarized here is an extension and specialization of this physics that is useful for the long wavelength x-ray region of 10-100 A.

For the low energy x-rays, the interaction can be defined as simply coherent scattering and photoelectric absorption. Incoherent scattering is negligible. The complete interaction with an atom may thus be described by a complex scattered amplitude defined by an atomic scattering factor, $f_1 + if_2$, as depicted in Figs. 1 & 2. The scattered amplitude is given by this factor multiplied by that amplitude which would be scattered if the atom were replaced by a free, Thomsonian electron. Here, r_o is the classical electron radius, m the electron mass, c the velocity of light and R the distance from the atom to the point of measurement. Because the wavelengths of interest are large as compared with the dimensions of the electron distributions within the atom, we make the important assumption here that essentially all electrons will scatter effectively in phase for all but the largest angles of scattering so that the atomic scattering factor components, f_1 and f_2, may be considered angle independent. The complex amplitude of atomic scattering therefore will be dependent only upon the angle of scattering, 2θ, through the polarization factor, P(2θ), of the Thomsonian term. P(2θ) is equal to unity or cos 2θ depending upon whether the incident electric vector is perpendicular to or parallel to the plane of scattering. As will be discussed below, the relative roles of the coherent scattering and the photoelectric absorption will be expressed through f_1 and f_2, respectively.

The relativistic quantum dispersion theory for atomic scattering and the calculation of the atomic scattering factors has been presented by Cromer and Lieberman [4] and by Jensen [5] (along with their references). In Fig. 2 are shown their results including the relativistic corrections, Δf_r, to the semiclassical, usual relations for f_1 and f_2. Here Z is the atomic number, h Planck's constant, mc^2 rest mass energy of the electron, E_{tot} the total energy of the atom and E the photon energy. Cromer and Lieberman have estimated E_{tot} (a negative quantity) for all the elements and from their table we have fit the following polynomial for the larger term in Δf_r.

$$\frac{5}{3}\frac{|E_{tot}|}{mc^2} = 2.19 \times 10^{-6}Z^3 + 1.03 \times 10^{-5}Z^2 .$$

LOW ENERGY X-RAY SCATTERING

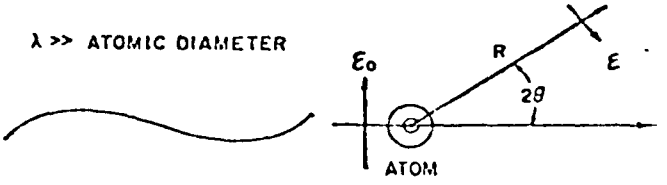

SINGLE ELECTRON SCATTERING AMPLITUDE × ATOMIC SCATTERING FACTOR

$$\mathcal{E}(\theta,\lambda) = -\left[\mathcal{E}_0\left(\frac{r_o}{R}\right)P(2\theta)\right](f_1(\lambda) + if_2(\lambda))$$

Figure 1

(74) Published in AIP Conference Proceedings No. 75, Low Energy X-Ray Diagnostics-1981, Monterey (American Institute of Physics, New York, 1981), pp. 85-96.

Low Energy X-Ray Spectroscopy with Crystals and Multilayers

B. L. Henke

University of Hawaii, Department of Physics and Astronomy, Honolulu, Hawaii 96822

ABSTRACT

The molecular and sputtered/evaporated multilayers and the acid phthalate crystals can be applied for relatively fast, high efficiency spectral analysis of constant and pulsed low energy x-ray sources in the 100 to 2000 eV region. Limits of resolution are about 1 eV. Reviewed here are the basic methods for the theoretical and the experimental characterization of these analyzers as required for absolute x-ray spectrometry. The design and absolute calibration of spectrographs for pulsed low energy x-ray source diagnostics are described.

I. INTRODUCTION--GRATING VS BRAGG SPECTROMETRY

Generally, the grazing incidence, diffraction grating spectrometry and the large angle Bragg diffraction spectrometry are complementary. Grating spectrographs can yield lower limits of resolution (<0.1 eV) but with relatively small aperture and low dispersion. The crystal/multilayer spectrographs are of higher limits of resolution (>0.5 eV) but with simpler and more flexible large angle geometry and with high dispersion. The crystal/multilayer spectrographs are of large aperture with an overall spectrographic speed that is considerably higher for constant source and somewhat higher for pulsed source spectroscopy. A precise intensity and window profile calibration of the crystal/multilayer instrument is more easily attainable. Having accurately characterized instrument window functions permits an effective resolution enhancement in the crystal/multilayer spectrometry by simple deconvolution procedures. The two spectrographic approaches are clearly complementary, and, ideally, both the grating and the crystal/multilayer spectrographs should be applied for an optimized analysis of many spectroscopic problems. (For a comprehensive review of grating spectrometry, see that by E. Källne in these Proceedings.)

Even with very intense excitation sources such as some synchrotron/storage ring and high temperature plasma sources, it may be that the crystal/multilayer spectrographs must still be used because the number of photons actually available for proper spectroscopic analysis is limited by other factors. The higher spectrographic speed may be required to achieve satisfactory statistics along with high temporal resolution in time-resolved spectroscopy. Primary monochromators may be required for needed selective excitation of spectroscopic samples which in turn may seriously limit the intensity available for high resolution spectroscopy. Finally, the spectroscopic sample may suffer appreciable radiation damage under the excitation dose that may be required for a given spectrographic measurement. An example of this type of problem is shown in Fig. 1. A low energy x-ray spectral analysis for the molecular orbital configuration of the crystalline solid sample of sodium perchlorate by a relatively fast, flat crystal spectrograph requires approximately three hours for one percent statistics. As shown here, with nine-minute scans through this period, the sample is steadily reduced through successive oxidation states with the last scan revealing the molecular orbital spectrum that is characteristic of NaCl. A successful analysis of this sample was possible [1,2] only by distributing the dosage over eight samples using selective excitation by photons of energy for which the photoionization process that is required has the highest cross section and using time resolved data collection which permitted an extrapolation to a "zero-dose" spectrum. Resolution enhancement was used to bring the energy resolution of this measurement to about 0.5 eV, using a lead myristate, molecular multilayer analyzer.

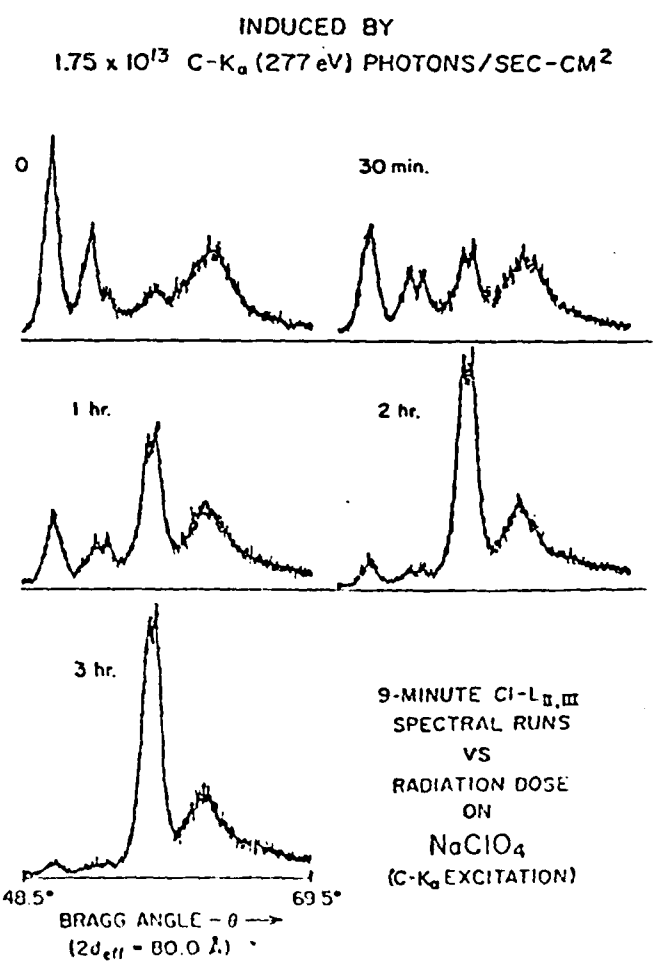

Figure 1

Published in AIP Conference Proceedings No. 75, Low Energy X-Ray Diagnostics-1981, Monterey (American Institute of Physics, New York, 1981), pp.340-388.

75

APPENDIX: THE ATOMIC SCATTERING FACTOR, $f_1 + if_2$, FOR 94 ELEMENTS AND FOR THE 100 TO 2000 eV PHOTON ENERGY REGION*

B. L. Henke, P. Lee, T. J. Tanaka,
R. L. Shimabukuro and B. K. Fujikawa

University of Hawaii
Department of Physics and Astronomy
Honolulu, Hawaii 96822

In a recent work,[1] a "state of the art" evaluation and fitting of the best available experimental and theoretical photoabsorption cross sections has been presented for the 30 to 10,000 eV region. Using the quantum dispersion relations, the atomic scattering factors were uniquely determined from the photoabsorption cross section data for the low-energy x-rays. In Ref. 1, the original data were given at fifty laboratory wavelengths along with compilation references and a description of the fitting procedures. Presented here are the f_1 and f_2 values which have been interpolated at regular intervals.

As discussed in the review papers of these Proceedings by Henke,[2,3] the f_1 and f_2 parameters may be applied to calculate the low-energy x-ray interactions--absorption, scattering, specular and Bragg reflection.

The corresponding value for the photoabsorption cross section is related to f_2 by $E\mu(E) = Kf_2$, where K for a given element is presented at the end of each f_1/f_2 table for a given element in keV-cm^2/gram units. For $E\mu(E)$ in eV-barns/atom units, K is equal to 6.987×10^7 for all atoms.

The tables are presented here at 125 values of photon energy, E(eV), and wavelength, λ(A), with logarithmically spaced intervals by truncating to the nearest electron volt the energy as given by

$$E = 100 \times 10^{(N \log 20)/124} \text{ eV}.$$

This expression may be used for convenient computer calculation and plotting of functions of f_1 and f_2 as indexed here by N. (f_1 and f_2 have been precisely interpolated for the truncated E values listed in these tables.) The approximate K, L and M absorption edge positions are identified within the tables.

For the shorter wavelengths and for the larger angles of scattering, the accuracy of these atomic scattering factors might be improved by the inclusion of two small correction terms for relativistics and charge distribution effects. Such corrections can become of relative importance when the magnitude of the scattering factor has been appreciably reduced by anomalous dispersion. As is discussed in Refs. 1 and 2, the modified scattering factor becomes simply $f = f_1 - \Delta f_r - \Delta f_e + if_2$, where the relativistic correction, Δf_r, is equal to $(5/3)|E_{tot}|/mc^2$, which has been tabulated by Cromer and Liberman[4] for Z = 3 to Z = 98; and the charge distribution correction, Δf_e, is equal to $(Z - f_0)$, where f_0 is the atomic form factor which recently has been tabulated as a function of $(\sin\theta/\lambda)$ by Hubbell and Overbo.[5] (Note: θ (Hubbell) = 2θ (Henke).) For $(\sin\theta/\lambda \leq .05$ A^{-1}, $f_0 = Z$, and for $(\sin\theta/\lambda) = 0.1$ A^{-1}, $f_0 \approx 0.9$ Z for most elements. An estimate of the value for the relativistic correction, Δf_r, may be given by[1,2]

$$\Delta f_r = \frac{5}{3}\frac{|E_{tot}|}{mc^2} = 2.19 \times 10^{-6}Z^3 + 1.03 \times 10^{-4}Z^2.$$

---

*The f_1/f_2 data as originally presented in the Monterey Conference Proceedings have been re-evaluated and some small improvements in the fittings have been included here in the photon energy region below about 300 eV for 26 elements as based, in part, upon newly acquired photoabsorption data.

[1] "Low Energy X-Ray Interaction Coefficients: Photoabsorption, Scattering and Reflection," B. L. Henke, P. Lee, T. J. Tanaka, R. L. Shimabukuro and B. K. Fujikawa, Atomic Data and Nuclear Data Tables 27 (1982).

[2] "Low Energy X-Ray Interactions: Photoionization, Scattering, Specular and Bragg Reflection," B. L. Henke, AIP Conference Proceedings No. 75, Low Energy X-Ray Diagnostics-1981, Monterey (American Institute of Physics, New York, 1981).

[3] "Low Energy X-Ray Spectroscopy with Crystals and Multilayers," B. L. Henke, AIP Conference Proceedings No. 75, Low Energy X-Ray Diagnostics-1981, Monterey (American Institute of Physics, New York, 1981).

[4] D. T. Cromer and D. Liberman, J. Chem. Phys. 53, 1891 (1970).

[5] J. H. Hubbell and I. Overbo, J. Phys. Chem. Ref. Data 8, 69 (1979).

This program is supported by a grant from the U.S. Air Force Office of Scientific

Volume 37, number 3 OPTICS COMMUNICATIONS 1 May 1981

X-RAY DIFFRACTION IN MULTILAYERS

Ping LEE *
University of Hawaii, Honolulu, Hawaii 96822, USA

Received 23 October 1980
Revised manuscript received 19 January 1981

Diffraction of X-rays in multilayer systems such as the molecular and the evaporated/sputtered multi-layers have been studied based upon the optics of thin films. General solutions for the intensity profiles of x-ray diffraction from multilayers of finite thickness have been obtained for angles of incidence outside the total reflection region. It is also shown that the optical expression for diffraction in the x-ray region by periodic systems agree with the conventional crystal diffraction theories.

1. Introduction

Improved experimental techniques have generated considerable interest in the application of evaporated [1] and sputtered [2] multilayers (ESM) as analyzers and monochromators in the ultrasoft x-ray region (10–100 Å). Variable film thicknesses and materials enable ESM to operate in regions between acid phthalate crystals and the molecular multilayers such as the Langmuir-Blodgett systems.

For crystals, there are two principle theories which may be invoked to account for the intensities observed in x-ray diffraction studies. The kinematical theory assumes that there is no appreciable absorption or multiple reflection of radiation in the crystal medium and hence is valid only for extremely thin crystals. Dynamical theory, on the other hand, takes into account all wave interactions within the crystal, and must be used whenever diffraction by large perfect crystals is of interest. As a general rule, if the thickness of the diffraction region and the reflection per plane are sufficiently small that multiple interplay of beams is negligible, then the results predicted by the dynamical diffraction formulae (i.e., Darwin-Prins or Ewald models) approach those predicted by the kinematical formula [3–5].

* Permanent address: Los Alamos Scientific Laboratory, P.O. Box 1663, Los Alamos, New Mexico 87544.

The calculated intensities of x-ray diffraction from ESM have been based upon the optics of thin films. This approach is the summation of all the reflection and refraction fields of x-rays at the plane interface of two adjacent media of different index of refraction, n. Numerous authors have given expressions for the intensity ratio of the incident beam to the reflected beam of a finite number of films in terms of recursion formulae [6–8]. Recently the peak reflectivity for ESM with two films per period has been obtained in closed form [9].

It is the intention of this communication to extend the theory of x-ray diffraction by ESM and to unify the crystal x-ray diffraction theory with the theory of interference films. Sect. 2.1 considers the case of N periodic multilayers with two films per period. Expressions for the profile of the diffracted beam has been derived in closed form for all angles of incidence outside the total reflection region. Sect. 2.2 deals with the general case of s layers per period. Sect. 3 generalizes the formalism developed in the previous section to the case of x-ray diffraction by crystals. Diffraction formulae valid for arbitrary number of layers are given. The final sect. 4 gives a comparison for various N, of the calculated diffraction profiles for a few of the crystals and multilayers of current interest.

Considerable algebraic simplification in the x-ray region results from the refractive index, n, being nearly

ATOMIC DATA AND NUCLEAR DATA TABLES 27, 1-144 (1982)

77

LOW-ENERGY X-RAY INTERACTION COEFFICIENTS: PHOTOABSORPTION, SCATTERING, AND REFLECTION*

E = 100-2000 eV Z = 1-94

B. L. HENKE, P. LEE, T. J. TANAKA, R. L. SHIMABUKURO, and B. K. FUJIKAWA

Department of Physics and Astronomy
University of Hawaii
Honolulu, Hawaii 96822

The primary low-energy x-ray interactions within matter are photoabsorption and coherent scattering, which can be efficiently described for photon energies outside the threshold regions by using atomic scattering factors. These may be uniquely determined through quantum dispersion relations from photoabsorption data. With the available fittings of the photoabsorption cross sections and with a new compilation of such data for the region 30-300 eV, continuous sets of the photoabsorption cross sections from 30 to 10 000 eV have been determined for 94 elements. With these, for the region 100-2000 eV, atomic scattering factors which are independent of scattering angle and which include the relatively strong anomalous dispersion structures have been obtained. Methods are reviewed and currently important examples of the application of atomic scattering factors to the detailed characterization of selected x-ray mirror monochromators and of Bragg multilayer and crystal analyzers for low-energy x-ray analysis are presented.

* This program in Low Energy X-Ray Physics is supported by the U. S. Air Force Office of Scientific Research under AFOSR Grant 79-0027, and by the U. S. Department of Energy under Supplemental Contract DE-AS08-81DP40153.

0092-640X/82/01001-144$02.00/0

CONTENTS

I. INTRODUCTION 3

II. DEFINING THE ATOMIC SCATTERING FACTORS 6

III. SYNTHESIS OF EXTENDED PHOTOABSORPTION CROSS-SECTION DATA 6

IV. CALCULATION OF THE f_1-VALUES 8

V. APPLICATION OF THE ATOMIC SCATTERING FACTORS 8

A. Reflection by X-Ray Mirrors 8

B. Reflection by Sputtered or Evaporated Multilayers 9

C. Reflection by Molecular Multilayers and Crystals 12

VI. COMPARISON WITH REFLECTIVITY MEASUREMENTS 13

VII. APPENDIX: DERIVATION OF DISPERSION RELATIONS FOR THE ATOMIC SCATTERING FACTOR COMPONENTS f_1 AND f_2 14

VIII. ACKNOWLEDGMENTS 16

IX. REFERENCES 16

X. EXPLANATION OF TABLES 19

XI. LOW-ENERGY X-RAY INTERACTION COEFFICIENT TABLES

I. Photoabsorption Cross Section μ (E = 30–10 000 eV) and Atomic Scattering Factor $f_1 + if_2$ (E = 100–2000 eV). Z = 1–94 22

II. Specular Reflectivity for Be, Al_2O_3, Al, Fused Quartz, Ni, Cu, and Au Mirrors. E = 100–1740 eV; Grazing Incidence Angle = 10–785 milliradians 116

III. Bragg Reflection Characteristics of Sputtered or Evaporated Multilayers for 100 Double Layers of W and C with $2d$-Values of 40, 50, 70, 80, and 100 Å ... 124

IV. Unit-Cell Data for the Molecular Multilayers of the Lead Salts of Straight-Chain Fatty Acids and for the Acid Phthalate Crystals of NH_4, Na, K, Rb, and Tl Cations 129

V. Structure Factor $F_1 + iF_2$ of Layered Analyzers for Lead Laurate, Myristate, Stearate, Behenate, and Lignocerate Molecular Multilayers and for the Acid Phthalate Crystals of Table IV 130

VI. Bragg Reflection Characteristics for Molecular Multilayers and for Acid Phthalate Analyzers. For First-Order Reflection from 200 d-Spacings of Lead Laurate, Myristate, Stearate, Behenate, and Lignocerate and for Thick Analyzers of the Acid Phthalates of Table IV 131

XII. REFERENCES FOR PHOTOABSORPTION DATA (FOR E < 300 eV) 141

Nuclear Instruments and Methods 207 (1983) 465–467
North-Holland Publishing Company

THE STABILITY OF CESIUM IODIDE X-RAY PHOTOCATHODES

K. PREMARATNE *, E.R. DIETZ and B.L. HENKE
University of Hawaii, Honolulu, Hawaii 96822, U.S.A.

Received 18 August 1982

For pulsed X-ray measurements as applied, for example, in high temperature plasma diagnostics, it has been established that the cesium iodide photocathode is very efficient for X-ray diode and streak camera applications. Its quantum yield (electrons/incident photon) is ten to one-hundred times higher than that for the gold photocathode in the 100–10000 eV region. The width of its secondary electron energy distribution is appreciably less than that for gold, allowing time resolved, streak camera measurements to be extended into the picosecond region. In this note an experimental study is described which demonstrates that the cesium iodide photocathode quantum yield and secondary electron energy distribution can be stable under practical conditions of preparation, handling, storage and short period exposures to the atmosphere.

1. Introduction

Quantitative measurements of X-ray emissions, as for high temperature plasma diagnostics, require accurately calibrated, often time-resolved spectroscopy. The sensitivity and reproducibility of X-ray detectors such as X-ray streak cameras and X-ray diodes depend primarily upon the X-ray photoemission characteristics of the photocathode material which is used for the conversion of incident X-ray photons to photoelectrons. Our recent investigations [1–4] and those of other investigators [5–9] have shown that cesium iodide can be a very practical photocathode material with important advantages as compared with those of the conventional photocathodes, gold and aluminum [10], because of its high quantum efficiency and its relatively narrow secondary energy distribution. We have also found that under-practical preparation conditions (10^{-6} Torr, LN-trapped vacuum evaporation), the reproducibility of the photocathode quantum yields and secondary electron distributions (batch to batch) is well within a few percent. This note describes an investigation of the *stability* of the cesium iodide photocathode under practical working conditions. For comparison, the stability of the gold photocathode has also been studied under similar working conditions.

2. The experiment

The photocathode samples were vacuum evaporated onto 1000 Å thick chromium substrates which were vacuum deposited upon microscope slides. The evaporation source was a tungsten boat with a perforated lid, placed 12 cm from the substrates. As previously determined [3] to be optimum for low-energy X-ray photocathodes, the thickness of the cesium iodide samples was chosen to be 2000 Å (measured by multiple-beam interferometry). Its purity was 99.99%. Gold samples were vacuum deposited to about 700 Å thickness using a tungsten spiral basket for the evaporation source. All samples were handled in a dry nitrogen atmosphere during transfer and storage. At the completion of evaporations, the samples were divided into four groups with two cesium iodide samples and two gold samples in each. One (group 1) was immediately placed in an instrument for absolute quantum yield measurement [3], and another (group 2) into a hemispherical analyzer electron spectrograph [1,3,10] for the secondary electron energy distribution measurements. The remaining two (groups 3 and 4) were stored in dry nitrogen and in argon, respectively. Total quantum yields of the samples were measured daily for thirty days. The pressure in the sample chamber was 10^{-7} Torr. The yield and secondary electron distribution measurements were made with Mg K_α (1254 eV) photon excitation. Shown in fig. 1 is a plot of the total quantum yield-vs-age for cesium iodide and gold samples which indicates that for both photocathodes the variation in quantum yield over thirty days in vacuum was not more than 2%.

At the completion of the quantum yield measurements as taken over the thirty-day period, the samples stored in dry nitrogen (group 3) and argon (group 4) were measured along with group 1 samples for a direct comparison of their quantum yields. Variations in the yield values among all of three groups were within 3% as shown in fig. 2.

* Present address: Department of Physics, University of Sri Lanka, Peradeniya Campus, Peradeniya, Sri Lanka

0167-5087/83/0000-0000/$03.00

(79)

Pulsed plasma source spectrometry in the 80–8000-eV x-ray region

B. L. Henke, H. T. Yamada, and T. J. Tanaka

Department of Physics and Astronomy, University of Hawaii, Honolulu, Hawaii 96822

(Received 4 February 1983; accepted for publication 10 June 1983)

The general characteristics are compared for the plane, convex, and concave fixed crystal analyzers which may be applied to the spectrometry of concentrated, intense plasma sources of x radiation involved, for example, in fusion energy and x-ray laser research. The unique advantages of the elliptical analyzer for precise and absolute spectral measurements are noted and detailed descriptions of its geometrical and physical optics are presented. With a source point at one of the foci of the elliptical analyzer profile, the spectrum is Bragg reflected ($45° < 2\theta < 135°$) at normal incidence upon a detection circle with its center at the second focal point, at which an effective scatter aperture and filter window is located. A primary monochromator consisting of a cylindrical, grazing-incidence mirror is placed between the source and the analyzer to provide an efficient cutoff for high-order diffracted background radiation and to focus the divergent rays so as to obtain an adjustable spectral line length at the detection circle. Photographic film may be transported along the detection circle. Linear position-sensitive electronic detection arrays or a streak camera slit window may be placed along a chord of the detection circle. Calibration procedures for absolute line and continuum intensity measurement are described and examples of calibrating spectra are presented as measured with elliptical analyzers of LiF, PET, KAP, and molecular multilayers for the 80–8000-eV photon energy region. The instrumental effects that contribute to the spectral line shape as measured by the elliptical analyzer spectrograph are defined and a simple line-shape analysis procedure is presented for the determination of the line-broadening contributions of the source. The effects of an off-axis positioning of a source point and of an extended source are analyzed and the application of the elliptical analyzer spectrograph for one- and two-dimensional imaging or an extended source at a given photon energy is discussed. Finally, methods and materials for the construction of the elliptical analyzers are described.

PACS numbers: 52.25.Ps, 52.70.Kz, 07.85. + n

INTRODUCTION

Through the last decade very intense and concentrated pulsed sources of x radiation have been developed. Notable among these have been the laser-produced plasma sources. In addition, improved versions of the discharge-type sources have become available, e.g., the Z-pinch, exploding wire, and imploding linear sources. These are being applied in high-temperature plasma physics research generally, in the spectroscopy of highly ionized atomic species, in fusion energy and x-ray laser research, and in the development of x-ray microscopy and lithography.

For the characterization and application of these new sources there has arisen an important need for precise and absolute pulsed x-ray source spectrometry for both large and narrow spectral range measurement.[1,2] To meet this need, a fixed elliptical analyzer spectrograph has been developed for the 100–10 000-eV photon energy region. Described here are its basic characteristics and design, its calibration, and its application.

In Sec. I a comparison is presented of pulsed source spectroscopy with plane, convex, and concave (elliptical) fixed analyzers. In Sec. II the geometrical optics for elliptical analyzer spectroscopy is presented. In Sec. III the determination, theoretically and experimentally, of the transmission characteristics of the elliptical analyzer spectrograph is described. Spectral line-shape functions are presented in Sec. IV. And, finally, discussed in Sec. V, are the effects of off-axis source points relative to alignment procedures for point sources and to one- and two-dimensional imaging for extended sources. In Appendix A methods for constructing the elliptically curved analyzers are discussed. In Appendix B a FORTRAN program is presented for resolution enhancement and line-shape analysis.

I. THE FIXED CRYSTAL ANALYZERS

The spectrum that is projected by the fixed crystal analyzers may be characterized geometrically by three basic parameters: (1) the angle χ of a ray from a point source that is reflected by a differential section of the diffracting analyzer; (2) the associated Bragg angle θ made at the point of incidence upon the analyzer, and (3) the angle β which is measured from a line through the *crossover point* of the differential bundle of rays as defined by the small variations $\Delta\chi$ and $\Delta\theta$. The relationship between the variables χ, θ, and β is illustrated in Fig. 1 and given by

$$\chi = 2\theta - \beta,$$

from which

$$d\chi/d\theta = 2 - d\beta/d\theta. \tag{1}$$

The angle β is intended here to measure effectively a position in the spectrum in the detection space. Because often one can choose a fixed crystal geometry for which the crossover positions are the same (or nearly so) for a relatively large spectral

 0034-6748/83/101311-20$01.30

Submitted for publication in
The Journal of the Optical Society of America

Low Energy X-Ray Response of Photographic Films:

Part I. Mathematical Models

B.L. Henke, S. L. Kwok, J. Y. Uejio,
H. T. Yamada and G. C. Young

University of Hawaii
Honolulu, Hawaii 96822

ABSTRACT

Relatively simple mathematical models are developed for optical density as a function of the x-ray intensity, its angle of incidence and photon energy in the 100-10,000 eV region for monolayer and emulsion types of photographic films. Semi-empirical relations have been applied to characterize a monolayer film, Kodak 101-07, and an emulsion type film, Kodak RAR 2497, which fit calibration data at nine photon energies well within typical experimental error.

(81)

Submitted for publication in
The Journal of the Optical Society of America

Low-Energy X-Ray Response of Photographic Films:

Part II. Experimental Characterization

B. L. Henke, F. G. Fujiwara, M. A. Tester

University of Hawaii
Honolulu, Hawaii 96822

C. H. Dittmore

Lawrence Livermore National Laboratory
Livermore, California 94550

M. A. Palmer

Sandia National Laboratory
Albuquerque, New Mexico 87185

ABSTRACT

Optical density vs exposure data have been obtained at nine photon energies in the 100-2000 eV x-ray region for five spectroscopic films (Kodak's 101-07, SB-392, RAR 2492, 2495 and 2497). These data were determined operationally by a direct comparison of the peak absolute intensities of spectral lines measured with a calibrated proportional counter and the microdensitometer tracings of the corresponding photographically recorded spectral lines. Film resolution limits were deduced from an analysis of contact microradiograms of linear zone plates constructed of gold bars. The relationship between the specular densities as measured here and the diffuse densities have been experimentally determined for the five films. Finally, experimental measurements of the optical density vs the angle of incidence of exposing radiation of constant intensity were obtained. These data, relating density to the x-ray intensity, its photon energy and angle of incidence are shown to be fit very satisfactorily in the 100-10,000 eV region by the semi-empirical mathematical model relations which have been derived in Part I of this work.

PHOTON COUNTING EFFICIENCY WITH HIGH AND LOW DENSITY CsI PHOTOCATHODES IN THE 100-10,000 eV REGION*

B. L. Henke, K. S. Tan and P. Y. Maeda

Department of Physics and Astronomy
University of Hawaii
Honolulu, Hawaii 96822

ABSTRACT

The low density CsI photocathodes have been optimized to yield relatively durable, stable and efficient systems for photon counting in the 100-10,000 eV x-ray region. Large area transmission photocathodes have been constructed which may be coupled to microchannel plate amplifiers for position-sensitive detection. The high density CsI is obtained by high vacuum evaporation. The low density, "fluffy" CsI is obtained by evaporation in 15-20 Torr of argon or nitrogen. For the low density CsI photocathodes, the photon counting efficiency is 60% at 100 eV and 20% at 6000 eV, and two to ten times higher than the efficiencies obtained with the high density CsI in the 100-10,000 eV region. The energy distributions of the photoemitted secondary electrons have been measured to be similar for the high and low density photocathodes and with about two eV full-width-at-half-maximum. The high efficiencies and relatively narrow emitted electron energy distributions have made the CsI transmission photocathodes particularly useful in x-ray streak camera applications. The electron generation statistics, such as the average number of electrons that are emitted per photon, have been determined by comparing the photon counting efficiencies to the corresponding absolute quantum yield values. For example, at 1254 eV, about 11 electrons per incident photon are emitted from a 2000 A, high density CsI transmission photocathode.

*This program is supported by the Air Force Office of Scientific Research under Grant No. 84-0001, and, in part, by a supplemental contract from the Department of Energy, No. DE-AS08-81DP40153.

(83)

X-Ray Diagnostics of Laser Plasmas with a Calibrated Elliptical Analyzer Spectrograph*

Tina J. Tanaka

Department of Physics and Astronomy
University of Hawaii
Honolulu, Hawaii 96822

ABSTRACT

An elliptical analyzer spectrograph was calibrated and applied to a laser produced plasma for the measurement of x-ray spectra from 100-2000 eV. Advantages of this particular spectrograph geometry include the focussing provided by the elliptical analyzer. A scatter aperture placed at a focal point of the ellipse serves to pass the reflected x-rays while blocking stray radiation. Another feature is normal incidence of the x-rays to the detector surface. Each component of the spectrograph was calibrated separately at characteristic line energies. These components include Langmuir-Blodgett multilayers and a potassium acid phthalate crystal bent into elliptical forms, flat fused quartz grazing incidence mirrors, thin film filters, and Kodak 2497 film. Each of these components except for the film were modeled using scattering factor tables by Henke et al. to estimate efficiencies for energies between calibration lines. Several models for calculation of Bragg reflection are presented for use with sputtered/evaporated multilayers which may be used in future spectrographs. The photographic sensitivity data was based on smooth curves fit through the calibration line data between the absorption edges. A Nd glass laser was used to produce plasmas from planar targets of aluminum, gold, teflon, boron carbide and nickel. The average laser intensity was $4.5 \pm 0.5 \times 10^{13}$ watts/cm^2 in a pulse length of 6.5ns. Other instruments used in the experiment included an x-ray photodiode array, a Si-PIN diode array, pinhole cameras, a de-Broglie KAP crystal spectrograph and a Thompson parabola ion analyzer. Absolute yields measured by the photodiode arrays were unfolded and compared to the results obtained with the elliptical analyzer over similar energy ranges. For energies about 300 eV, the integrated absolute yields were within a factor of 5 of each other while below 300 eV, the integrated yields were a factor of 1000 different. Line intensities of hydrogen-like and helium-like ions were used to calculate the temperatures of the B_4C, teflon and aluminum plasmas. These were calculated from local thermodynamic equilibrium and coronal models. For the aluminum plasma a temperature of 775 ± 50 eV was measured using the coronal model, while using the continuum slope from the photodiode arrays yielded temperatures of 400 ± 100 eV and 1000 ± 100 eV. These two temperatures were obtained over different photon energy ranges. Electron densities which were calculated using a coronal model were found to be $(5.5 \pm 0.6) \times 10^{16}$ electrons/cm^3 for the aluminum plasma.

A dissertation submitted to the graduate division of the University of Hawaii in partial fulfillment of the requirements for the degree of Doctor of Philisophy in Physics, May 1983.

A TWO-CHANNEL, ELLIPTICAL ANALYZER SPECTROGRAPH FOR ABSOLUTE, TIME-RESOLVING/TIME-INTEGRATING SPECTROMETRY OF ICF PLASMAS IN THE 100-10,000 eV REGION*

B. L. Henke and P. A. Jaanimagi

Department of Physics and Astronomy
University of Hawaii
Honolulu, Hawaii 96822

A new spectrograph system has been recently developed and calibrated for absolute spectrometry of ICF plasmas in the 100-10,000 eV region. This spectral region is analyzed with fixed elliptically curved crystals of LiF, PET and RAP, and with molecular multilayers of 2d-values in the 70-160 A range. Twin channels are utilized for simultaneous time-integrating photographic recording and for time-resolving, x-ray streak camera recording. Absolute calibrations of the elliptical analyzers, of the photographic film and of gold and low and high density CsI transmission photocathodes have been made using monoenergetic, DC laboratory x-ray sources. The instrument has been designed for mounting upon a 4-inch port of a two-meter diameter source chamber and includes an appendage, high-vacuum, sputter-ion pumping system. The final testing and application of this new spectrograph will be on the University of Rochester's LLE 24-beam Omega source.

---

*This program on Low-Energy X-Ray Physics and Technology is supported by AFOSR Grant 79-0027 and by DOE/NLUF Contract No. DE-AS08-82DP40175.

(85)

300-CHANNEL, LARGE APERTURE PICOSECOND X-RAY STREAK CAMERA*

P. A. Jaanimagi and B. L. Henke

Department of Physics and Astronomy
University of Hawaii
Honolulu, Hawaii 96822

We report on the design of a picosecond x-ray streak camera for laser plasma interaction studies in the 100 eV to 10 keV spectral range. The camera incorporates a 1 mm by 40 mm input slit and demagnified electron imaging, and can resolve 300 spatial resolution elements with a 10 ps time resolution. A numerical electron optics ray trace code has enabled optimization of the electrode geometry. Comparisons of Au, CsI and low density CsI for x-ray photocathode materials are also reported.

---

*This research is supported by DOE/NLUF Contract No. DE-AS08-82DP40175 and by AFOSR Grant 79-0027.

Presented at the 25th Annual Meeting of the Division of Plasma Physics, American Physical Society, Los Angeles, Session 5U, November 9, 1983.

NOTES ON THE MODIFICATIONS AND USAGE OF THE SLAC-UH ELECTRON TRAJECTORY PROGRAM, LENS

P. A. Jaanimagi

Department of Physics and Astronomy
University of Hawaii
Honolulu, Hawaii 96822

ABSTRACT

This report is to be used with SLAC Report No. 166 (September 1973), and additional notes by J. P. Knauer on the use of the LENS program at the University of Hawaii. The modifications to the LENS program can be categorized under three sections and are discussed. 1) In the spirit of saving computational time and space, sections of the FORTRAN source code were redone or "cleaned up." A few examples are given. 2) The quantitative accuracy of the program was questioned as problems were encountered with energy conservation for even simple electron trajectories through "smooth" electrostatic gradients and fields. 3) Some variables were added to allow more user control in the program's operation.

(87)

A NEW, HIGH SENSITIVITY, LOW-ENERGY X-RAY SPECTROGRAPHIC FACILITY

B.L. Henke

Department of Physics and Astronomy
University of Hawaii
Honolulu, Hawaii 96822

This report describes a "state of the art" focussing spectrograph with position sensitive detection for the low-energy x-ray region (100-1000 eV). It utilizes curved "crystal" analyzers as the molecular multilayers which have been developed in this laboratory and the new sputtered/evaporated multilayer analyzers which are now being evaluated by this project. The 2d spacings of these multilayers analyzers range from 30 to 160 A. A major effort of this long-standing program has been the development of precise and efficient spectroscopy for the low-energy x-ray region. This new focussing system will complement well the scanning flat crystal spectrometry and the fixed, elliptically curved crystal spectrometry that have been established under this program. The two established spectrographs have been developed for the absolute, low-energy measurements--the focussing system is aligned for studies for which maximum spectroscopic sensitivity is required (e.g., time resolved spectroscopic analyses of radiation damage).

Pulsed plasma source spectrometry in the 80–8000-eV x-ray region

B. L. Henke, H. T. Yamada, and T. J. Tanaka

Department of Physics and Astronomy, University of Hawaii, Honolulu, Hawaii 96822

(Received 4 February 1983; accepted for publication 10 June 1983)

The general characteristics are compared for the plane, convex, and concave fixed crystal analyzers which may be applied to the spectrometry of concentrated, intense plasma sources of x radiation involved, for example, in fusion energy and x-ray laser research. The unique advantages of the elliptical analyzer for precise and absolute spectral measurements are noted and detailed descriptions of its geometrical and physical optics are presented. With a source point at one of the foci of the elliptical analyzer profile, the spectrum is Bragg reflected ($45° < 2\theta < 135°$) at normal incidence upon a detection circle with its center at the second focal point, at which an effective scatter aperture and filter window is located. A primary monochromator consisting of a cylindrical, grazing-incidence mirror is placed between the source and the analyzer to provide an efficient cutoff for high-order diffracted background radiation and to focus the divergent rays so as to obtain an adjustable spectral line length at the detection circle. Photographic film may be transported along the detection circle. Linear position-sensitive electronic detection arrays or a streak camera slit window may be placed along a chord of the detection circle. Calibration procedures for absolute line and continuum intensity measurement are described and examples of calibrating spectra are presented as measured with elliptical analyzers of LiF, PET, KAP, and molecular multilayers for the 80–8000-eV photon energy region. The instrumental effects that contribute to the spectral line shape as measured by the elliptical analyzer spectrograph are defined and a simple line-shape analysis procedure is presented for the determination of the line-broadening contributions of the source. The effects of an off-axis positioning of a source point and of an extended source are analyzed and the application of the elliptical analyzer spectrograph for one- and two-dimensional imaging or an extended source at a given photon energy is discussed. Finally, methods and materials for the construction of the elliptical analyzers are described.

PACS numbers: 52.25.Ps, 52.70.Kz, 07.85 + n

INTRODUCTION

Through the last decade very intense and concentrated pulsed sources of x radiation have been developed. Notable among these have been the laser-produced plasma sources. In addition, improved versions of the discharge-type sources have become available, e.g., the Z-pinch, exploding wire, and imploding linear sources. These are being applied in high-temperature plasma physics research generally, in the spectroscopy of highly ionized atomic species, in fusion energy and x-ray laser research, and in the development of x-ray microscopy and lithography.

For the characterization and application of these new sources there has arisen an important need for precise and absolute pulsed x-ray source spectrometry for both large and narrow spectral range measurement.[1,2] To meet this need, a fixed elliptical analyzer spectrograph has been developed for the 100–10 000-eV photon energy region. Described here are its basic characteristics and design, its calibration, and its application.

In Sec. I a comparison is presented of pulsed source spectroscopy with plane, convex, and concave (elliptical) fixed analyzers. In Sec. II the geometrical optics for elliptical analyzer spectroscopy is presented. In Sec. III the determination, theoretically and experimentally, of the transmission characteristics of the elliptical analyzer spectrograph is described. Spectral line-shape functions are presented in Sec. IV. And, finally, discussed in Sec. V, are the effects of off-axis source points relative to alignment procedures for point sources and to one- and two-dimensional imaging for extended sources. In Appendix A methods for constructing the elliptically curved analyzers are discussed. In Appendix B a FORTRAN program is presented for resolution enhancement and line-shape analysis.

I. THE FIXED CRYSTAL ANALYZERS

The spectrum that is projected by the fixed crystal analyzers may be characterized geometrically by three basic parameters: (1) the angle γ of a ray from a point source that is reflected by a differential section of the diffracting analyzer; (2) the associated Bragg angle θ made at the point of incidence upon the analyzer, and (3) the angle β which is measured from a line through the *crossover point* of the differential bundle of rays as defined by the small variations $\Delta\gamma$ and $\Delta\theta$. The relationship between the variables γ, θ, and β is illustrated in Fig. 1 and given by

$$\gamma = 2\theta - \beta,$$

from which

$$d\gamma/d\theta = 2 - d\beta/d\theta. \tag{1}$$

The angle β is intended here to measure effectively a position in the spectrum in the detection space. Because often one can choose a fixed crystal geometry for which the crossover positions are the same (or nearly so) for a relatively large spectral

 0034-6748/83/101311-20$01.30

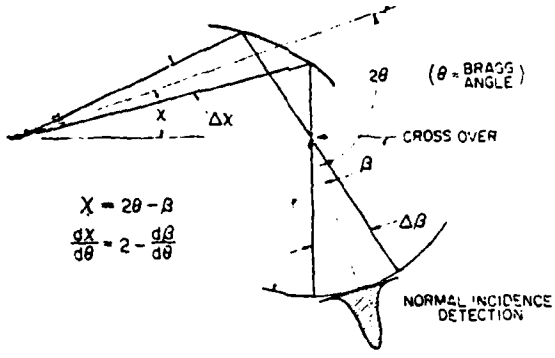

FIG. 1. Defining the basic geometrical parameters for fixed crystal analyzer spectroscopy: χ, the angle of the radiation from the source point in the plane of dispersion; and β, the angle of the Bragg reflected ray as measured from a line through the crossover (real or virtual).

range, a spectrum may then be established along a circular arc for normal-incidence detection with this crossover position as its center.

Using these variables, the general expressions that relate the measured spectral intensities to the spectral characteristics of the source may be readily established for a point source geometry. The reflection efficiency of the Bragg analyzer is defined by its reflectivity curve $I(\Delta\theta)$ and by the area under this reflectivity curve, the integrated reflectivity R. $I(\Delta\theta)$ is the fraction of the incident intensity that is reflected at a $\Delta\theta$ position from the Bragg diffraction peak position θ_0 for a given photon energy E ($\Delta\theta = \theta - \theta_0$).

In order to predict the number of photons per unit area-second at the detector, we need two length parameters, viz., L, the distance from the point source to the differential reflecting region at the analyzer added to that from the analyzer to the detection position, and r, the radial distance from the crossover position to the detection point.

Finally we shall assume here that the analyzer is of some small extension normal to the plane of Fig. 1 with its cross section invariant in all planes parallel to that of Fig. 1 (cylindrically curved). We may therefore effectively use an angle ψ subtended by this horizontal extension of the diffracting region as measured from the point source to define the differential solid angle from the source of the diffracted beam as $\psi\, d\chi$. And the length of the spectral "line" in the detection space is then essentially $L\psi$.

For a point source of sharply defined photon energy E and of intensity i_0 *photons/steradian-second*, the number of photons/sec, dN, diffracted at the Bragg angle θ within a differential $d\theta$ is simply given as

$$dN = i_0\psi(d\chi/d\theta)d\theta I(\theta - \theta_0).$$

And the total number of photons per second that is reflected within the measured spectral line becomes

$$N = i_0\psi \int_{-\infty}^{\infty} (d\chi/d\theta) I(\theta - \theta_0)d\theta$$
$$= i_0\psi\, \overline{(d\chi/d\theta)} R, \qquad (2)$$

where the integrated reflectivity R is equated to $\int_{-\infty}^{\infty} I(\theta - \theta_0)d\theta$. And for a continuum source, slowly varying with photon energy, of intensity at photon energy E equal to S_0 *photons/steradian-second-eV*, the photons per unit area-second measured for the continuum spectrum at the detector may be given by

$$\frac{dN}{dA} = \frac{S_0}{rL}\int_{-\infty}^{\infty}\left(\frac{d\chi}{d\theta}\right)\left(\frac{d\theta}{d\beta}\right)\left(\frac{dE}{d\theta}\right) I(\theta - \theta_0)d\theta$$
$$= \frac{S_0}{rL}\overline{\left(\frac{d\chi}{d\theta}\right)\left(\frac{d\theta}{d\beta}\right)\left(\frac{dE}{d\theta}\right)} R. \qquad (3)$$

Here we have equated the differential area dA of the diffracted beam at the detector to $(L\psi r\, d\beta)$. Because the reflectivity function $I(\theta - \theta_0)$ has effectively a nonzero value only when $(\theta - \theta_0)$ is near zero values, we have considered the quantities $d\chi/d\beta$, $d\beta/d\theta$, and $dE/d\theta$ to be essentially constants

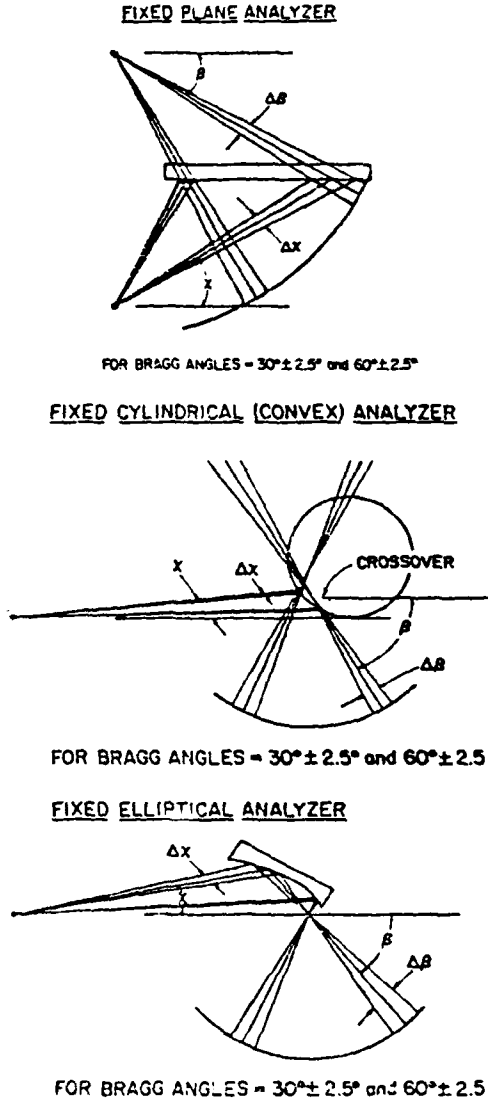

FIG. 2. Comparing, for the plane, convex, and elliptical fixed analyzers, the reflected ray systems for Bragg angles θ equal to $30° \pm 2.5°$ and for $60° \pm 2.5°$, illustrating the virtual or real crossover positions which may be applied as centers for normal-incidence detection circles. The source-to-analyzer distances at 45° Bragg angle are the same for the three analyzers. The radii of curvature for the convex and the elliptical analyzers for the 45° reflection are set to be equal. Here the computed ray traces are for a relatively small working distance to the source.

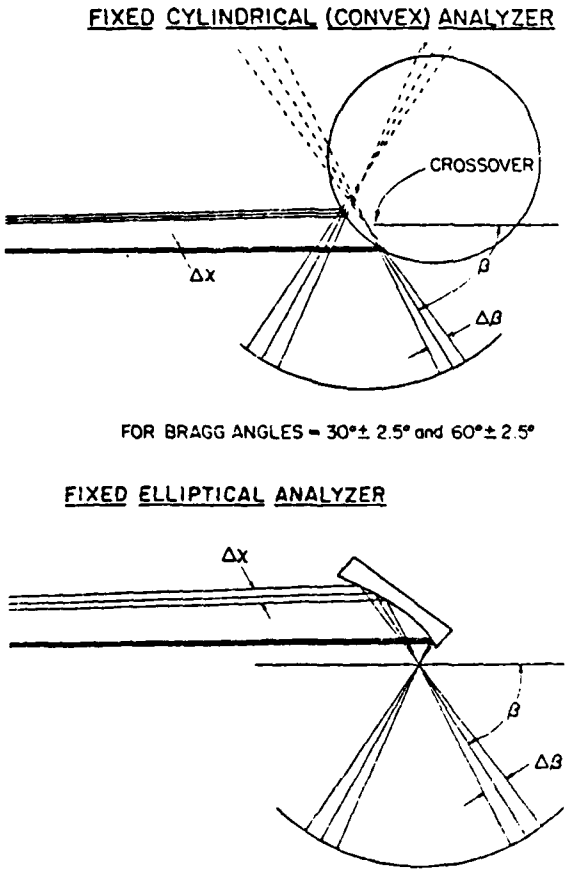

FIG. 3. Comparison of the reflected ray system for the convex and the elliptical fixed analyzers as described in Fig. 2, and for a relatively large working distance to the source. (The plane analyzer has a severely limited spectral range for large source distances.) Illustrated here is that the crossover center position is not fixed for the convex analyzer as it is for the elliptical analyzer.

and to be taken outside the integral as their values at θ_0, the Bragg angle for the given photon energy.

The curvature of the fixed analyzer determines the magnitude of the basic parameter, $d\chi/d\theta$, and, by Eq. (1), that of $d\beta/d\theta$. In Figs. 2 and 3 are presented computer-plotted ray traces for Bragg reflections at 30° and 60° (± 2.5°) for fixed analyzers of three types: (1) plane; (2) convex (circular cylinder); and (3) concave (elliptical cylinder). And in Table I are listed for these fixed analyzer geometries the analytical expressions for $d\chi/d\theta$ and for $d\chi/d\beta$ which determine the line and continuum measured intensities, respectively, according to Eqs. (2) and (3).

In these ray traces, the values for r and L have been chosen to be the same for the three analyzers at the 45° Bragg reflection. The radius of curvature for the elliptical analyzer was chosen to be equal to that of the convex analyzer for this intermediate 45° Bragg angle. Because the number of photons that are diffracted by the analyzers is proportional to $\Delta\chi$ for a given Bragg angular width $\Delta\theta$, it is clearly illustrated here that the plane analyzer has the highest angular aperture.[3,4] It is also immediately evident, however, that only for relatively small source distances, not very different from the length of the plane analyzer, can an appreciable spectral range be reflected with the plane analyzer. The convex and the concave analyzers will allow a large spectral range to be measured with crystals of practical dimensions and for large working distances to the source (as illustrated in Fig. 3).

An important advantage of the plane and the elliptical analyzers is that their crossover points are fixed for all Bragg reflections, thus allowing a *normal-incidence detection circle* to be established with positions in the measured spectrum precisely determined by the angle β. *The unique advantage of the elliptical analyzer is that its crossover is real rather than virtual as for the plane or the convex analyzer* as established at a focal point for the given elliptical geometry. With the elliptical analyzer, therefore, an effective scatter aperture can be located at this crossover position. This can be of considerable importance because then only the small diffracting region of the analyzer can be "seen" at the associated point on the detection circle, thus essentially eliminating the effect of the diffuse and/or fluorescent background radiation from the total illuminated surface of the analyzer.

Another general characteristic of fixed analyzer geometries is that a crossover point can be developed by allowing the analyzer (rather than to be cylindrically curved as described above) to have a second curvature as generated by rotating the analyzer section (as presented in Fig. 1) about an axis that passes through the source point and in the plane of Fig. 1. For example, if this axis is chosen as that which passes through the source and the detection point, all of the photons that were diffracted into a "line" region (as described above to be of dimensions $L\,dr\,d\beta$) will now be concentrated into a "point" crossover region of dimensions $r\,d\beta$. If the detector system can integrate the photon flux not along a spectral line region but only at a point (as within the slit window of a streak camera), this type of focusing could result

TABLE I. Comparison of photometric parameters.

Analyzer	$\lvert d\chi/d\theta\rvert$	$\lvert d\beta/d\theta\rvert$	$\lvert d\chi/d\beta\rvert$	Geometry
Plane	Unity	Unity	Unity	Spectral range limited
Convex				a—cylinder radius
$(a/s)\ll 1$	$(a/s)\sin\theta$	2	$\frac{1}{2}(a/s)\sin\theta$	s—source-to-cylinder axis
Elliptical				h, R_h as defined
$(h/R)\ll 1$	$(h/R_h)/\sin^2\theta$	2	$(h/R_h)/2\sin^2\theta$	in Eqs. (4) and (5)

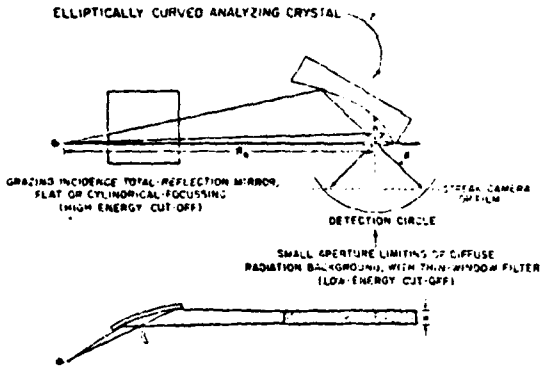

FIG. 4. Schematic of an elliptical analyzer spectrograph system. The source point is at one of the foci of the elliptical profile and the center of a *normal-incidence detection circle* is at the second focal point and is located within an effective scatter aperture. A filter may be placed over the scatter aperture to effect a transmission band and low-energy cutoff. A cylindrical, grazing-incidence mirror is used to establish a high-energy cutoff of high-order diffracted background radiation, and may be applied to focus the divergent beam from the source so as to adjust the length of the spectral line at the detector. Photographic film may be transported along the detection circle; a linear, position-sensitive electronic detection array or a streak camera slit may be located along a chord to the detection circle. For the linear detectors, the mirror may be focused to infinity, thereby placing a uniform, constant-length spectral line along a chord to the detection circle.

in a considerable gain in spectrographic efficiency or speed. It should be noted, however, that this second crossover point can be precisely generated only at the two intersection positions along a *normal-incidence* detection circle. This focal region can be somewhat extended when the axis of rotation of the analyzer surface passes tangentially to the detection circle, and therefore only for a relatively small region of the spectrum. For example, a very large aperture spectroscopy can be obtained for a small spectral range and at non-normal incidence on a linear detection region by using the *Hamos geometry*.[5,6] This is done by rotating the section for a plane analyzer shown in Fig. 2, about a horizontal line through the source which becomes the axis of a cylindrical section analyzer and the linear locus of focal crossover points corresponding to different Bragg angles. In the next section a simple method is described for achieving point focusing along the entire detection circle with the elliptical analyzer of single curvature.

II. THE GEOMETRICAL OPTICS OF THE ELLIPTICAL ANALYZER SYSTEM

For pulsed source spectrometry which can be simply and precisely calibrated, the elliptically curved fixed analyzer system has several important and unique advantages. As noted above, a real crossover point is established at one of the foci of the elliptical arc which becomes (1) a fixed center for a normal-incidence detection circle and (2) a position for an effective scatter aperture. In addition, (3) the magnitude of the parameters L and r [as defined above and for Eq. (3)] are essentially constant for this analyzer, and (4) because of the invariance of L, a cylindrical total-reflection mirror may be utilized, as shown in Fig. 4, to provide not only a very effective cutoff for high-order diffracted background radiation, but also to focus the spectrum at a second crossover for *all* positions along the detection circle.

For a precise and absolute calibration of the elliptical analyzer spectrographic system, characteristic x-ray lines from a laboratory point or line x-ray source may be used with a slit-window proportional counter scanned along a goniometer circle (inside a vacuum calibration chamber) that is coincident with this detection circle. For pulsed-source spectrometry, photographic film may be mounted along the detection circle. Alternatively, active, linear position-sensitive electronic detector arrays or a streak camera slit window may be located tangentially to the detection circle.

Specific examples of crystal and multilayer elliptical analyzers which have been successfully applied in this laboratory for the *80–8000-eV region* are presented in Table II.

We summarize here the geometrical relations for the elliptical analyzer which will allow the determination of the absolute transmission functions as may be defined by Eqs. (2) and (3). The elliptical arc of the analyzer may be described by the radial distance ρ from the focal point (at the scatter aperture) to the analyzer as measured back along the exit ray defined by the angle β (see Fig. 4), and given by

$$\rho = h/(1 - \epsilon \cos\beta). \tag{4}$$

Here h is chosen as a characteristic size parameter of the elliptical analyzer and is the distance ρ to the analyzer for $\beta = 90°$. The parameter ϵ is the eccentricity of the ellipse and may be given by

$$\epsilon = \sqrt{1 + (h/R_0)^2} - h/R_0, \tag{5}$$

TABLE II. Spectral ranges for selected elliptical analyzers.

Crystal	$2d$ (Å)	E (eV) 2θ 45°	E (eV) 2θ 90°	E (eV) 2θ 135°	λ (Å) 2θ 45°	λ (Å) 2θ 90°	λ (Å) 2θ 135°
LiF	4.027	8045	4354	3332	1.54	2.85	3.72
PET	8.742	3706	2006	1535	3.35	6.18	8.08
KAP	26.64	1216	658.2	503.7	10.19	18.84	24.61
Laurate	70	462.8	250.5	191.7	26.79	49.50	64.67
Stearate	100	324.0	175.3	134.2	38.27	70.71	92.39
Lignocerate	130	249.3	134.9	103.2	49.75	91.92	120.1
Melissate	160	202.5	109.6	83.9	61.23	113.1	147.8

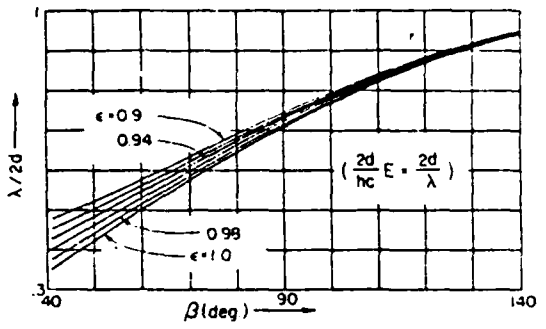

FIG. 5. Wavelength dispersion along the detection circle.

where R_0 is the working distance to the point source equal to the distance between the foci for the given ellipse.

We may relate the Bragg angle θ for the reflection at the analyzer to the spectrum angle β for this elliptical geometry, obtaining

$$\theta = \tan^{-1}\left(\frac{1-\epsilon\cos\beta}{\epsilon\sin\beta}\right),$$
$$\beta = \theta + \cos^{-1}\left(\frac{\cos\theta}{\epsilon}\right). \tag{6}$$

[Note: For very large R_0 and thus for nearly parallel, axial radiation into the analyzer, $\epsilon = 1$ and the arc becomes parabolic. Then Eq. (6) yields $\theta = \beta/2$.]

Neglecting here the small crystal refraction effects (see Sec. IV), the angle θ_0 is given through the Bragg equation in terms of the wavelength λ and the photon energy E by

$$m\lambda = 2d\sin\theta_0 = mhc/E, \tag{7}$$

where d is the spacing of the diffracting planes, m is the diffraction order number, and h and c are Planck's constant and the velocity of light, respectively ($hc = 12.398$ eV-Å). Using Eqs. (6) and (7), the wavelength and photon energy positions as functions of β along the detection circle may be obtained. These dispersion relations are plotted in Figs. 5 and 6. Here we have anticipated that an optimum working range for the spectrum angle β is 45° to 135° (e.g., to maximize dispersion and to minimize background by avoiding the smaller angles, and to satisfy typical spectrographic mechanical constraints for larger-angle diffractions). It is also straightforward to present the dispersion relations for linear detection arrays along a chord of the detection circle. As an example, these are plotted in Figs. 7 and 8 for a linear detection array or streak camera window which embraces the entire spectral range of $\beta = 45°$ to 135°.

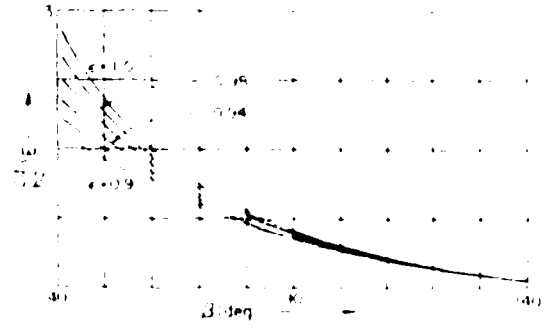

FIG. 6. Energy dispersion along the detection circle.

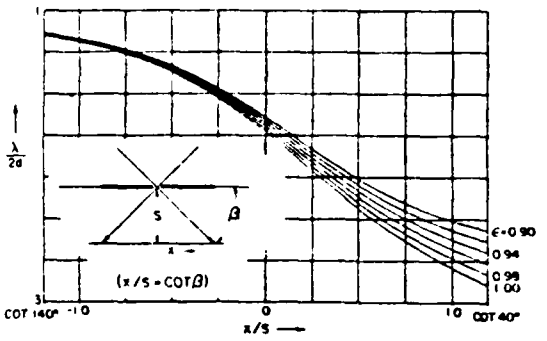

FIG. 7. Wavelength dispersion for a linear detector which embraces the full spectral range along a chord to the detection circle.

Differentiating Eq. (6), we obtain

$$\frac{d\beta}{d\theta} = \frac{\epsilon^2 + 1 - 2\epsilon\cos\beta}{\epsilon(\epsilon - \cos\beta)}. \tag{8}$$

With Eq. (1), we obtain

$$\frac{d\chi}{d\theta} = \frac{\epsilon^2 - 1}{\epsilon(\epsilon - \cos\beta)}$$

and

$$\frac{d\chi}{d\theta}\frac{d\theta}{d\beta} = \frac{d\chi}{d\beta} = \frac{\epsilon^2 - 1}{\epsilon^2 + 1 - 2\epsilon\cos\beta}. \tag{9}$$

Plots of $d\beta/d\theta$ and $d\chi/d\theta$ are presented in Figs. 9 and 10, respectively.

The pathlength for all rays from the source point as reflected to the focal point (exit aperture) is characteristically a constant for the elliptical reflector and equal to $\sqrt{h^2 + R_0^2} + h$. We may, therefore, write for the size parameter L for the total pathlength to the detection circle [applied in Eq. (3)]:

$$L = \sqrt{h^2 + R_0^2} + h + r, \tag{10}$$

where r is the radius of the detection circle.

Finally, the quantity $dE/d\theta$, which also appears in the transmission relation described in Eq. (3), may be obtained through differentiating Eq. (7) to be

$$\frac{dE}{d\theta} = -\frac{E}{\tan\theta}. \tag{11}$$

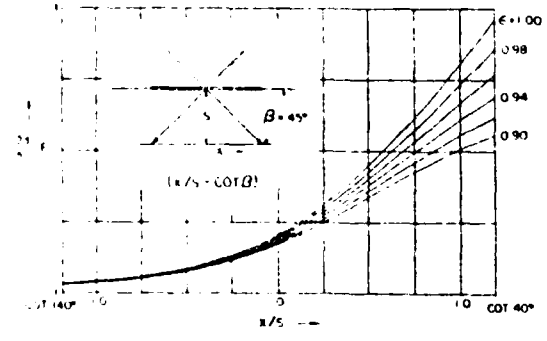

FIG. 8. Energy dispersion for a linear detector which embraces the full spectral range along a chord of the detection circle.

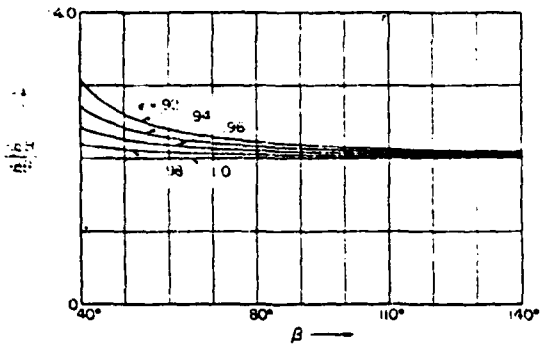

FIG. 9. Photometric parameter $d\beta/d\theta$ vs β for elliptical analyzers of eccentricity ε.

for which E and $\tan\theta$ can be readily computed as a function of β using Eqs. (6) and (7).

The high-energy cutoff characteristics of a primary monochromator with a mirror and transmission filter as combined with the elliptical analyzer are set by the grazing angle of incidence, ϕ, at the mirror (and by an appropriately chosen transmission band of the filter). The length of the spectral line at the detection circle, as suggested earlier, is determined by the divergence angle ψ and by the curvature of the mirror. A relatively long spectral line on a photographic film may be of advantage because an integration can then readily be accomplished with modern scanning microdensitometers over a larger number of exposed grains without saturation at higher photographic densities in film detection. An integration along a relatively long spectral line may also be important with two-dimensional position-sensitive electronic arrays in reducing the electron current to below saturation values required per channel or pixel. To accommodate a one-dimensional detection slit, as for a streak camera, a cylindrical mirror may be applied, as noted above, to place image points of a point source along the detection circle to which the slit would be tangent.

For the flat mirror, the length of the spectral line at the detection circle is $L\psi$. The radius of the mirror that is required for the plot imaging of the source at the detection circle is given by

$$r_c = \frac{2pq}{(p+q)\sin\phi} = \frac{2p(L-p)}{L\sin\phi}, \tag{12}$$

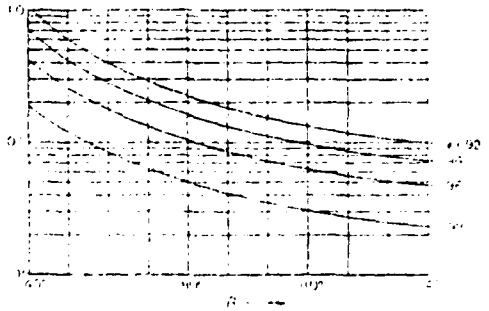

FIG. 10. Photometric parameter $d\chi/d\theta$ vs β for elliptical analyzers of eccentricity ε.

where p and q are the path distances from the mirror center to the source and detection circle, respectively.

For a shortened spectral line of length $\rho\psi$ with parallel radiation forming the spectral line along its length (at the detection circle), we let $q \to \infty$ in Eq. (12), and obtain for the required radius of the mirror

$$r_\infty = 2p/\sin\phi. \tag{13}$$

III. THE TRANSMISSION FUNCTIONS FOR THE ELLIPTICAL ANALYZER SPECTROGRAPH

As described above, the elliptical analyzer can be directly calibrated using a slit-window proportional counter measurement along a goniometer circle that is coincident with the detection circle and using laboratory line sources. If the source contains an isolated, characteristic emission of i_0 photons/steradian-second, it may be measured directly on the direct beam with an appropriate filter and pulse-height window of the proportional counter. The counter is then scanned through the β-angular region of the diffracted line in order to integrate for the total number of photons, N, that are diffracted within the spectral line for the given photon energy E. The ratio $N/i_0\psi$, thus measured at different source photon energies, may be defined as the line transmission function T_l.

Using the parameters that characterize the individual elements of the spectrographic system (the filter, the mirror, and the crystal or multilayer elliptical analyzer), it is of considerable value to predict, by calculation, the combined transmission functions. These can be useful (1) for optimizing the design of a particular measurement within a given spectral and intensity range, (2) for estimating the rejection ratio for high-order diffracted background radiation, and (3) to "fit" the experimental point measurements of the transmission function. Two examples are presented here of the calculation of a transmission function for measurements in the 100–200- and 550–1000-eV spectral channels.

Using Eq. (2), we may write for the line transmission function $N/i_0\psi$ for a spectrographic system

$$N/i_0\psi \equiv T_l = FMR\,(d\chi/d\theta), \tag{14}$$

where, at a particular photon energy E, $F(E)$ is the fraction of the radiation that is transmitted by a filter, $M(E)$ is the fraction of the incident radiation that is reflected by the mirror, and $R(E)$ is the integrated reflectivity that is characteristic of the crystal or multilayer. Methods for calculating these parameters have been reviewed recently in Refs. 2, 7, and 8.

For the spectral measurement in the 100–200-eV channel, a lead lignocerate multilayer of 200 d spacings has been chosen. Its reflection characteristics have been calculated and given in Ref. 8 and plotted here in Fig. 11. (This molecular multilayer has a high and monotonically varying reflectivity in this spectral range.) In Fig. 12 are plotted the transmission factors F for appropriate filter thicknesses of carbon foils, and M, the percent reflectivity for a gold mirror surface as set for reflection angle θ around 100 mrad. Also plotted here is the integrated reflectivity R and the characteristic parameter $d\chi/d\theta$ for the elliptical analyzer. The particular filter, mirror, and multilayer which have been chosen here

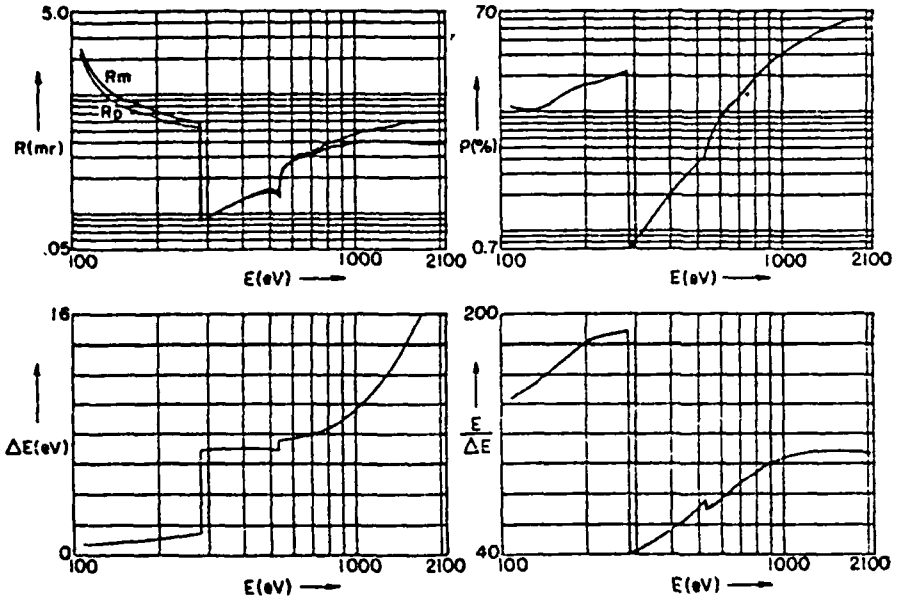

FIG. 11. Characterization of the molecular multilayer, lead lignocerate of 200 d spacings ($2d = 130$ Å). R, the integrated reflectivity; P, the percent peak reflectivity; ΔE, the energy width of the reflectivity curve; and $E/\Delta E$, the resolving power. These have been determined as described in Ref. 8.

have sharp cutoffs for photon energies beyond 280 eV for effective high-energy background rejection. In Fig. 13, the combined response function, as given in Eq. (14), has been plotted. Finally, in Fig. 14, a rejection ratio for second-order diffracted background radiation is plotted as defined by the ratio $N(E)/N(2E)$ for the total number of photons diffracted at first order to that at second order as measured at the same value of β for two monoenergetic sources of equal i_0 values and of photon energy E and $2E$, respectively. These ratios have been calculated for systems with and without the primary mirror (gold at 100 mrad) in order to indicate the appreciable gain in background rejection resulting from the use of the mirror element.

For spectroscopy in approximately the 500–1000-eV channel, we have chosen a potassium acid phthalate crystal which has relatively high reflectivity that is monotonically varying above about 550 eV (above the oxygen–K edge structure).[9] Its reflectivity characteristics have been calculated[8] and are plotted here in Fig. 15. An aluminum foil filter is used which has a transmission band for this spectral region with an absorption band beginning at the Al–K edge (1560 eV). A 30-mrad reflection from an aluminized glass mirror surface will have a high-energy cutoff also at about this energy.[2] (The oxide film on the aluminum mirror does not effectively change this reflectivity characteristic in this spectral region.) In Fig. 16 have been plotted the transmission factors $F(E)$, $M(E)$, and $R(E)$ and the geometrical parameter $d\chi/d\theta$. These are combined, by Eq. (14), to yield the spectrographic transmission function $N/i_0\psi$, which is plotted in Fig. 17. The high-order rejection ratio $N(E)/N(2E)$ for this channel, and as defined above, has been plotted in Fig. 18, illustrating the important improvement resulting from the mirror cutoff characteristic.

A transmission function can similarly be obtained for the ratio of the photons/microns^2-second, dN/dA, as measured at the detection circle to the photons/steradian-eV-second, S_0, from a point source of continuum radiation. By

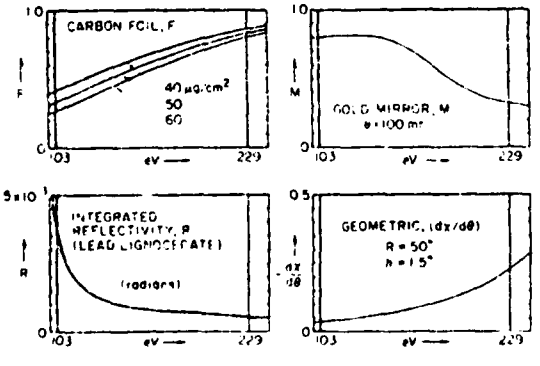

FIG. 12. Spectrographic transmission factors for the lignocerate channel, 103–229 eV. F, the filter transmission; M, the mirror reflectivity; R, the crystal analyzer integrated reflectivity efficiency; and $d\chi/d\theta$, the spectrographic aperture ratio.

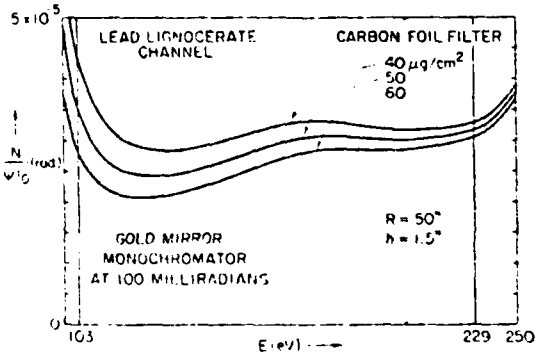

FIG. 13. Product of the transmission factors of Fig. 12, yielding the overall spectrographic response for the lead lignocerate channel [i.e., the line transmission function $(N/\psi i_0)$, as given in Eq. (14)].

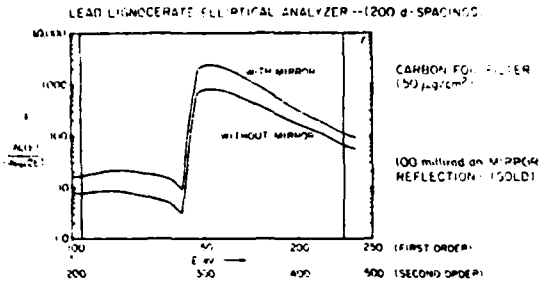

FIG. 14. First-order to second-order response ratio as calculated for the lead lignocerate channel. (This is the ratio of the line transmission functions, $N/\psi i_0$, at the same angle, β, for first- and second-order diffraction and for photon energies E and $2E$, respectively.) Illustrated here is the marked improvement of this rejection ratio effected by the primary mirror monochromator.

incorporating the factors M and F with Eq. (3), we may obtain

$$\frac{dN/dA}{S_0} = \frac{(dE/d\theta)[MF(d\chi/d\theta)R]}{rL(d\beta/d\theta)} = \left(\frac{dE/d\theta}{rL(d\beta/d\theta)}\right)\left(\frac{N}{i_0\psi}\right), \quad (15)$$

for which $N/i_0\psi$, $d\beta/d\theta$, and $dE/d\theta$ can be obtained from Eqs. (14), (8), and (11), respectively. Here we have given the *continuum transmission function* $(dN/dA)/S_0$ as proportional to the *line transmission function* $N/i_0\psi$, which, as discussed above, can be directly measured using laboratory characteristic line sources.

Examples of experimentally measured spectral lines for characteristic emissions from laboratory sources are shown in Figs. 19–23 using five elliptical analyzers that have been applied in this laboratory (crystals of *LiF*, PET, and *KAP*, and molecular multilayers, lead laurate, and lead melissate). As indicated in Table II, these can be applied for spectral analysis in the 80–8000-eV region. The characteristic lines that are shown here were for mid-range positions for each channel and, for each, an approximate value for the line transmission $N/i_0\psi$ is given [with $F = M = 1$ in Eq. (14)].

The procedure for measuring the transmission function $N/i_0\psi$ [and, therefore, $FMR(d\chi/d\theta)$ by Eq. (14)] is as follows:

In a vacuum calibration chamber, with a slit-window flow proportional counter translated along a goniometer circle that is coincident with the detection circle, a spectral line (isolated by a filter transmission band) is scanned at an angular rate of ω_0 radians per second in the β angle. The total number of counts that are collected while scanning over the line (or principal line series) is collected as N_x. A pulse-height "window" of the proportional counter is chosen to include only the counts for the characteristic line (or narrow group of lines). With the elliptical analyzer and scatter-slit assembly translated out of the direct beam and the counter in the position for $\beta = 0$, the number of counts per second on the direct beam from the filtered x-ray line source (of intensity i_0) is measured as I_x. I_x is related to photons per steradian-second, i_0, of the source by

$$I_x = i_0\psi\frac{t}{(R_0 + r)Q},$$

where t is the counter slit width and $R_0 + r$ is its distance to the x-ray tube slit. Q is the photon counting efficiency of the counter.

The total counts per second, N_x, that are collected as the line is scanned may be related as follows:

$$dN_x = Q\left(\frac{d^2n}{dt\,d\beta}\right)d\beta\left(\frac{\Delta\beta}{\omega_0}\right),$$

where the quantity $d^2n/dt\,d\beta$ is the photons/second-radian at the detection circle in the spectral line, and $\Delta\beta$ is the angular width of the counter acceptance and equal to t/r. (r is the

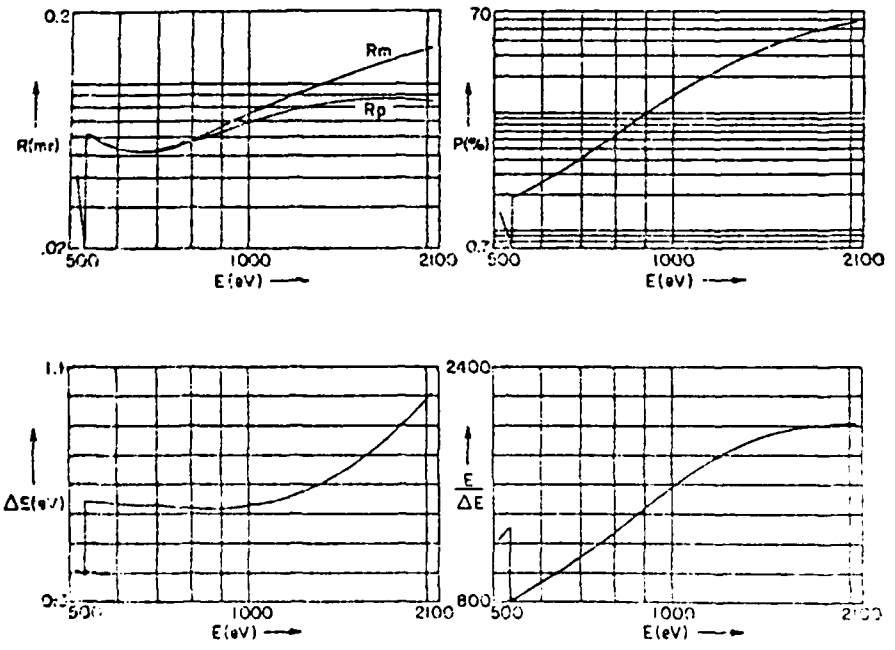

FIG. 15. Characterization of the potassium acid phthalate crystal analyzer, KAP ($2d = 26.63$ Å). As for Fig. 11.

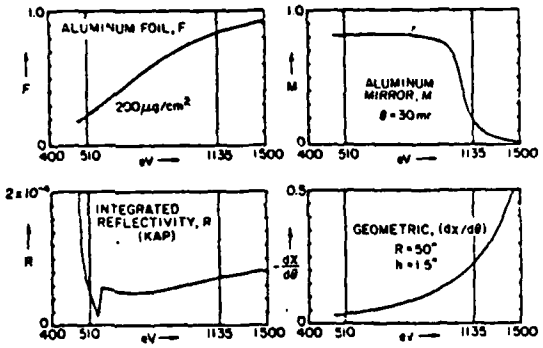

FIG. 16. Transmission factors for the KAP channel, 550–1000 eV. As for Fig. 12.

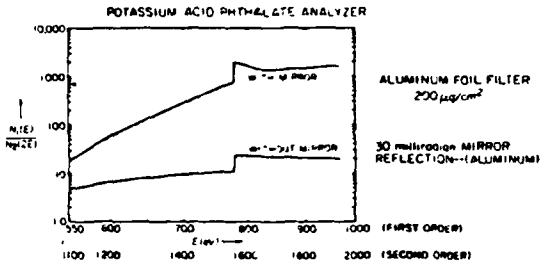

FIG. 18. First-order to second-order response ratio for the KAP channel. As for Fig. 14.

radius of the detection circle.) Integrating over the spectral line distribution in β, we obtain

$$N_x = \frac{Q(t/r)}{\omega_0}\left(\frac{dn}{dt}\right),$$

where dn/dt is the total number of photons/second within the spectral line distribution and defined as N in Eq. (2). And finally, combining these measurements, we obtain the transmission function $N/i_0\psi$, experimentally using the following relation:

$$\frac{N}{i_0\psi} = \frac{\omega_0 N_x}{I_x}\left(\frac{r}{R_0 + r}\right). \tag{16}$$

(Note: this relation is independent of the value of the optimized counter efficiency Q.)

IV. SPECTRAL LINE SHAPE WITH THE ELLIPTICAL ANALYZER SPECTROGRAPH

The natural emission linewidths for a point source are instrumentally broadened only by the effective reflectivity curve of the analyzer (the fractional intensity reflected as a function of the angle $\Delta\theta$ from the Bragg maximum).

If the spectral emission is sharply monoenergetic at photon energy E, and from a point source, the residual analyzer diffraction broadening may usually be well approximated by a Lorentzian for the low-energy x rays and given by

$$\frac{dN}{d\theta} = \frac{N(\omega/2\pi)}{(\theta - \theta_0)^2 + (\omega/2)^2} = \frac{T_l\, i_0\psi(\omega/2\pi)}{(\Delta\theta)^2 + (\omega/2)^2}. \tag{17}$$

The normalization of this expression is performed by setting the total area under the curve, $dN/d\theta$, equal to the total number per second, N, of photons of energy E that are allowed to diffract from the analyzer around the associated Bragg angle θ_0 [assuming a Lorentzian rocking curve $I(\Delta\theta)$]. And here N is equated to $T_l\, i_0\psi$, where T_l is the line transmission function $N/i_0\psi$ that may be measured and/or computed as discussed above. ω is the full width at half-maximum (FWHM) of the reflectivity curve which may be considered to be the perfect crystal width increased somewhat by the mosaic quality of the crystal (and usually must be verified experimentally).

Rewriting Eq. (17) in terms of the angle variable β that measures the spectral line position, we obtain

$$\frac{dN}{d\beta} = \left(\frac{d\beta}{d\theta}\right)\frac{(\omega/2\pi)T_l\, i_0\psi}{(\Delta\beta)^2 + (\phi/2)^2}. \tag{18}$$

In this expression, $\Delta\beta$ is the small angle that measures a position in the spectral line from the spectral line peak position at β_0 and is essentially equal to $\Delta\theta\,(d\beta/d\theta)$. ϕ is the measured angular FWHM, in β, and is equal to $\omega(d\beta/d\theta)$.

Finally, for the number of photons per micron^2-second, dN/dA, that is measured at the detection circle within a dif-

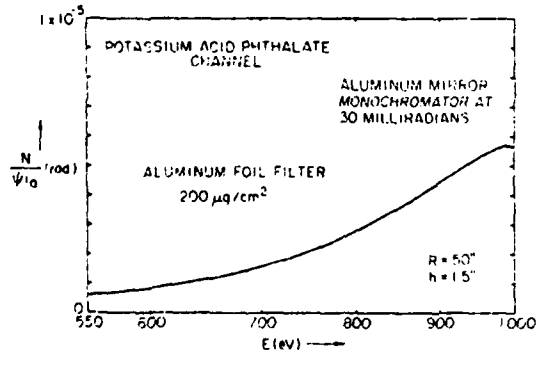

FIG. 17. Product of the transmission factors of Fig. 16, yielding the overall spectrographic response for the KAP channel [i.e., the line transmission function as given in Eq. (14)].

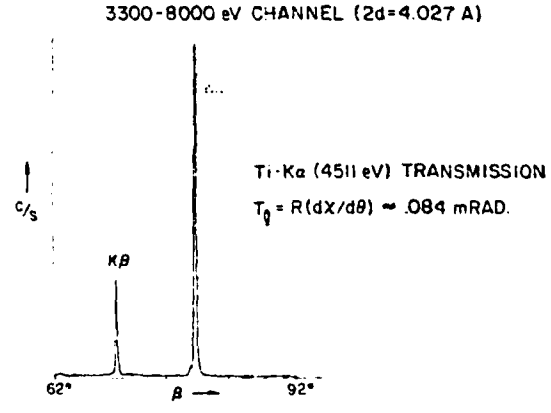

FIG. 19. Spectral measurement with the LiF elliptical analyzer—3300–8000-eV channel ($2d = 4.027$ Å). Calibrating x-ray source-and-proportional counter combined window is Gaussian of FWHM = 0.2° in β.

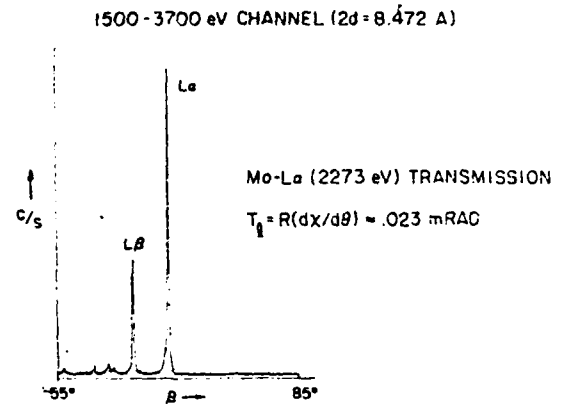

FIG. 20. Spectral measurement with the PET elliptical analyzer—1500–3700-eV channel ($2d = 8.742$ Å). Calibrating instrument window as for Fig. 19.

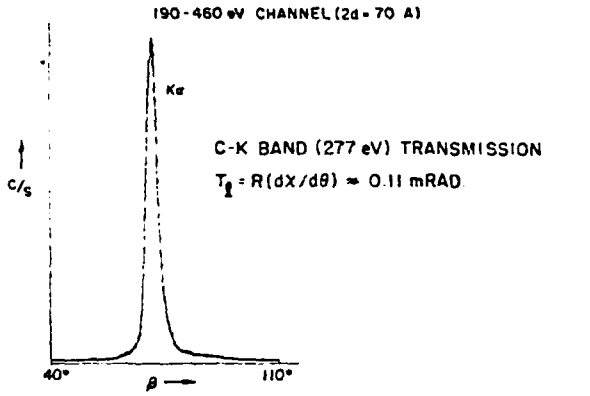

FIG. 22. Spectral measurement with the lead laurate elliptical analyzer—190–400-eV channel ($2d = 70$ Å). Calibrating instrument window as for Fig. 19.

ferential interval of angular width $d\beta$, we obtain from Eq. (18)

$$\frac{dN}{dA} = \left(\frac{d\beta/d\theta}{rL}\right)\frac{(\omega/2\pi)T_l\, i_0}{(\Delta\beta)^2 + (\phi/2)^2}. \tag{19}$$

Here we have let $dA = L\psi r\, d\beta$ as defined in Sec. I.

It should be noted that if the measured spectral line position β_0 is used for a precise determination of the photon energy with Eqs. (6) and (7), a small *crystal refraction correction* may be needed, particularly for the lower photon energies. This is accomplished by simply replacing the angle θ_0 corresponding to β_0, using Eq. (6), by the refraction-corrected peak position and equal to $[\theta_0 + \delta_0/\sin\theta_0 \cos\theta_0]$. Here δ_0 is the real part of the unit decrement of the refractive index of the crystal, and θ_0 is derived from the photon energy or wavelength through Eq. (7).

The crystal width ω may be determined by a calibrating measurement of an emission source of a known natural linewidth ϵ [in angle $\Delta\theta$ units given by Eq. (11)]. Because such calibrating lines can usually be described as Lorentzian in their shape, the result of the convolution of the emission line and a Lorentzian crystal reflectivity curve will be a spectral line that is also Lorentzian, of area equal to N (given by $T_l\, i_0\psi$, where i_0 is now the total number of photons/steradian-second from the given emission line source of finite energy width). This measured Lorentzian will have a FWHM equal to simply the sum of the widths, $\omega + \epsilon$. Therefore, from the measured width on a calibration line, ω may be determined if ϵ is known or is negligibly small (see, for example, Ref. 10).

Now, if an experimental emission line source can be assumed to have a Lorentzian distribution in ΔE [and therefore as ϵ_x in $\Delta\theta$, using Eq. (11)], we may apply the same argument as used above, simply replacing ω in Eq. (16) by $\omega + \epsilon_x$, where ϵ_x is the FWHM of the Lorentzian emission line. In this way, ϵ_x may be measured by the experimental spectral line shape.

If, alternatively, the emission line is well approximated as a Gaussian distribution in ΔE and, therefore, in $\Delta\theta$ (as resulting, for example, from Doppler broadening), the convolution of the Gaussian distribution with the crystal's assumed Lorentzian diffraction profile will yield a *Voigt* distri-

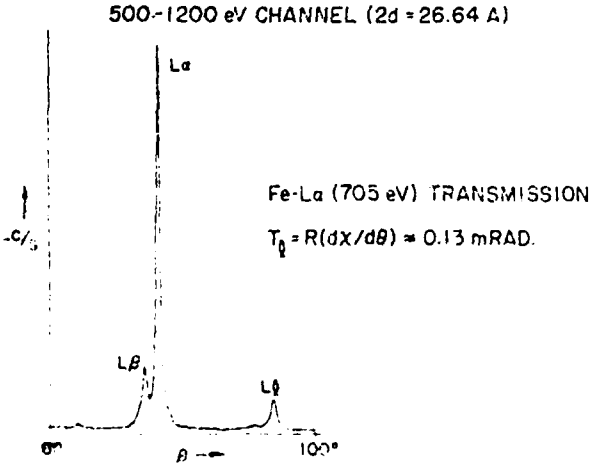

FIG. 21. Spectral measurement with the KAP elliptical analyzer—500–1200-eV channel ($2d = 26.64$ Å). Calibrating instrument window as for Fig. 19.

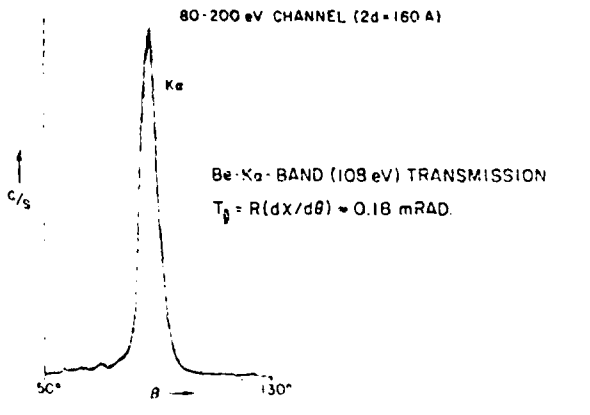

FIG. 23. Spectral measurement with the lead monostearate elliptical analyzer—80–200-eV channel ($2d = 160$ Å). Calibrating instrument window as for Fig. 19.

bution, again with an associated area equal to N.

Generally, an emission line shape, at least for the wings of the distribution, may be attributed to the combined effects of both Gaussian and Lorentzian broadening of the energy distribution of the source,[11] along with the instrumental diffraction broadening of the elliptical analyzer which is essentially Lorentzian for the low-energy x-ray region. The shape of the Voigt distribution (with unit peak intensity) may be given as a function of $\Delta\beta$ as measured from a peak position β_0 by the convolution integral

$$V(\alpha)=\int_{-\infty}^{\infty}\frac{\exp(-y^2)dy}{(\alpha-y)^2+a^2}\left(\int_{-\infty}^{\infty}\frac{\exp(-y^2)dy}{y^2+a^2}\right)^{-1}. \tag{20}$$

Here $\alpha=(\ln 2)^{1/2}(2\Delta\beta/g)$ and $a=(\ln 2)^{1/2}(l/g)$. Here g and l are given in terms of the FWHM, *in energy*, of a Gaussian-broadened component d (e.g., Doppler) and that of a Lorentzian-broadened component s (e.g., Stark) of the emission line source by the following relations:

$$g=d\left(\frac{d\theta}{dE}\right)\left(\frac{d\beta}{d\theta}\right) \tag{21}$$

and

$$l=s\left(\frac{d\theta}{dE}\right)\left(\frac{d\beta}{d\theta}\right)+\omega\left(\frac{d\beta}{d\theta}\right), \tag{22}$$

where, for a given emission line, $d\theta/dE$ and $d\beta/d\theta$ are evaluated at the Bragg peak position and given by Eqs. (11) and (8), and ω is the measured Lorentzian FWHM diffraction width of the analyzer.

By numerically integrating Eq. (19), we have shown that the FWHM, v, of this Voigt distribution can be related to the Gaussian and Lorentzian component FWHM, g and l, approximately by the following (see Ref. 10):

$$l\simeq v[1-(g/v)^2], \tag{23}$$

which yields

$$v\simeq\tfrac{1}{2}[l+(l^2+4g^2)^{1/2}]. \tag{24}$$

And in Ref. 10, we have shown that this integral Voigt function (of unit peak height) can usually be simply and accurately represented by a linear mix of the Gaussian and the Lorentzian by the analytical approximation

$$v(x)=\delta G(x)+(1-\delta)L(x), \tag{25}$$

where $G(x)=\exp[-(\ln 2)x^2]$ and $L(x)=(1+x^2)^{-1}$ in which the variable x is equal to $2\Delta\beta/v$, and v is the FWHM of the Voigt distribution.

From precise Voigt function tables we have taken Voigt distributions as characterized by given l/v and g/v ratios and least-square fit these, using Eq. (25), to determine corresponding (and a complete range) of δ values. Least-square fitting these data yields, within a very good approximation, the following relations for the FWHM component widths, l and g:

$$l=v(1-\delta^{1.036}) \text{ and } g=v\delta^{0.568}. \tag{26}$$

This mixing parameter, δ, varies from zero to unity as distribution ranges from a pure Lorentzian to a pure Gaussian.

We may, therefore, present a relation for the number dN of photons/second that are measured within a differential angular interval $d\beta$ as

$$dN/d\beta=P_0[\delta G(x)+(1-\delta)L(x)], \tag{27}$$

where P_0 is the central peak value of $dN/d\beta$ for the Voigt distribution. And if the area dA of the spectral line component of angular interval $d\beta$ as measured at the detection circle is $L\psi r\,d\beta$ (as defined earlier), we may write for the number of photons per second-micron^2 at the detection circle (at the photographic film or position-sensitive electronic detector)

$$dN/dA=(P_0/rL\psi)[\delta G(x)+(1-\delta)L(x)]. \tag{28}$$

If, for example, self-absorption within the emission source is significant, the central position of the spectral line may be depressed and then only the wings may be accurately fit to a Voigt distribution. Then P_0 must be interpreted to be the central maximum of a Voigt distribution as fit to the wings only of the measured line. Assuming no self-absorption effects, we may integrate Eq. (27) over the entire distribution to obtain the total number of photons per second within the spectral line, N, and to relate this number to the total number of photons per steradian-second, i_0, for the source using the spectrographic line transmission function T_l as defined earlier in Eq. (14):

$$N=\tfrac{1}{2}P_0v[\delta\sqrt{\pi/\ln 2}+(1-\delta)\pi]=T_l\,i_0\psi. \tag{29}$$

By fitting the Voigt portion of the measured spectral line, P_0, v, and δ can be determined. With v and δ the FWHM parameters g and l can then be obtained through Eqs. (23) and (26) and finally the energy widths d and s can be obtained using Eqs. (21) and (22). The source intensity i_0 for the given emission is determined using Eq. (29).

In order to test the assumptions and procedures outlined above for line profile analysis, the spectral line shape for the molybdenum–Mζ (192.6 eV) emission as reflected from a lead behenate molecular multilayer elliptical analyzer was measured and is illustrated in Fig. 24. A relatively simple least-squares fitting of the proportional counter step-scanned profile was applied to determine the best peak position β_0, the FWHM value for an assumed Voigt distribution, v, and a least-squares value for the mixing parameter δ. In Appendix B is presented a program for this fitting procedure. Using these values as described above, the Lorentzian and the Gaussian components, l and g, were determined. These fit parameters based upon the experimental data are presented in Fig. 24. The same parameters were predicted as follows: the energy FWHM of the emission line, 1.53 eV, and the crystal reflectivity curve FWHM, ω, equal to 3.54 mrad [as calculated for this analyzer of 200 layers ($2d=120$ Å)] were converted into equivalent widths in β angle, l_i and l_ω, to be equal to 0.695° and 0.491°, respectively. The predicted Lorentzian width l is the sum of these values and equal to 1.19°. Using the results of Sec. V, the image of the source slit at the detection circle was estimated to subtend an angle $\Delta\beta$, equal to 0.15°, and that subtended by the counter slit width was matched to be about the same value, 0.15°. The convolution of these effects was assumed to be well approximated as a Gaussian and of FWHM equal to 0.2°. (These slit widths were chosen so as to have negligible effect upon the characteristic line profiles used in our calibrations.) As can be noted

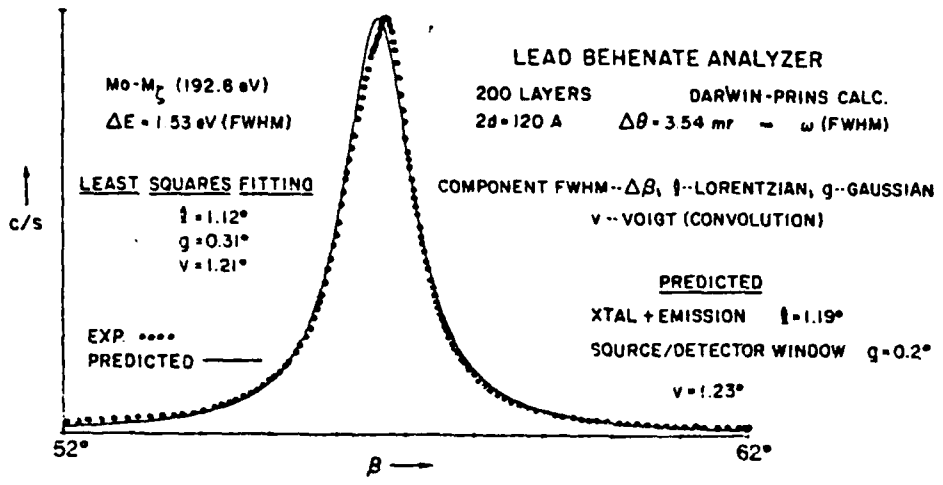

FIG. 24. Combining the measured energy width of the Mo–Mζ line with the energy width of the lead behenate analyzer (from Ref. 8) and using Eqs. (21) and (22), a predicted Lorentzian width l in the angle β is predicted to be 1.19°. The measured width, using the least-squares fitting procedure presented here, yields the value for l equal to 1.12°. Another example of this procedure for reducing a spectral line distribution to its Gaussian and Lorentzian components is given in Appendix B.

in Fig. 24, the agreement between the predicted and the measured Voigt line shape parameters is very satisfactory. This agreement is also illustrated in the fit of the predicted (smooth) curve to the experimental points.

As discussed in Ref. 10, this procedure for fitting the line shapes with Voigt distributions has been extended to the analysis of overlapping spectral lines by a straightforward, multiple parameter least-square fitting program.

V. THE EFFECT OF OFF-AXIS POINTS

Usually, for the purposes of alignment of the elliptical spectrograph, a laser beam may be focused at the proper target point position within the pulsed x-ray source chamber. The beam then proceeds through an opposite chamber port at which the spectrograph is mounted (and with sufficient divergence to fully illuminate its elliptical analyzer). For a preliminary alignment, the crystal analyzer may be replaced with a blank with the same contour as that of the mounted crystal analyzer, but with a mirror finish. A sharp line image of the point source will then be centered within the scatter aperture if the analyzer is aligned.

Typically the distance from the analyzer to this focal point is small as compared with the working distance of the analyzer to the source point so that a vertical shift in the source point will result in a strongly "demagnified" shift in the line image within the scatter aperture. In addition, the source image brightness changes very slowly with such an off-axis position. Initial alignment might be more sensitively accomplished by simply using a pair of "gun sights" precision fixed on the analyzer mount and with vertical and horizontal slits, respectively, at the entrances and with point photodiodes at the exits of these "sights." A "knife-edge" test may then be made by placing a sharp edge (or narrow slit) at the proper focal point position at the scatter aperture and by testing for uniform laser light illumination along the detection circle. (Correspondingly, a crystal mounting technique may be tested by directly aluminizing a crystal analyzer surface to render it mirror like).

The effects of an off-axis position of a monoenergetic x-ray point source is even more limited than those of the laser light source because the x-ray reflection must also satisfy the Bragg relation requirement and be at a constant angle θ. This is illustrated in the ray traces presented in Figs. 25–27 for a set of rays from source points subtending an angular range (measured from the second focal point) of $\pm$ 1°, and for constant-θ reflections at 22.5°, 45°, and 67.5°, respectively. The

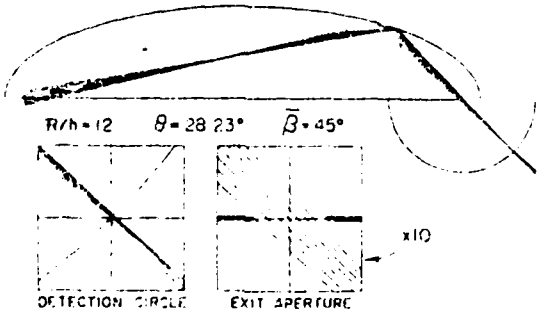

FIG. 25. Effect of off-axis source points. The rays from monochromatic source points within a two-degree range about the axis (as measured from the scatter aperture) are computer traced for a constant Bragg angle reflection from the elliptical analyzer. Illustrated here is the uniform spacing of these rays as they pass through the scatter aperture and intercept the detection circle (shown magnified ten times in the inserts). The crossovers that are generated by the constant Bragg angle reflections correspond to the Johann focusing points characteristic of the average radius of curvature of the analyzer at the point of reflection. Shown here is the ray system with a central ray reflection for β equal to 45°.

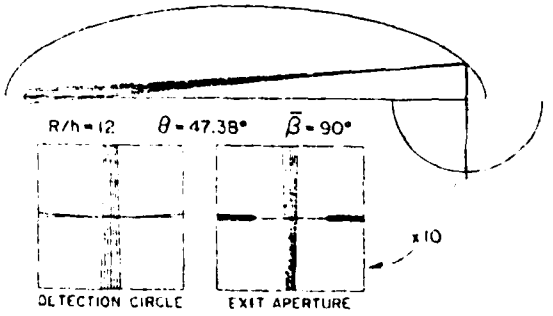

FIG. 26. Effect of off-axis source points for β equal to 90°. As for Fig. 25.

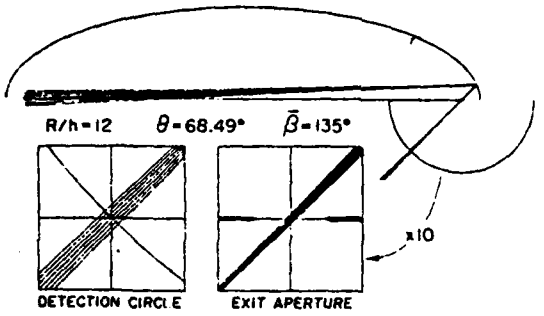

FIG. 27. Effect of off-axis source points for β equal to 135°. As for Fig. 25.

ray systems generate crossover points that correspond to the *Johann focusing geometry* for the average radius of curvature of the elliptical arc in the allowed reflection region. As illustrated here, if the spectral line is measured at the crossover position below the scatter aperture, then its position is fixed and is essentially independent of the source point position. This effect can be very useful for spectral line measurements on sources which are not constant in their position. The locus of these crossover points is easily determined and is not circular as is illustrated in Fig. 28.

As is illustrated here (and schematically in Fig. 29), source points at vertical positions y are uniformly "mapped" to corresponding image points at z within the scatter aperture and at ΔS along the detection circle at positions above and below the Johann crossover points. Again, as noted above for the usual spectrographic geometry with relatively large working distances to the source ($R_0/h \gg 1$), the shift in the reflected line for a monoenergetic x-ray point source as presented at the scatter aperture and along a detection circle is very small as compared with a vertical shift in the source point position. If, however, the detection arc is located farther away from this Johann crossover, a spectral line shift is larger and the effect can be used to obtain one-dimensional imaging of an extended source in the y direction. The constancy of the magnification with source position is illustrated in the plots of ΔS vs source point position y, presented in

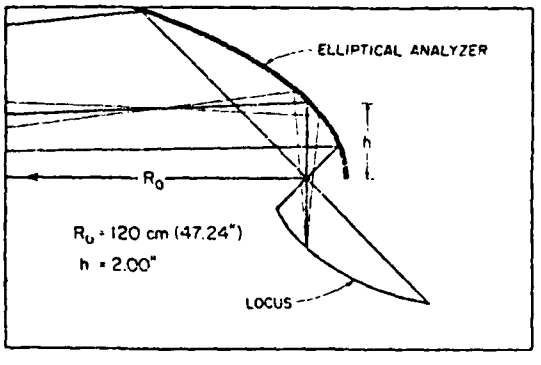

FIG. 28. Locus of the Johann focusing points in detection space. If a spectral line is measured with a detector along this locus, the line position, intensity, and shape are essentially constant, independent of a shift in the position of the source point. (The distances of these Johann crossovers along the central ray to the analyzer are equal and given by $r \sin\theta$, where r is the radius of curvature of the analyzer for the Bragg reflection angle θ.)

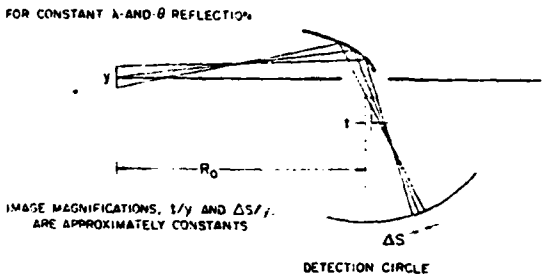

FIG. 29. y-dimensional imaging of a monochromatic source point in the dispersion plane. Defining the object position y and its image position ΔS from the central ray. (y and ΔS are easily related, using the Johann focusing point geometry.)

Fig. 30. In addition, except for the smaller β angles, the value of $d\chi/d\theta$ which determines the spectral line or image brightness is slowly varying with source point position as is illustrated in Fig. 31.

A one-dimensional imaging along the length of the spectral line for source points along the x direction (normal to the plane of dispersion) can be obtained by establishing an effective vertical slit between the source and the analyzer. This projection geometry is shown in Fig. 32. The image magnification is essentially constant and given by

$$\frac{x'}{x} = \frac{L-s}{s} \approx \frac{L-d}{d}. \tag{30}$$

Here L, the pathlength from source to detection circle, is a constant characteristic of the elliptical focusing geometry and is given by Eq. (10).

This effect of a vertical slit may also be gained by placing a knife edge directly in front of an entrance, plane mirror that is used to obtain a total-reflection high-energy cutoff which has been described earlier. In addition, as discussed earlier, a larger aperture can be obtained by using a cylindrically curved mirror, rather than a plane mirror, which focuses points along the x direction to corresponding points along the x' direction with the same magnification, x'/x, as given in Eq. (30).

Finally, by locating a small effective slit aperture at the first Johann crossover, a two-dimensional image of an ex-

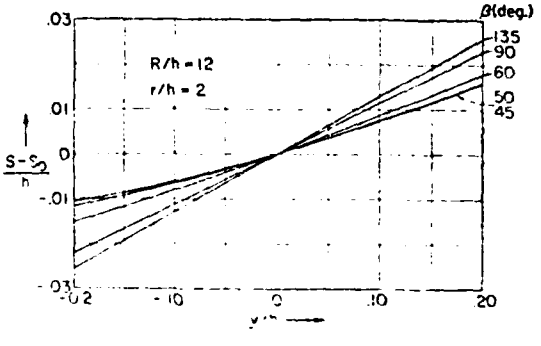

FIG. 30. Computed image position S as a function of the source position y (defined in Fig. 29) for different central ray angles β. Illustrated here is the essential constancy of the y-dimensional magnification for a given photon energy.

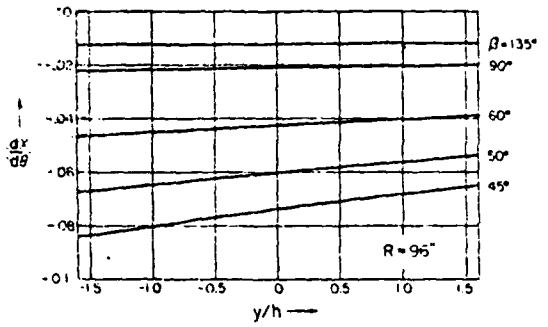

FIG. 31. The photometric parameter $d\chi/d\theta$ that determines the total brightness of the diffracted line is also relatively constant for a given photon energy as the source point position y varies.

tended source may be obtained for a selected photon energy. Such two-dimensional images can be presented at several positions along the detection circle for different photon energies by establishing several corresponding small apertures in front of the analyzer. This two-dimensional imaging is illustrated in Fig. 33.

VI. CONCLUSIONS

As based upon analyses and results which have been presented here, the authors conclude that the elliptical analyzer spectrograph can provide relatively simply and flexibly a precise and absolute spectrometry of concentrated, bright sources of pulsed x radiation in the photon energy region of 100–10 000 eV. Its unique geometrical advantages permit (1) measurement with minimum background, (2) effective use of primary monochromator mirrors for a high-energy cutoff and for complete adjustment of the spectral line length along the detection circle in order to accommodate a given detection mode, and (3) a one- or two-dimensional imaging of an extended source for a given photon energy.

A simple and direct experimental calibration procedure for the determination of the transmission functions of the elliptical analyzer spectrograph (for line and continuum measurement) has been demonstrated. These, along with the measured spectral line shapes, have been found to be in good agreement with the prediction of the geometric and physical optics for this spectrographic system.

A first application of the elliptical analyzer spectrograph for the 100–2000-eV region has been accomplished using planar targets at a 100-μ focal spot of a 20 J/6 ns pulsed laser source (1.06 μ) at the Sandia National Laboratory. A report is now in preparation by one of the authors (T.T.) and collaborators.[12] In Fig. 34 is shown an example of the results obtained with the Sandia source on an aluminum target. (The hydrogen- and helium-like principal lines use a KAP elliptical analyzer in second order–single shot.)

For precise, absolute spectrometry, well-calibrated detection is also required. In a companion paper,[13] we present absolute, operational calibrations of five photographic films that have been found to be effective particularly for 100–2000-eV spectroscopy (Eastman-Kodak 101, 2492, 2495, 2497, and SB392). An important advantage of photographic detection is its relatively large dynamic range (>1000). A photographic option is particularly useful for obtaining initial "survey" spectra and for determining the effective levels of the source intensities.

Work is now in progress on coupling streak camera detection to the elliptical spectrograph for time-resolved spectroscopy in the picosecond region for both wide and narrow spectral range diagnostics on the large laser-produced plasma sources of the Lawrence Livermore National Laboratory[14] and at the University of Rochester's Laboratory for Laser Energetics.[15] At this laboratory, a collaborative effort has also been initiated on the comparative evaluation and calibration of "state of the art" position-sensitive, self-scanning electronic detection systems as coupled to the elliptical analyzer spectrograph for the 100–10 000-eV region and for both pulse and photon counting detection modes.

Finally it should be noted that the elliptical analyzer spectrograph systems that have been described here can have some important advantages as applied to the very intense synchrotron x-ray continuum sources. Because the

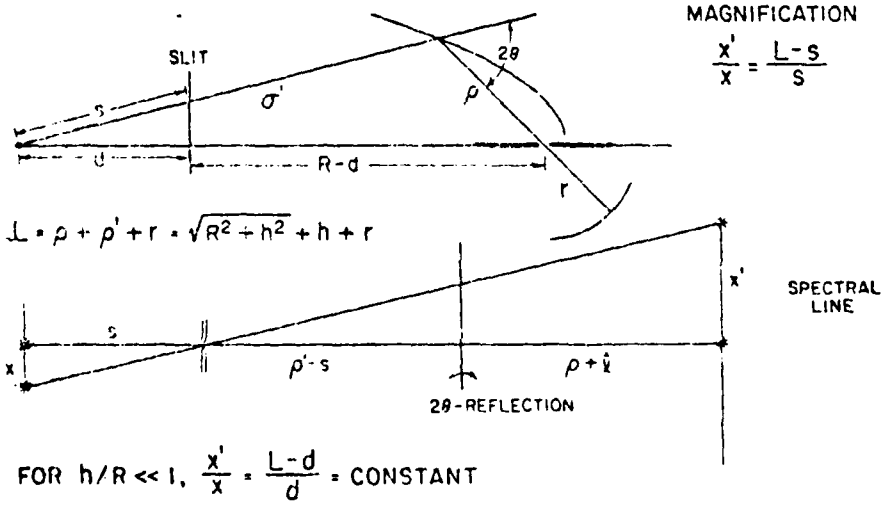

FIG. 32. x-dimensional imaging of a monochromatic source point in the plane normal to that of dispersion, effected by establishing a vertical slit (or a cylindrical focusing mirror) at position d from the source. For the typically large values of R_c/h, the magnification x'/x is essentially constant and equal to $(L-d)/d$, where L is the characteristic constant pathlength for the elliptical analyzer system.

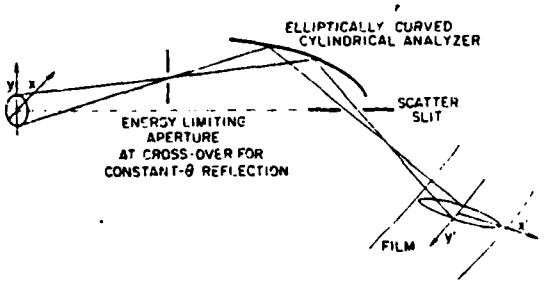

FIG. 33. x- and y-dimensional imaging of an extended source by placing a short, vertical slit at the first Johann crossover point corresponding to a given photon energy E and Bragg angle θ. By establishing several of these small slits in front of the analyzer, two-dimensional images for the several photon energies are formed along the detection circle.

grazing-incidence mirrors and certain crystals and multilayers (e.g., the sputtered/evaporated multilayers) can be used which are stable under the very high total intensity of the synchrotron radiation, these mirror-elliptical analyzer systems can be very effective *primary* monochromators with good high- and low-energy rejection and low background. In addition, when applied as high-resolution spectrographs, these systems can be used to present an absorption spectrum along the detection circle, utilizing the continuum x-radiation source and with the absorption sample over the scatter aperture. Important measurements on photoabsorption for condensed matter over a relatively large spectral range can thus be made and, in particular, those of the extended x-ray absorption fine structure (EXAFS) can be made simply and accurately on very small samples.

ACKNOWLEDGMENTS

This program is supported by the Air Force Office of Scientific Research under Grant No. 79-0027 and, in part, by the Department of Energy under Contract No. DE-AS08-81DP40153. The authors gratefully acknowledge the invaluable assistance in this work of Priscilla Piano and of Murray A. Tester, of many student assistants who have been involved in the development of the molecular multilayer systems, and of Gerald C. Young for his considerable help in the developing of the line-shape analysis computer program. Finally, we wish to thank Dr. Kenneth Glibert of the Sandia National Laboratory for his interest and help in initiating the first tests of an elliptical analyzer spectrograph on a pulsed plasma x-ray source.

APPENDIX A: CONSTRUCTION OF THE ELLIPTICAL ANALYZERS

As noted in Sec. I (e.g., Figs. 2 and 3), for fixed analyzer spectroscopy with relatively large spectral range coverage (as with the convex and the elliptical analyzers), a given spectral line is diffracted by only a narrow region of the crystal. Therefore, for precise, quantitative measurement on line intensities and shapes there is a strong requirement for accurate, smooth, and continuous profiling of these analyzers. Meeting this requirement is more easily accomplished with cylindrically bent crystals (rather than with the higher-strained double curvature systems) as have been the basis of the spectrographic design applied in this work. Presented here is a brief description of materials and mounting procedures that have been found to be useful for the construction of the elliptical analyzers.

A. Crystals for $E > 500$ eV

In Table A1 we have listed some practical crystal materials that have been successfully cleaved and bent to analyzer radii of curvature as small as one inch.[16] These have good stability and relatively high reflectivity[17,18] and have been

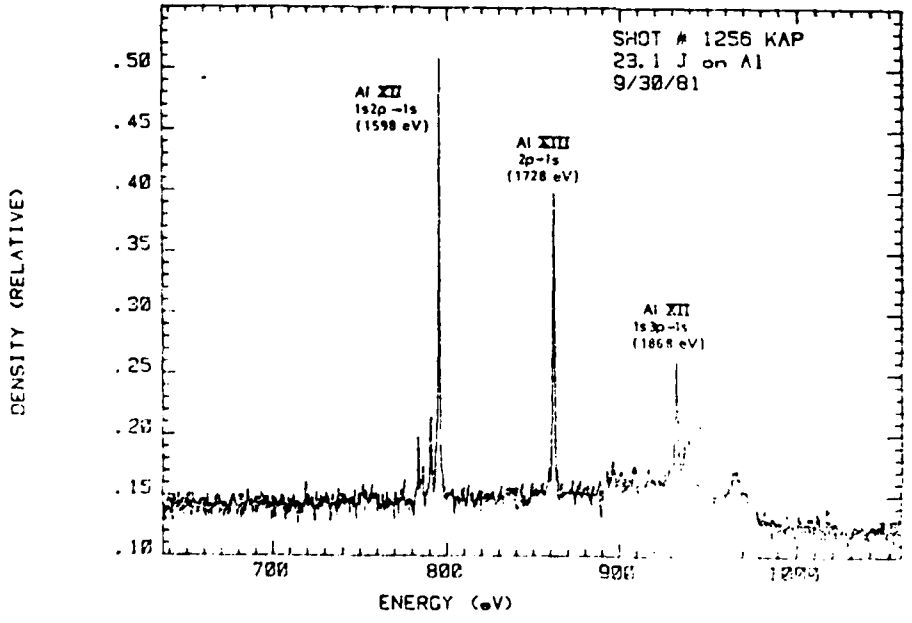

FIG. 34. Spectral measurement of a laser-produced plasma source with an elliptical analyzer spectrograph. The 20-J/6 ns (1.06-micron light) laser facility of the Sandia National Laboratory was used. The h and R_0 values of the analyzer were 1 and 12 in., respectively. The plasma source was produced at a 100-μ-diam focal spot on a planar aluminum target. A 1400-Å parylene/700-Å aluminum filter was used and without a primary, grazing-incidence mirror monochromator. Shown here is a microdensitometer plot of the spectrum as recorded on Eastman-Kodak 2497 film (along a 2.15-in.-radius detection circle) from a single-shot exposure. In this measurement are the principal lines of the helium- and hydrogen-like series of aluminum as diffracted in second order with a KAP analyzer.

TABLE A1. Some practical crystal systems for curved analyzer applications (2d values and approximate forming parameters).

Crystal	$hkl - 2d$ (Å)	P—plastic e—elastic	Thickness (mils)	Temperature (°C)	Bonding
LiF	220–2.848	P	8–20	700°	Epoxy
LiF	200–4.027	P	8–20	700°	Epoxy
PET	002–8.742	e/P	8–10	90°	Wax
EDDT	020–8.808	e/P	8–10	90°	Wax
ADP	101–10.64	P	8–15	90°	Wax
Mica (muscovite)	002–19.84	e	5–10	20°	Epoxy
RAP	$10\bar{1}0$–26.12	e	5–10	20°	Epoxy
KAP	$10\bar{1}0$–26.63	e	5–10	20°	Epoxy

typically applied in focusing x-ray emission analysis instrumentation.[19]

Crystals that are plastic, as LiF, can be preformed at the indicated elevated temperatures[20] over a convex curved surface of stainless steel or graphite that is a negative replica of the elliptical substrate. At room temperature the elastic crystal and preformed plastic crystal segments (of typical thicknesses as listed here) are pressed and held against the elliptically curved substrates which are coated with a thin layer of filtered, low-viscosity epoxy resin of a slow curing rate.[21] A small bench vise is used with a gentle pressure established through a silicon–rubber pad which is molded from the substrate blank surface. It has been found that crystals as PET and EDDT bend more easily at hot-plate temperatures and these are preformed against the substrate which is coated with melted wax, and then held until cooled to room temperature under the light pressure of the silicon–rubber pad.

The smaller thicknesses for the crystal analyzers in the range indicated in Table A1 are required when bending to radii as small as one inch. The crystal thicknesses should be chosen to be no smaller than is required for the particular bending radii of curvature because the quality of the analyzer is usually improved when using the thicker material.

High-quality, single crystals can be cleaved from blocks that are commercially available of about four inches in length as cut from boules of the synthetically grown material. (The natural crystal, mica, can also be obtained with excellent quality in this length.) For given values of R_0 and h

TABLE A2. Dependence of spectral range and beam dimensions upon h (for R_0 = 120 cm (47.24 in.) and for analyzer length = 4.0 in.).

h	β_1 (deg.)	(2d)E_1(A-eV)	β_2(deg)	(2d)E_2(A-eV)	a_1	a_2	Δa	r_1	r_2
1.0	41.3	3.28E+04	138.7	1.32E+04	2.50"	0.38"	2.12"	18.43"	1.21"
1.5	50.0	2.74E+04	130.0	1.36E+04	3.05"	0.71"	2.34"	16.13"	1.99"
2.0	56.4	2.45E+04	123.6	1.40E+04	3.55"	1.09"	2.46"	15.36"	2.87"
2.5	61.2	2.27E+04	118.8	1.43E+04	4.03"	1.50"	2.53"	15.27"	3.82"
3.0	64.9	2.15E+04	115.1	1.45E+04	4.51"	1.94"	2.57"	15.53"	4.81"
3.5	67.8	2.06E+04	112.2	1.47E+04	4.99"	2.40"	2.59"	15.99"	5.83"
4.0	70.2	1.99E+04	109.3	1.48E+04	5.47"	2.87"	2.60"	16.56"	6.87"

r_1 and r_2 are radii of curvature at β_1 and β_2

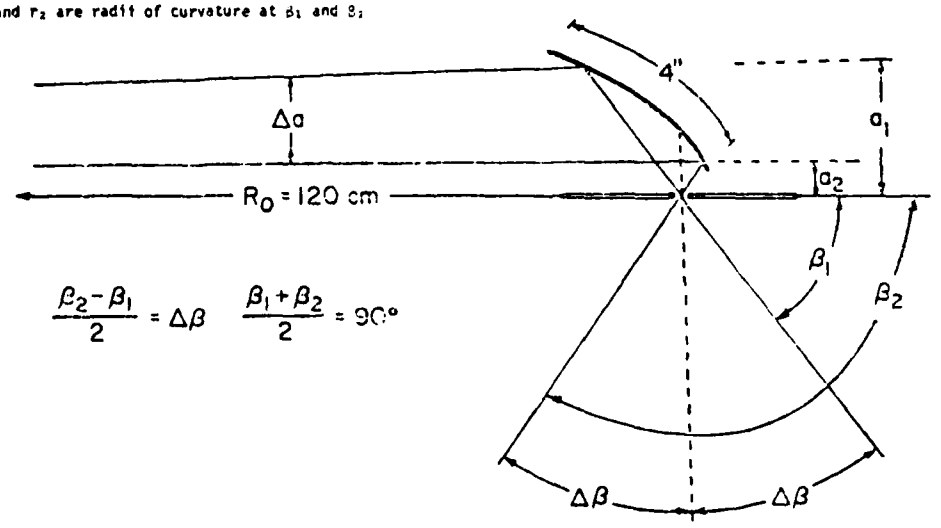

$$\frac{\beta_2 - \beta_1}{2} = \Delta\beta \qquad \frac{\beta_1 + \beta_2}{2} = 90°$$

TABLE A3. Profile parameters for 4-in. crystal analyzer [R_0 = 120 cm (47.24 in.)].

h	ϵ	x_0	y_0	x_1	y_1	x_2	y_2	m
1.0	0.9791	0.750	1.500	4.463	0.760	0.565	0.954	−0.8137
1.5	0.9688	0.750	2.000	4.488	0.641	0.589	1.090	−0.6894
2.0	0.9586	0.750	2.500	4.566	0.606	0.668	1.196	−0.6045
2.5	0.9485	0.750	3.000	4.685	0.615	0.786	1.284	−0.5429
3.0	0.9385	0.750	3.500	4.835	0.648	0.934	1.362	−0.4961
3.5	0.9287	0.750	4.000	5.006	0.695	1.103	1.432	−0.4591

this substrate block no larger than necessary for required mechanical rigidity in order to allow flexible spectrograph mounting and for the bench-vise handling in the crystal-mounting procedures as described above. For the molecular multilayer construction this minimum size is essential because the substrates are stacked six high for the dipping tank operation in the direct depositing of these analyzers. This standardized substrate design is detailed in Fig. A1. All dimensions are simply related to the locating centers of the hole-and-slot positions (used with fixed mounting posts within the spectrograph) and to the position of the focal point within the scatter aperture.

The computer-controlled milling machine that has been used generates a prescribed radius of curvature between successive points along the required elliptical arc. The spacing for these points is chosen in order that this circular-arc approximation is of error that is no greater than the tolerance of the milling machine (~0.2 mil). This typically requires fewer than 100 incremental positions along the four-inch arc for the analyzer substrates used in this work.

In addition to specifying the standardized back and side surfaces and locating hole and slot, a listing is also presented for the milling machine instructions of the x, y and radius of curvature, r, associated with each position along the elliptical arc. All coordinates are given using the back and side surfaces of the substrate block as the x and y axes as shown in Fig. A1. The points along the elliptical arc portion are calculated using the parametric relations in variable β. From Eq. (4), the radial position from the focal point to the arc is given by

$$\rho = \frac{h}{1 - \epsilon \cos\beta}.$$

Using the coordinates as defined in Fig. A1, we may then write

$$x = x_0 + \frac{h\cos(\beta - \theta_0)}{1 - \epsilon\cos\beta}$$

and

$$y = y_0 - \frac{h\sin(\beta - \theta_0)}{1 - \epsilon\cos\beta}.$$

The corresponding radius of curvature, r, at the angular position β is given by

$$r = \frac{h(1 - 2\epsilon\cos\beta + \epsilon^2)^{3/2}}{(1 - \epsilon\cos\beta)^3}.$$

At the β position of one end of the symmetrically centered, four-inch crystal segment (and at corresponding coordinates, x_2 and y_2), the profile is allowed to continue as a straight tangential section to the end of the substrate block as shown in Fig. A1 and with a slope m equal to that at x_2-y_2 for the elliptical arc. By eliminating the elliptical arc at this end (with its smaller radii of curvature), the crystal segment may be more easily translated back and forth along the substrate in the mounting process of establishing a good epoxy contact and centering.

In Table A3 we have listed, for h values in the range of 1–3.5 in. and for R_0 = 120 cm, the values for x_0, y_0, x_1, y_1, x_2, y_2, m, and ϵ which permit the complete specification of the curved profile portion of the standard elliptical analyzer substrate described in Fig. A1.

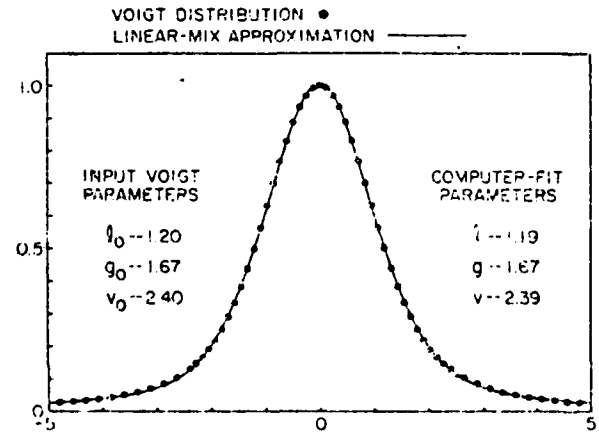

FIG. B1. Compared here, as for Table B1, are the predicted, computer-fit FWHM values for l, g, and v with those characterizing the 60, uniformly spaced point data for an exact Voigt distribution. Demonstrated here is the high accuracy of such fitting by the relatively simple analytical approximation to the Voigt convolution integral given in Eq. (25) and applied here.

APPENDIX B: SINGLE SPECTRAL LINE ANALYSIS

Assuming that a measured spectral line distribution may be precisely described as a convolution of Lorentzian

TABLE B1. l, q, and v values for different mixing parameters δ.

Input Voigt parameters			Computer-fit parameters			Mixing parameter
v_0	l_0	g_0	v	l	g	δ
3.95	3.20	1.67	3.94	3.22	1.64	0.202
2.68	1.60	1.67	2.67	1.58	1.69	0.432
2.40	1.20	1.67	2.39	1.19	1.67	0.521
2.01	0.60	1.67	2.00	0.59	1.67	0.720

that characterize the elliptical analyzer, the spectral range that may then be covered is determined by the effective length of the crystal. In Table A2, the limiting values for the spectrum angles, β_1 and β_2, as set by a four-inch length of crystal analyzer are presented for h values in the 1–4-in. range. An R_0 value of 120 cm (47.24 in.) has been chosen here as being an appropriate value for most of the large inertially and magnetically confined plasma sources which are currently in operation. The corresponding limiting $(2d)E$ values have been calculated and are presented here, which will yield the photon energy limits, E_1 and E_2, derived by using the $2d$-crystal values as those presented, for example, in Table A1. The associated beam limits, a_1 and a_2, and the linear aperture Δa are given. Finally, the radii of curvature, r_1 and r_2, of the analyzer profile at the corresponding β_1–β_2 angle limits are also presented here.

B. Multilayers for $E < 500$ eV

For spectroscopy below the carbon–K edge (at ~280 eV), we have developed molecular multilayer analyzers of the Langmuir–Blodgett type using the lead salts of the straight-chain fatty acids, lauric, myristic, stearic, behenic, lignocerate, and melissic. These are of $2d$ values equal to 70, 80, 100, 120, 130, and 160 Å, respectively. Our molecular multilayer analyzers are typically with 200 d spacings. Their characteristics and methods of construction have been reported elsewhere.[2,8,10,22,23] For these, the reflecting planes are dense double layers of lead atoms separated by a low-density matrix of the carbon chains. Because the carbon matrix is of particularly low absorption for photon energies below the carbon–K edge, the reflectivity and resolution of these molecular multilayers are relatively high. (Energy resolution is typically around 1 eV.)

These multilayers are deposited directly upon the elliptical analyzer substrate blanks which are clad with 10-mil glass sheet material. The thin glass segments are preformed at a "sagging" temperature and annealed upon stainless-steel elliptical analyzer substrates.[24] These are then epoxied to the elliptical substrates with a procedure as noted above.

A unique advantage of the molecular multilayers is that these may be deposited upon substrates of any shape (for example, of double curvature and of radii of curvatures in the millimeter range).

For spectroscopy in the 300–500-eV range, the molecular multilayers are generally not as efficient as the sputtered/evaporated multilayers of nonorganic, low-density/high-density layered pair systems.[2,8,25,26] These may be constructed with $2d$ values in the required 30–60-Å range. The high-density layer may, for example, be of an element such as tungsten. The low-density layer may be a compatible lighter element with a particularly low absorption for photon energies in the desired 300–600-eV region. These may be deposited most accurately upon *flat* surfaces (for example, upon the same 10-mil glass sheet material as used for molecular layer substrates) which may then be elastically bent and epoxy mounted as described above for elastic crystal segments.

C. Construction of the elliptical substrates

The elliptical profiles are machined into a suitable substrate material using a computer-controlled vertical milling machine. Considerations involved in the choice of the substrate material include machinability, surface smoothness, and the temperature coefficient of expansion (as may approximately match that of the attached crystal or glass segment). Typically, stainless steel, aluminum, and plastics have been used. A low atomic number substrate material may be important to minimize objectionable fluorescent x-radiation background from the substrate when a given source spectrum contains an appreciable high-energy x-ray background component.

We have attempted to design the crystal-mounting block to be of convenient dimensions that are suitable for analyzers of R_0 values in the 10–100-in. range and h values in the 1–4-in. range. It is important to have the dimensions of

UNIVERSAL ELLIPTICAL ANALYZER MOUNTING BLOCK

FOR $\theta_0 = 30°$

POSITION	x	y
0	0.7500"	h + 0.5000"
3	0	h 5000"
4	5.0000"	0
5	4.2500"	0.2500"
6	2.5000"	0.2500"
7	0.7500"	0.2500"

5–7 LOCATING HOLE AND SLOT DIAM = 0.2500"

6 CLEARANCE HOLE DIAM = 0.165"

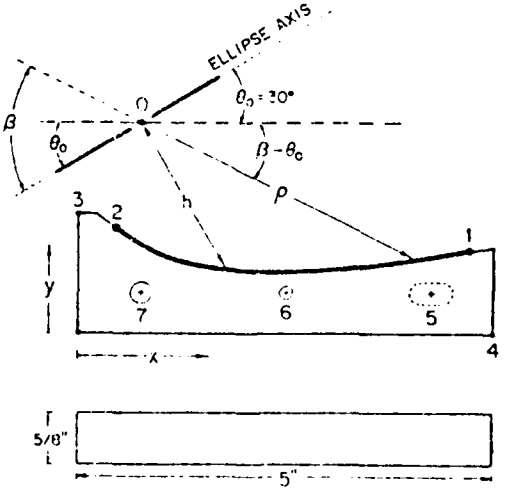

FIG. A1. Universal elliptical analyzer mounting block for four-inch crystal segments and for R_0 and h values in the ranges 10–100 and 1–4 in., respectively. The parameters that specify the curved profile that is machined into this block, for a given h value, are presented in Table A3.

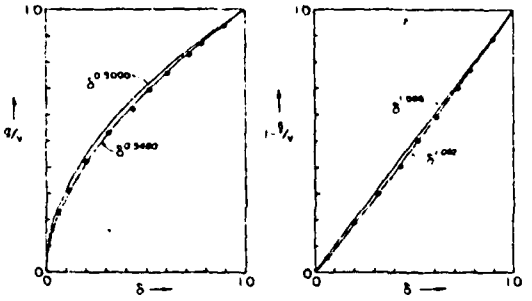

FIG. B2. Plotted here are the relations that are used to determine the g/v and l/v ratios from the computer-fit values of δ. The exponents that are used here were based upon least-square fitting over evenly spaced values of δ as shown here in the 0.1 to 0.9 range. The ratios used in these plots were those that characterize the corresponding, exact Voigt distributions that were fit for these δ values. For comparison are shown the simpler functions that have been used to obtain the approximate analytical relations that are given in Eqs. (23) and (24).

and Gaussian components (and therefore as a Voigt distribution), and using the linear-mix analytical approximation described by Eq. (25), a FORTRAN program has been written[27] that will then allow the computation from a line intensity profile data set $I(\beta)$ for the following values:

δ	:	linear-mixing parameter
I_0	:	peak intensity
β_0	:	peak position in spectrum angle,
v	:	FWHM of the best Voigt distribution fit
l	:	Lorentzian component FWHM
g	:	Gaussian component FWHM
N	:	area under the best-fit distribution.

The linear-mix approximation to the Voigt function may be written as

$$I(\beta) = I_0[\delta G(x) + (1-\delta)L(x)],$$

where $G(x) = \exp[-(\ln 2)x^2]$ and $L(x) = (1+x^2)^{-1}$ and for which $x = 2(\beta - \beta_0)/v$.

For a given value of v, a linear least-squares fitting yields a value for δ and for I_0. In this program, v is varied in order to find its "best" value which renders a minimum absolute least-square fitting error. The entire line profile data set is used for this fitting procedure. In order to begin this minimum-error search process, a first approximation for the value of v is obtained by least-square fitting the two sides of the distribution (using intensity points in the range of $I_0/3$ to $2I_0/3$) to a cubic in I/I_0. From these fits, the FWHM value v and the peak position β_0 are first determined. With these values, the minimum-error fitting of the above linear-mix function may proceed.

In Fig. B1 are plotted exact Voigt distribution points as characterized by the parameters l_0, g_0, and v_0. Also plotted here is the linear-mix approximation curve as developed by this program along with its computed values of l, g, and v. Similarly, in Table B1 are presented the l, g, and v values for different mixing parameters δ, comparing the original Voigt values to the derived, computer-fit values. As discussed above, the g and l parameters are determined from the values for δ and for v using the following relations [from Eq. (26)]

$g = v(\delta^{0.548})$ and $l = v(1-\delta^{1.062})$. These exponents were determined from least-square fitting to the computer-fit δ values in the 0.1 to 0.9 range as shown in the plots of Fig. B2.

Note. If the central region of the spectral line departs from a Voigt distribution (e.g., depressed by the effect of self-absorption within the source), only the intensity points for the wings of the distribution are entered as the line profile data set. In this case, the program will stop and ask the operator to enter an estimated peak position and intensity (corresponding to an "extrapolated Voigt distribution" near the distribution center). A region in the wings that is affected by contributions from an overlapping, nearby spectral line may be eliminated and represented by a few points that are estimated Voigt extrapolations and which reflect the symmetry as required for the single line that is being analyzed. It is important that all background intensity under the spectral line be subtracted from the original intensity profile data.

[1] V. A. Boiko, S. A. Pikuz, and A. Ya. Faenov, Instrum. Exp. Tech. (USSR) 23, 291 (1980).

[2] B. L. Henke, Nucl. Instrum. Methods 177, 161 (1980); B. L. Henke, "Low energy x-ray spectroscopy with crystals and multilayers," in *AIP Conference Proceedings No. 75 on Low Energy X-Ray Diagnostics, Monterey, California*, edited by D. T. Attwood and B. L. Henke (American Institute of Physics, New York, 1981), p. 85.

[3] B. Yaakobi, T. C. Bristow, and A. Hauer, Opt. Commun. 14, 336 (1975); B. Yaakobi and A. Nee, Phys. Rev. Lett. 36, 1077 (1976).

[4] R. W. Lee, D. L. Matthews, S. M. Lane, E. M. Campbell, L. Koppel, J. Scofield, J. Auerback, and T. Lim, J. Phys. B 15, L317 (1982).

[5] B. Yaakobi, R. E. Turner, H. W. Schnopper, and P. O. Taylor, Rev. Sci. Instrum. 50, 1609 (1979).

[6] E. Källne and J. Källne, MIT Plasma Fusion Center Report No. PFC/JA-82-17, August 1982.

[7] B. L. Henke, "Low energy x-ray interactions: photoionization, scattering, specular and Bragg reflection," in *AIP Conference Proceedings No. 75 on Low Energy X-Ray Diagnostics, Monterey, California*, edited by D. T. Attwood and B. L. Henke (American Institute of Physics, New York, 1981), p. 146.

[8] B. L. Henke, P. Lee, T. J. Tanaka, R. L. Shimabukuro, and B. K. Fujikawa, At. Data Nucl. Data Tables 27, No. 1 (January 1982).

[9] D. M. Barrus, R. L. Blake, H. Felthauser, E. E. Fenimore, and A. J. Burek, "Spectrophotometric properties of crystals for low energy x-ray diagnostics," in *AIP Conference Proceedings No. 75 on Low Energy X-Ray Diagnostics, Monterey, California*, edited by D. T. Attwood and B. L. Henke (American Institute of Physics, New York, 1981), p. 115.

[10] B. L. Henke, R. C. C. Perera, E. M. Gullikson, and M. L. Schattenburg, J. Appl. Phys. 49, 480 (1978).

[11] W. L. Weise, "Line broadening," in *Plasma Diagnostic Techniques*, edited by R. H. Huddleston and S. Leonard (Academic, New York, 1965), p. 265.

[12] T. J. Tanaka, M. A. Palmer, J. P. Anthes, K. Glibert, J. Martin, and B. L. Henke, "An elliptical analyzer x-ray spectrograph: application to a laser produced plasma" (in preparation).

[13] B. L. Henke, F. G. Fujiwara, M. A. Tester, T. S. Dutland, H. T. Yamada, M. A. Palmer, and C. H. Dittmore, "The characterization of five photographic films for quantitative, low energy x-ray spectroscopy" (in preparation).

[14] R. L. Kauffman, Lawrence Livermore National Laboratory (private communication).

[15] National Laser Users Facility, University of Rochester, B. L. Henke, P. A. Jaanimagi, and M. C. Richardson (in preparation).

[16] J. V. Nicholas, X-Ray Optics, Inc., Bloomington, IN (private communication).

[17] [illegible] Alexander-Saltzman and Co., Co. Goleta, Appl. Spectrosc. 28, 155 (1974); A. Jones, Space Sci. Instrum. 2, 53 (1976).

[18] [illegible] *Principles and Practice of X-Ray Spectrometric Analysis*, 2nd ed. (Plenum, New York, 1975).

[19] [illegible] Rev. Sci. Instrum. 41, 1229 (1970).

[20] Nicrotel II 6175 Dexter HYSOL Potting Compound, vendor Plastic and Potting Materials, Inc., Paramount, CA.

and Tooling Materials, Inc., Paramount, CA.
[22]B. L. Henke and M. A. Tester, "Techniques of low energy x-ray spectroscopy (0.1 to 2 keV region)," in *Advances in X-Ray Analysis* (Plenum, New York, 1975), Vol. 18, p. 76.
[23]B. L. Henke and K. Taniguchi, J. Appl. Phys. 47, 1027 (1976).
[24]Material used: 10-mil Corning Microsheet, Garner Glass Company, Claremont, CA (private communication, T. H. Garner).
[25]T. W. Barbee, Jr., "Sputtered layered synthetic microstructure (LSM) dispersion elements," in *AIP Conference Proceedings No. 75 on Low Energy X-Ray Diagnostics, Monterey, California*, edited by D. T. Attwood and B. L. Henke (American Institute of Physics, New York, 1981), p. 131.
[26]E. Spiller, "Evaporated multilayer dispersion elements for soft x-rays," in *AIP Conference Proceedings No. 75 on Low Energy X-Ray Diagnostics, Monterey, California*, edited by D. T. Attwood and B. L. Henke (American Institute of Physics, New York, 1981), p. 124.
[27]See AIP document No. PAPS RSINA-54-1311-5 for 5 pages of the FORTRAN listing. Order by PAPS number and journal reference from the American Institute of Physics, Physics Auxiliary Publication Service, 335 East 45th Street, New York, NY 10017. The price is $1.50 for each microfiche (98 pages) or $5.00 for photocopies of up to 30 pages, and $.15 for each additional page over 30 pages. Airmail additional. Make checks payable to the American Institute of Physics.

RESEARCH PUBLICATIONS BY THE PRINCIPAL INVESTIGATOR AND CO-WORKERS ON THIS RESEARCH PROGRAM

1973 - 1983

43. "Ultrasoft X-Ray Reflection, Refraction and Production of Photoelectrons (100-1000 eV Region)," *Physical Review A6*, 94-104 (1972).

44. "Electron Interactions within Solids--Electron Spectroscopy" and "Light Element Analysis" *Proceedings of the U.S.-Japan Seminar on Fundamentals of Scanning Electron Microscopy* (Osaka, Japan, November-December 1972).

45. "Low Energy X-Ray and Electron Absorption within Solids (100-1500 eV Region)," Interim Report, AFOSR 72-2174 (August 1973) (w/ Eric S. Ebisu).

46. "Low Energy X-Ray and Electron Absorption within Solids (100-1500 eV Region)," *Advances in X-Ray Analysis* (Plenum, New York, 1974) (w/ Eric S. Ebisu).

47. "Ultrasoft X-Ray Bragg and Specular Reflection: The Effects of Anomalous Dispersion," Interim Report, AFOSR 72-2174 (August 1974) (w/ Rupert C. C. Perera and Ronald H. Ono).

48. "Demountable Ultrasoft X-Ray Source," (informal notes, August 1974).

49. "Techniques of Low Energy X-Ray Spectroscopy (0.1 to 2 keV Region)," *Advances in X-Ray Analysis* (Plenum, New York, 1975) (w/ Murray A. Tester).

50. "Techniques of Low Energy X-Ray Spectroscopy (0.1 to 2 keV Region)," Interim Report, AFOSR 75-2762 (November 1974) (w/ Murray A. Tester).

51. "Valence Band Spectroscopy in the Ultrasoft X-Ray Region (50 to 100 A), *Advances in X-Ray Analysis* (Kendall/Hunt, Dubuque, 1976), Vol. 19 (w/ Kazuo Taniguchi).

52. "Parameters for the Calculation of X-Ray Absorption Coefficients for H (1) through Ge (32) in the 100-1500 eV Region," *Advances in X-Ray Analysis* (Kendall/Hunt, Dubuque, 1976), Vol. 19 (w/ Mark L. Schattenburg).

53. "Quantitative Low Energy X-Ray Spectroscopy (50-100 A Region)," *J. Appl, Phys.* 47 (1976) (w/ Kazuo Taniguchi).

54. "Sulfur LII,III Emission Spectra and Molecular Orbital Studies of Sulfur Compounds," *J. Chem. Phys. 64* (1976) (w/ Kazuo Taniguchi).

55. "X-Ray Calibration Sources for the 100-1000 eV Region," *Proceedings of the 1976 ERDA Symposium on X- and Gamma-Ray Sources and Applications* (University of Michigan, Ann Arbor, May 1976).

56. "Secondary Electron Energy Distributions for Gold as Excited by C-Kα (277 eV) and Al-Kα (1487 eV) X-Rays," *Appl. Phys. Lett. 29* (1976) (w/ J. A. Smith and D. T. Attwood).

57. "0.1 to 10 keV X-Ray-Induced Electron Emissions from Solids--Models and Secondary Electron Measurements," *J. Appl. Phys. 48*, 1852 (1977) (w/ J. A. Smith and D. T. Attwood).

58. "High Efficiency Low-Energy X-Ray Spectroscopy in the 100-500 eV Region," *J. Appl. Phys. 49*, 480 (1978) (w/ R. C. C. Perera, E. M. Gullikson and M. L. Schattenburg).

59. "Cl-$L_{II,III}$ Fluorescent X-Ray Spectra Measurement and Analysis for the Molecular Orbital Structure of ClO_4^-, ClO_3^- and ClO_2^-," *J. Chem. Phys. 68*, 3692 (1978) (w/ R. C. C. Perera and D. S. Urch).

60. "Some Recent Studies in Low Energy X-Ray Physics," *Proceedings of the 8th International Conference on X-Ray Optics and Microanalysis* (Boston, August 1977).

61. "Models and Measurement for the Response of Dielectric X-Ray Photocathodes," Scientific Reports, AFOSR 75-2762-F and DOE E(04-3)235-PA15, March 1978.

62. "Low Energy X-Ray Emission Spectroscopy in the 100-500 eV Region: Molecular Orbital Interpretation," (PhD Thesis by R. C. C. Perera) Special Scientific Report, AFOSR 75-2762-F, May 1978.

63. "The Secondary Electron Emission Photocathode Characteristics for Time Resolved X-Ray Spectroscopy," *Proceedings of the International Conference on X-Ray and XUV Spectroscopy* (Sendai, Japan, August 1978); *Jap. J. Appl. Phys. 17*, Suppl. 17-2, p. 23 (1978) (w/ K. Premaratne).

64. "C-K and Cl-L Emission Spectra and Molecular Orbital Analysis of CCl_4" *Proceedings of the International Conference on X-Ray and XUV Spectroscopy* (Sendai, Japan, August 1978); *Jap. J. Appl. Phys. 17*, Suppl. 17-2, p. 23 (1978) (w/ R. C. C. Perera).

65. "A Soft X-Ray Spectrometer for the Study of Plutonium and Plutonium-based Materials," *X-Ray Spectrometry 7* (1978) (w/ P. L. Wallace, W. L. Haugen and E. M. Gullikson).

66. "Soft X-Ray Induced Secondary Electron Emission from Semiconductors and Insulators: Models and Measurements," *Phys. Rev. B19*, 3004 (1979) (w/ J. Liesegang and S. D. Smith).

67. "Low Energy X-Ray Emission Spectra and Molecular Orbital Analysis of CH_4, CCl_4 and $CHCl_3$," *J. Chem. Phys. 70*, 5398 (1979) (w/ R. C. C. Perera).

68. "The Characterization of Photocathodes for Application to Time-Resolved X-Ray Spectroscopy," Technical Progress Report, AFOSR 79-0027 and DOE DE-AS03-76SF00235, April 1979.

69. "Multilayer X-Ray Spectrometry in the 20-80 A Region: A Molecular Orbital Analysis of CO and CO_2 in the Gas and Solid States," *X-Ray Spectrometry 9*, 81 (1980) (w/ R. C. C. Perera).

70. "X-Ray Spectrometry in the 100-1000 eV Region," *Nucl. Instrum. Methods 177*, 161 (1980).

71. "Evaluation of High Efficiency CsI and CuI Photocathodes for Soft X-Ray Diagnostics," *Appl. Opt. 19*, 748 (w/ E. B. Saloman and J. A. Pearlman).

72. "The Characterization of X-Ray Photocathodes in the 0.1-10 keV Photon Energy Region," *J. Appl. Phys.* (March 1981) (w/ J. P. Knauer and K. Premaratne).

73. "Low Energy X-Ray Interactions: Photoionization, Scattering, Specular and Bragg Reflection," *AIP Conference Proceedings No. 75 on Low Energy X-Ray Diagnostics, Monterey, California* (American Institute of Physics, New York, 1981) D. T. Attwood and B. L. Henke, Editors.

74. "Low Energy X-Ray Spectroscopy with Crystals and Multilayers," *AIP Conference Proceedings No. 75 on Low Energy X-Ray Diagnostics, Monterey, California* (American Institute of Physics, New York, 1981) D. T. Attwood and B. L. Henke, Editors.

75. "Appendix: The Atomic Scattering Factor, f + if , for 94 Elements and for the 100 to 2000 eV Photon Energy Region," *AIP Conference Proceedings No. 75 on Low Energy X-Ray Diagnostics, Monterey, California* (American Institute of Physics, New York, 1981) D. T. Attwood and B. L. Henke, Editors (w/ P. Lee, T. J. Tanaka, R. L. Shimabukuro and B. K. Fujikawa).

76. "X-Ray Diffraction in Multilayers," *Opt. Commun. 37* (1981), (P. Lee).

77. "Low-Energy X-Ray Interaction Coefficients: Photoabsorption, Scattering and Reflection," *Atomic Data and Nuclear Data Tables 27*, No. 1 (1982) (w/ P. Lee, T. J. Tanaka, R. L. Shimabukuro and B. K. Fujikawa).

78. "The Stability of Cesium Iodide X-Ray Photocathodes," *Nucl. Instrum. Methods 207*, 465 (1983) (w/K. Premaratne and E. R. Dietz).

79. "Pulsed Plasma Source Spectrometry in the 80-8000 eV X-Ray Region," *Rev. Sci. Instrum. 54*, 1311 (1983) (w/ H. T. Yamada and T. J. Tanaka).

80. "Low-Energy X-Ray Response of Photographic Films: Part I. Mathematical Models," submitted to *J. Opt. Soc. America* (w/ S. L. Kwok, J. Y. Uejio, H. T. Yamada and G. C. Young).

81. "Low-Energy X-Ray Response of Photographic Films: Part II. Experimental Characterization," submitted to *J. Opt. Soc. America* (w/ F. G. Fujiwara, M. A. Tester, C. H. Dittmore and M. A. Palmer).

82. "Photon Counting Efficiency with High and Low Density CsI Photocathodes in the 100-10,000 eV Region," (w/ K. S. Tan and P. Y. Maeda), in preparation.

83. "X-Ray Diagnostics of Laser Plasmas with a Calibrated Elliptical Analyzer Spectrograph," Doctoral Thesis, University of Hawaii, Tina J. Tanaka, May 1983.

84. "A Two-Channel, Elliptical Analyzer Spectrograph for Absolute, Time-Resolving/Time-Integrating Spectrometry of ICF Plasmas in the 100-10,000 eV Region," (w/ P. A. Jaanimagi), in preparation.

85. "300-Channel, Large Aperture Picosecond X-Ray Streak Camera," (w/ P. A. Jaanimgai), in preparation.

86. "Notes on the Modifications and Usage of the SLAC-UH Electron Trajectory Program, LENS," (w/ P. A. Jaanimagi), in preparation.

87. "A New, High Sensitivity, Low-Energy X-Ray Spectrographic Facility," in preparation.

In Preparation:

88. "Multilayer Analyzers for Low-Energy X-Ray Spectroscopy (100-500 eV): Part I. Mathematical Models," (w/ H. T. Yamada).

89. "Multilayer Analyzers for Low-Energy X-Ray Spectroscopy (100-500 eV): Part II. Construction and Characterization," (w/ N. Balakrishnan and R. E. Tackaberry).

90. "Reflectivity Characteristics of Low-Energy X-Ray Mirror Monochromators," (w/ F. G. Fujiwara, R. E. Tackaberry and D. Kania).

RESEARCH PUBLICATIONS BY THE PRINCIPAL INVESTIGATOR LISTED IN THE Science Citation Index* (Institute for Scientific Information, Inc., Philadelphia, Pennsylvania) 1965-1979

1965-1969

HENKE BL

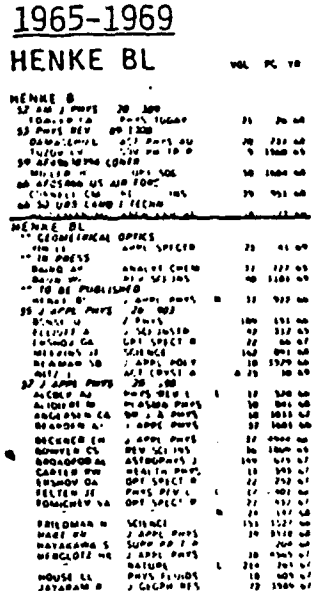

HENKE B

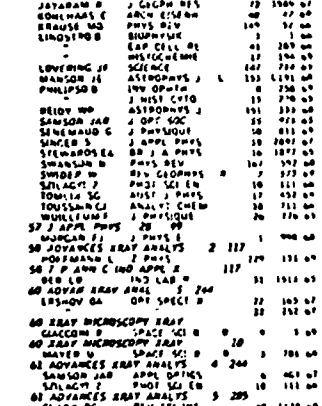

1970-1974

HENKE BL

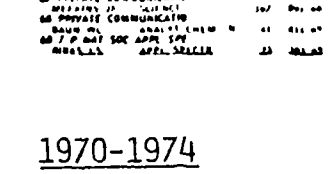

HENKE B

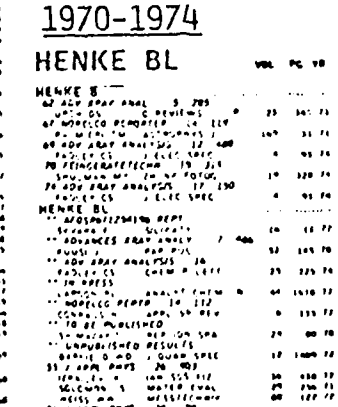

*Note: The Science Citation Index lists: 1) previously published items referred to (cited) in current literature; 2) who is doing the citing; and 3) in what journals the citing is being made.

1975-1979

HENKE BL

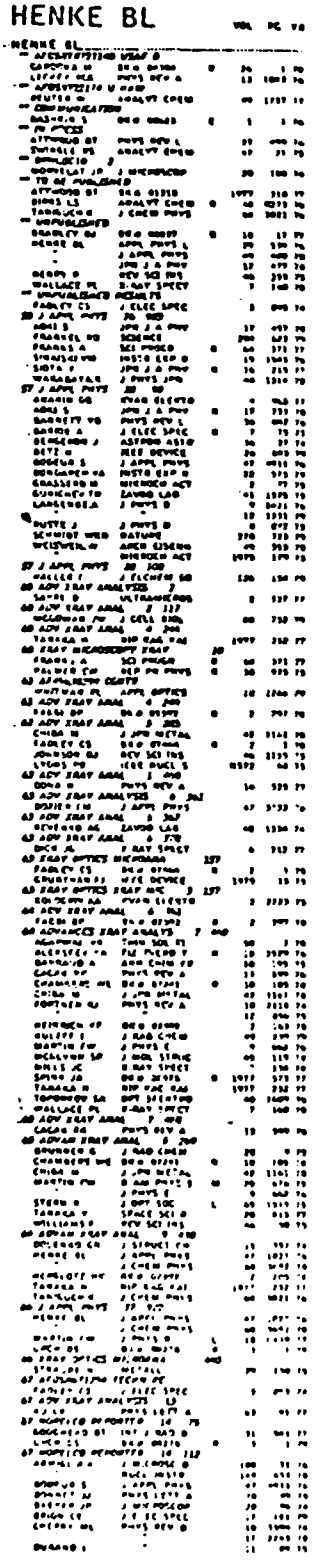

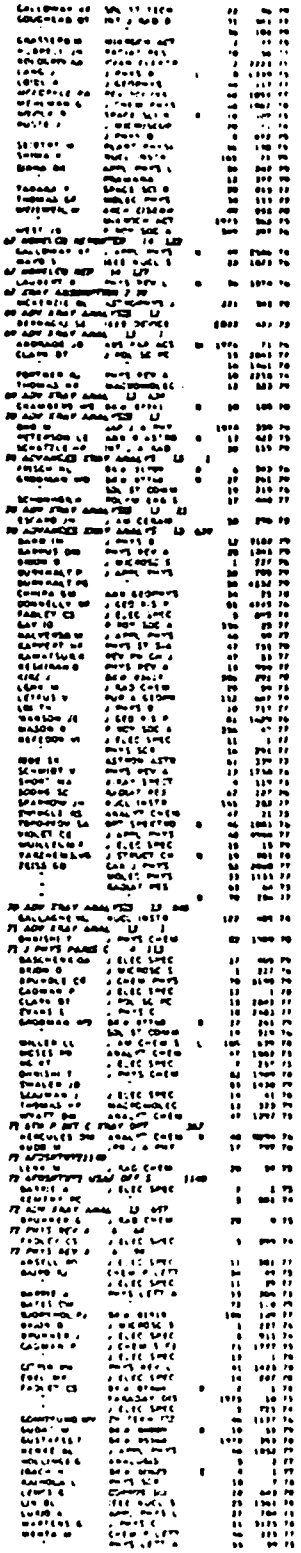

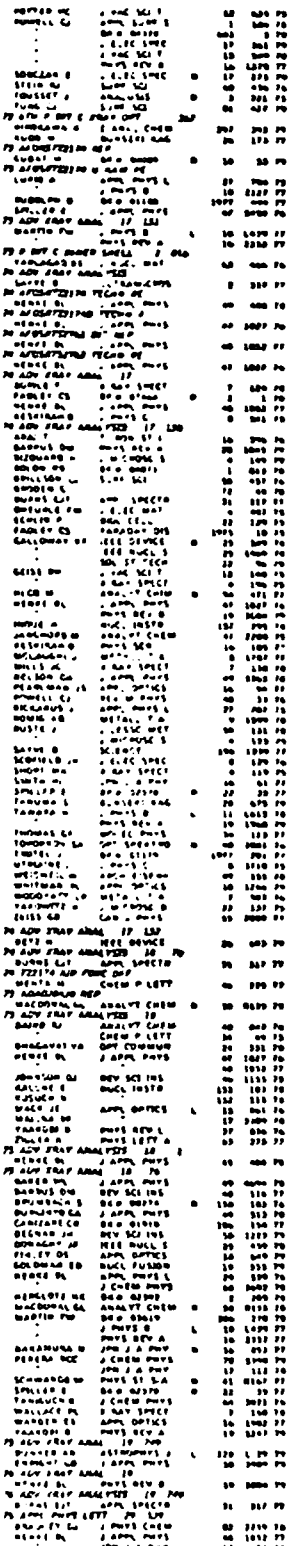

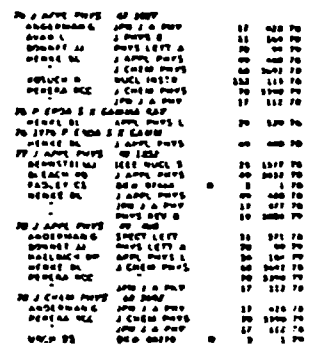

Citations for publications during the period 1980-1985 are currently unavailable.

IV. INVITED AND CONTRIBUTED RESEARCH PAPERS PRESENTED BY THE PRINCIPAL INVESTIGATOR

1978 - 1983

1978

- *A Systematic Study of the Characteristics of X-Ray Photocathodes*, Poster presentation, American Physical Society Second Topical Conference on High Temperature Plasma Diagnostics, Santa Fe, New Mexico, February 28 - March 3, 1978
- *Application of Low Energy X-Ray Spectroscopic Techniques to High Temperature Plasma Diagnostics*, Physics seminar lecture, Los Alamos Scientific Laboratory, June 1978
- *The Optimization of X-Ray Photocathodes for Time Resolved X-Ray Spectroscopy in Laser-Produced Fusion Research*, Physics colloquium lecture, University of California Lawrence Livermore Laboratory, June 1978
- Participated in a workshop on the Absolute Calibration of X-Ray Photocathodes as Applied in X-Ray Detectors (XRD's) sponsored by the National Bureau of Standards at the Lawrence Livermore Laboratory, June 1978. The results of the calibrations of two detectors that were calibrated by each of the six participating laboratories, including this one, were evaluated.
- *The Secondary Electron Emission Photocathode Characteristics for Time Resolved X-Ray Spectroscopy*, International Conference on X-Ray and XUV Spectroscopy, Sendai, Japan, August 28 - September 1, 1978
- *C-K and Cl-L Emission Spectra and Molecular Orbital Analysis of CCl_4* International Conference on X-Ray and XUV Spectroscopy, Sendai, Japan, August 28 - September 1, 1978
- *A Review of X-Ray Photocathode Characteristics that Affect Picosecond Streak Camera Operation*, 1978 American Physical Society Annual Meeting of the Division of Plasma Physics, Colorado Springs, October 30 - November 3, 1978
- *Physics and Application of Multilayer 'Crystals' for Spectral Analysis in the 50-100 A Region*, Invited paper, American Crystallographic Assn. Meeting (Joint with Japanese Crystallographic Society), Honolulu, Hawaii, March 26-30, 1979.

1979

- Seminar at Lawrence Livermore Laboratory, June 20, 1979
- Seminar at Los Alamos Scientific Laboratory, June 26, 1979
- Seminar at Kirtland Air Force Base and Sandia Laboratories, Albuquerque, New Mexico, June 28, 1979
- Seminar at Maxwell Laboratories, Inc., San Diego, June 29, 1979
- *X-Ray Spectroscopy in the 100-1000 eV Region*, Invited review paper, Japan-U.S.A. Seminar on Synchrotron Radiation Facilities, East-West Center, University of Hawaii, November 5-9, 1979

1979 (cont.)

- *The Characterization of X-Ray Photocathodes*, 21st Annual Meeting of the Division of Plasma Physics, American Physical Society, Boston, November 12-16, 1979
- Seminar at Department of Physics, Pomona College, Claremont, California, November 1979
- Seminar at Massachusetts Institute of Technology, Center for Space Research, Cambridge, Massachusetts, November 1979

1980

- Seminar at Lawrence Livermore Laboratory, August 1980
- Seminar at Los Alamos Scientific Laboratory, August 1980
- Seminar at Kirtland Air Force Base and Sandia Laboratories, Albuquerque, New Mexico, August 1980
- *Some Recent Developments in Low Energy X-Ray Spectroscopy*, 1980 Annual Meeting of the Division of Plasma Physics, American Physical Society, San Diego, November 10-14, 1980

1981

- Co-organizer of a special Topical Conference on Low Energy X-Ray Diagnostics sponsored by the American Physical Society, June 8-10, 1981, Monterey, California. Contributions for this program included the following:

  1. *Low Energy X-Ray Spectroscopy with Crystals and Multilayers.*
  2. *Low Energy X-Ray Interactions: Photoionization, Scattering, Specular and Bragg Reflection.* (Review paper)
  3. *An Absolute Calibration of RAR 2497 Film for Low Energy X-Ray Spectroscopy.* (with E. R. Dietz and M. A. Tester) (Review paper)
  4. *The Atomic Scattering Factor, $f_1 + if_2$, for 94 Elements and for the 100 to 2000 eV Photon Energy Region.* (with P. Lee, T. J. Tanaka, R. L. Shimabukuro and B. K. Fujikawa).

Proceedings of this Conference were published by the American Institute of Physics, New York, 1981: *AIP Conference Proceedings No. 75 on Low Energy X-Ray Diagnostics*, D. T. Attwood and B. L. Henke, Editors.

TOPICAL CONFERENCE ON LOW ENERGY X-RAY DIAGNOSTICS
Monterey, California
8-10 June 1981

The meeting will provide a forum for active researchers in differing scientific fields to meet and discuss common interests in the rapidly evolving technologies of low energy (100 eV to 1 KeV) x-ray generation, manipulation, and detection, as well as the physical phenomena these developments make accessible. Papers are solicited in the areas of low energy x-ray sources, detectors and spectroscopy, as well as reflective and diffractive optics. The meeting is expected to emphasize, through invited papers, new developments in microfabrication techniques, applications to the diagnosis of high density, high temperature plasmas, and x-ray lithographic applications in science and industry. Conference Co-chairmen are David Attwood of the Lawrence Livermore National Laboratory and Burton Henke of the University of Hawaii. The meeting is jointly sponsored by the American Physical Society, the U. S. Department of Energy, and the Lawrence Livermore National Laboratory.

Because only a small number of rooms have been reserved in this popular tourist region, participants are urged to reserve rooms quickly and directly at the Doubletree Inn, Monterey, California [telephone: (408) 649-4511]. In doing so, refer to the "X-Ray Conference". Further information regarding presentation of papers, program details, and preregistration can be obtained by writing to David T. Attwood, P. O. Box 5508, L-479, Lawrence Livermore National Laboratory, Livermore, Calif. 94550. The registration fee of approximately $60 includes a subsequent copy of the meeting's proceedings, bound in book form by the American Institute of Physics. All presentations must be available in camera-ready form at the time of the meeting, to APS journal standards, for inclusion in the published proceedings. ■

- Seminar at Lawrence Livermore National Laboratory, September 1981
- Seminar at Los Alamos National Laboratory, September 1981
- Seminar at Sandia National Laboratory, September 1981
- Seminar at University of Rochester, Laboratory for Laser Energetics, September 1981
- Seminar at Eastman-Kodak Company, Rochester, New York, September 1981

1982

- Seminar at Lawrence Livermore National Laboratory, August 1982
- Seminar at Los Alamos National Laboratory, August 1982
- Seminar at Sandia National Laboratory, August 1982
- Seminar at KMS Fusion, Ann Arbor, Michigan, August 1982
- *An Elliptically Curved Fixed Analyzer Spectrograph for the Diagnostics of Inertial Fusion Targets in the 80-8000 eV Region; The Characterization of Five Photographic Films for Quantitative, Low Energy X-Ray Spectroscopy*, 24th Annual Meeting of the Division of Plasma Physics of the American Physical Society, November 1-5, 1982, New Orleans

1983

- *Some Recent Work in Low-Energy X-Ray Measurement and Theory*, Seminar at the Department of Physics, State University of New York at Stony Brook, May 1983.

- *Some Recent Work in Low-Energy X-Ray Measurement and Theory*, Seminar at Brookhaven National Laboratory, Upton, New York, May 1983.

- *Some Recent Work in Low-Energy X-Ray Measurement and Theory*, Seminar at Philips Electronic Instruments, Inc., Mahwah, New Jersey, May 1983.

- Seminar on *Characterization of Multilayer Analyzers*, Energy Conversion Devices, Inc., Troy, Michigan, June 1983.

V. SOME OF THE LABORATORY FACILITIES OF THIS PROGRAM

Figure 1. Ultrasoft X-Ray Vacuum Spectrograph. A 2-to-4 kilowatt, demountable x-ray source of characteristic radiation directly, or be used to excite a fluorescent line source of slightly lower photon energy than the exciting line. Langmuir-Blodgett type multilayer analyzers specially developed in this laboratory with 2d-values in the 80-160 A range are employed for spectral analysis in the 20 to 150 A region (100-500 eV region). Pulse-height discriminating proportional counter detection is utilized to effectively reduce hard and soft background with better than 60% photon counting efficiency. Appropriate filter-windows in the tenth micron thickness range are used with a vacuum isolation window-gate on the x-ray source and for the proportional counter that is "pressure-tuned" for a given photon energy at subatmospheric pressures, typically 50-to-100 mm of propane counter gas. Spectral data is step-scanned, recorded on paper tape which is then processed on a small laboratory computer. This system is also used for the absolute calibration of x-ray detectors (XRD's) as shown here.

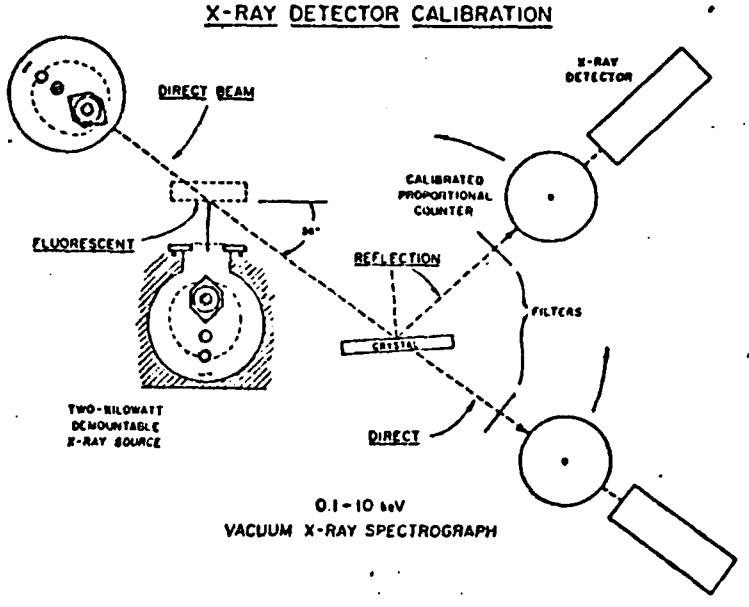

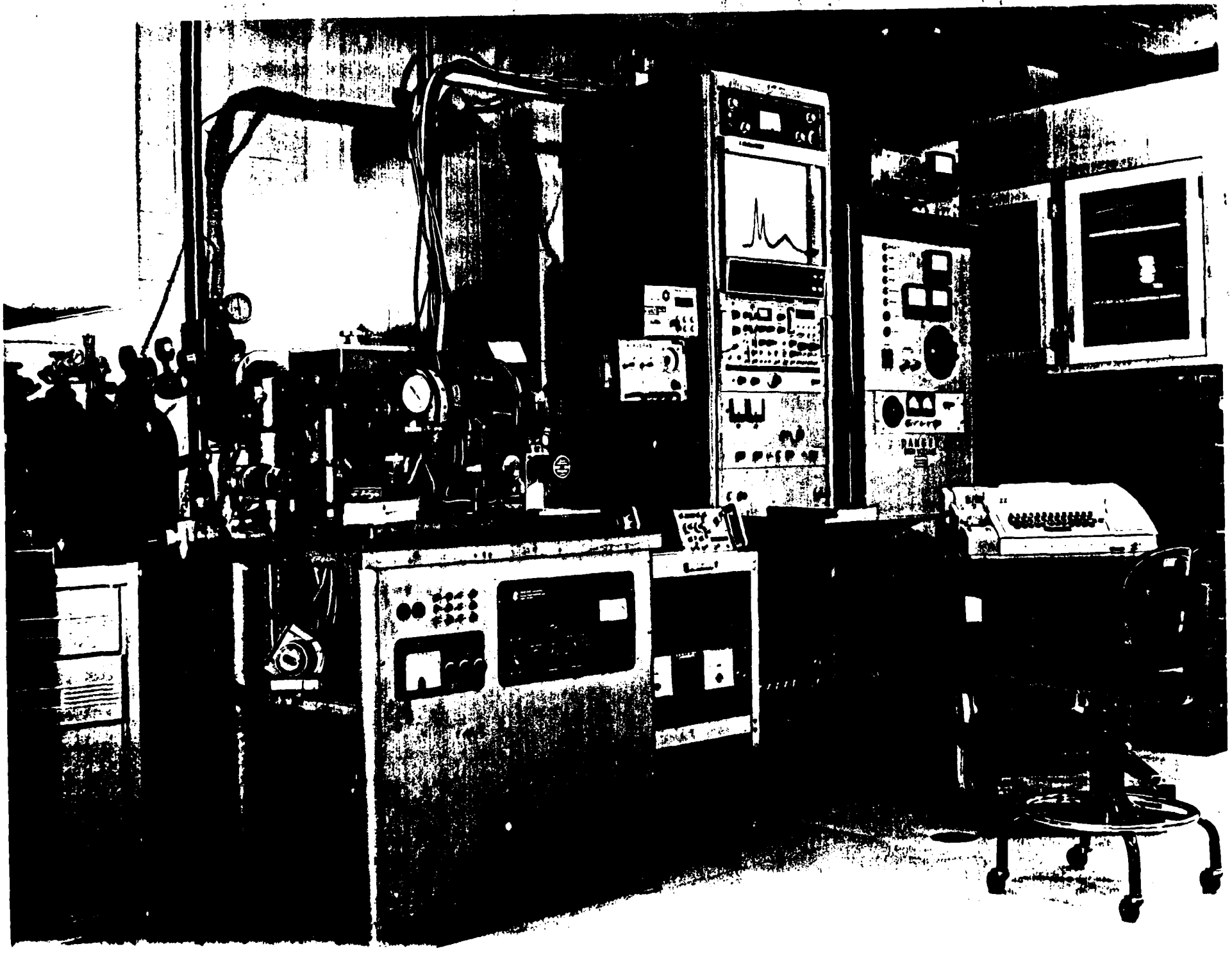

Figure 2. Calibration Facility for Pulsed X-Ray Source Spectrometers and Monochromators. A demountable, 2-4 kilowatt x-ray source may be mounted at any desired working distance from the fixed-crystal using extension vacuum pipe sections. Specially chosen, characteristic lines (K, L and M) in the 0.1 to 10 keV region are used with appropriate filters on the x-ray tube and counter windows. Pulse height discrimination against background with sensitive, photon counting is obtained with flow-proportional counters that are "pressure tuned" for each wagelength. The monochromaticity of the direct beam is monitored by a multichannel analyzer connected to the proportional counter. The orientation of the fixed crystal spectrograph with respect to the direct beam is adjustable from outside the vacuum chamber and this module can also be shifted in and out of the direct beam from outside. The proportional counter scans about a spectrograph axis using a precision goniometer and from 0° (direct beam) through 150° in 2θ.

After an absolute intensity spectrum is recorded with a proportional scan along the detection circle of the elliptical analyzer spectrograph, a camera may be introduced which places a photographic film along the same detection circle in order to obtain the corresponding, calibrated spectrum photographically. A comparison of the two measured spectra permits an absolute calibration of the photographic film.

This calibration facility is also applied to obtain the absolute total-reflection characteristics of x-ray mirror monochromators and of x-ray multilayer and crystal analyzers.

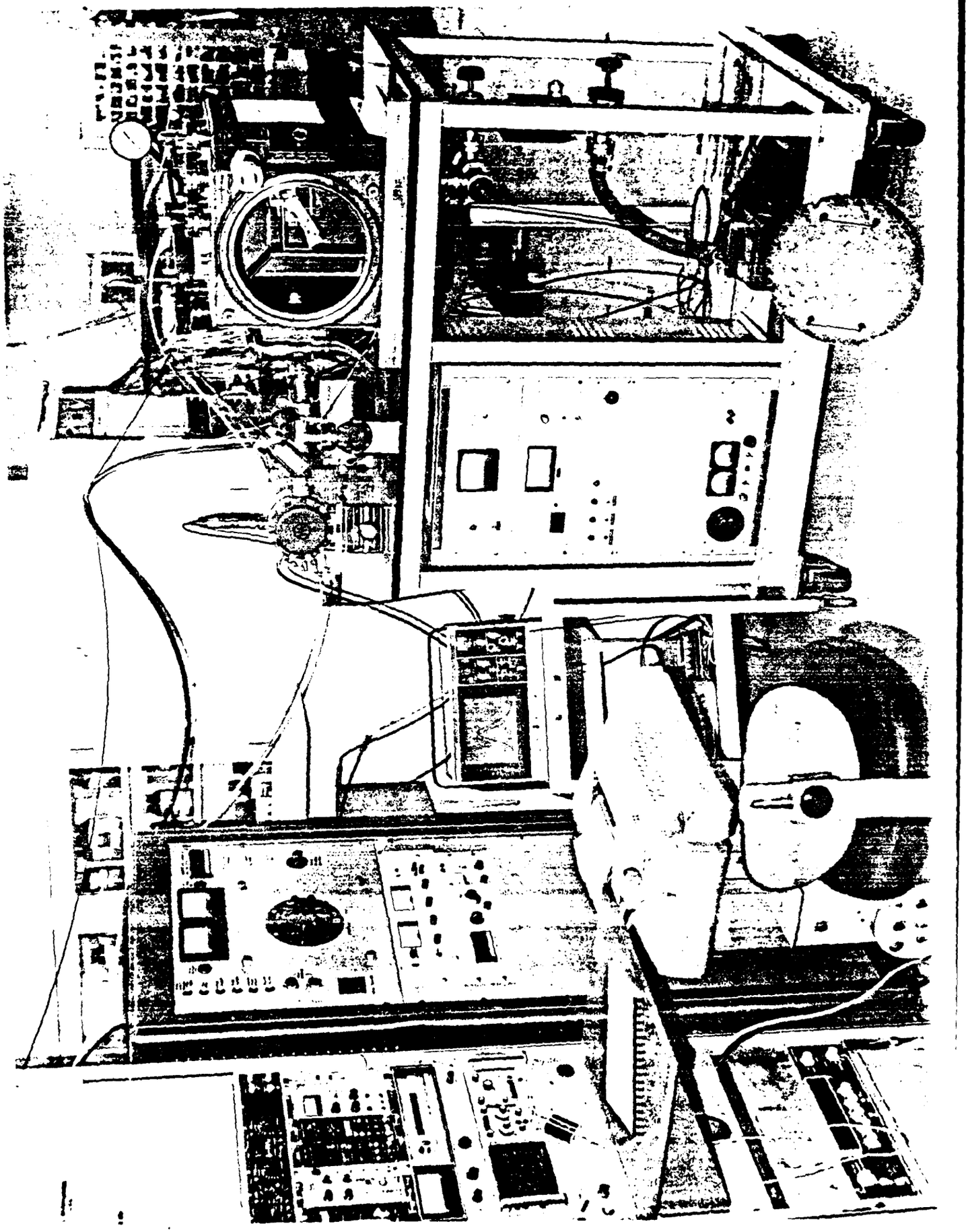

Figure 3. High Resolution, Low-Energy Electron Spectrograph. A filtered, characteristic line source of low-energy x-radiation is used to excite the photoelectron and subsequent Auger electron and secondary electron spectra from one of eight samples in a rotating holder. The emitted electrons are analyzed with a relative energy resolution of better than 0.3% by a hemispherical lens electrostatic analyzer of mean diameter of 20 inches. The electron counting is with a 16-stage electron multiplier tube. For the measurement of the secondary electron energy distributions of x-ray photocathode materials, the acceptance energy is typically fixed at 15 eV and the accelerating voltage applied to the sample is step-scanned and the spectra are recorded on paper tape and subsequently processed and plotted with a small laboratory computer system. The measured resolution of the secondary electron energy distributions is better than .05 eV.

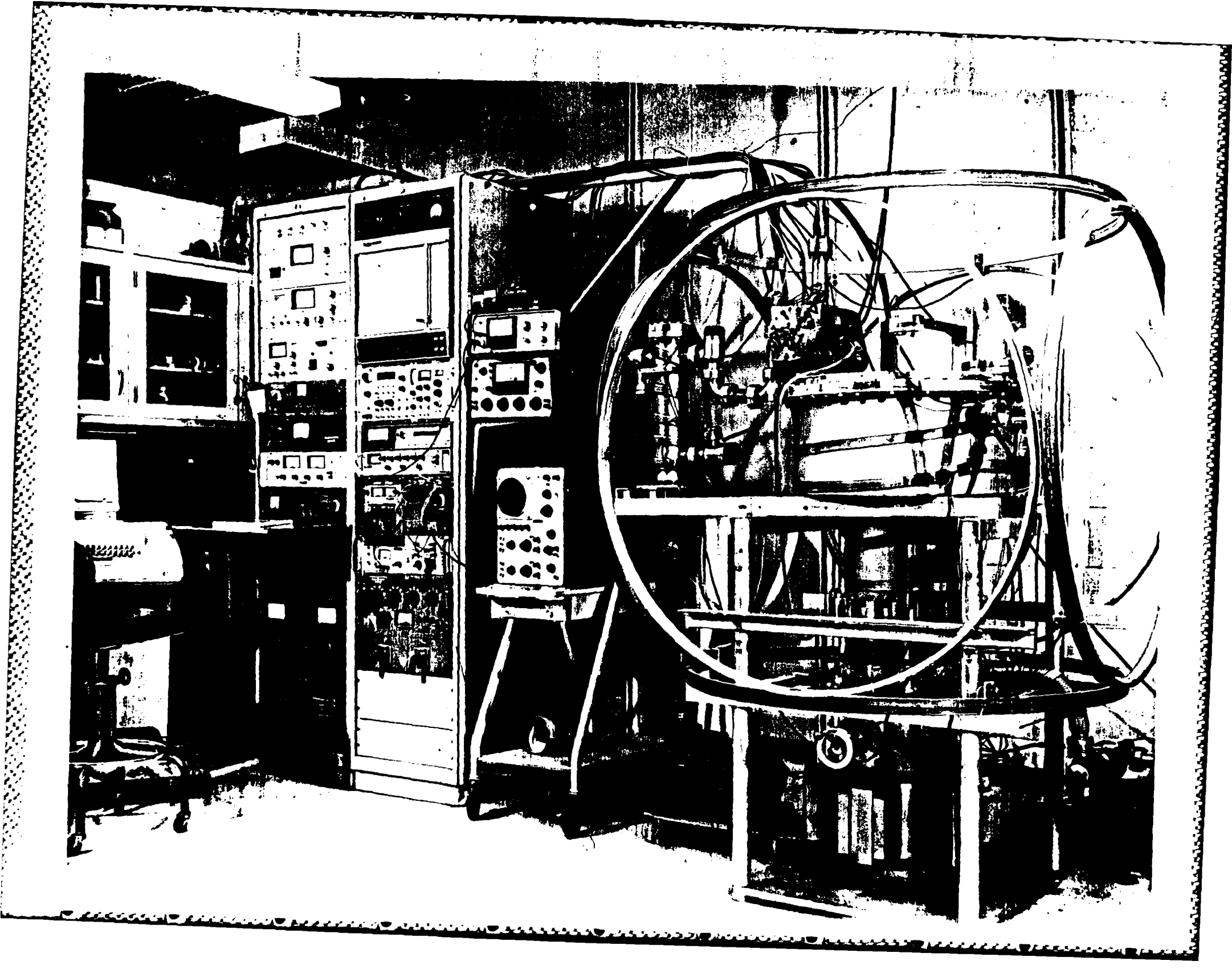

Figure 4. Facility for the Measurement of the Absolute Quantum Efficiency (for Total and Secondary Emission) of X-Ray Photocathode Materials.

A 2-to-4 kilowatt, filtered characteristic line source of x-radiation in the 0.1 to 10 keV region is closely coupled for the excitation of fluorescent line sources of energy just below that of the excitation source. Six fluorescent radiators are mounted on a rotating holder, permitting precise relative measurements. The sample in the radiated position is directly connected to a Carey 401 electrometer system and the photoelectric currents are monitored on an x-ray plotter. Cylindrical electrode systems are used to apply plus-minus 30 volt accelerating potentials to permit a differential measurement for the total and secondary electron yields for either thick or thin (transmission) photocathodes. The photons/steradian flux from the fluorescent source is measured by a calibrated flow proportional counter with the same filter-window as also introduced between the fluorescent source and the photocathode sample. Because of the relatively high photon intensity that is required for precise yield measurements, the absolute photon counter must be on an extended vacuum-pipe path and with an accurately calibrated "pinhole" window. For transmission photocathode studies, a second x-ray detector is used to measure the transmission of the photocathode system to permit a measurement of both the electron yield per incident photon and per transmitted photon.

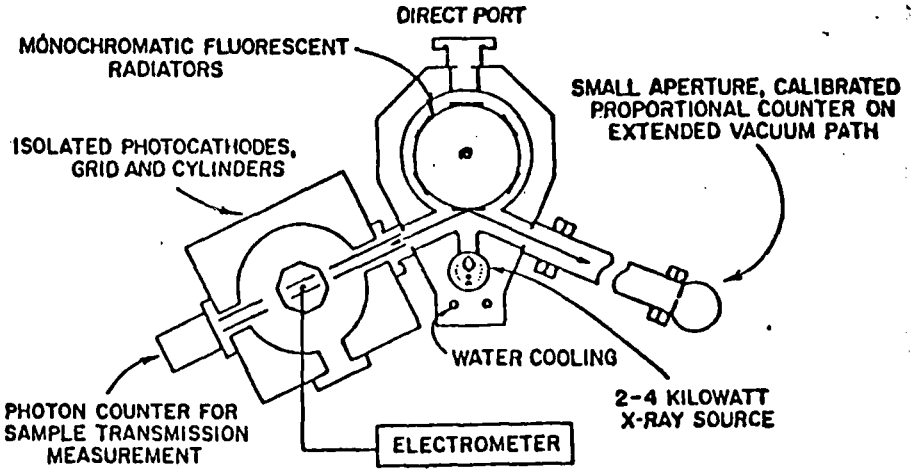

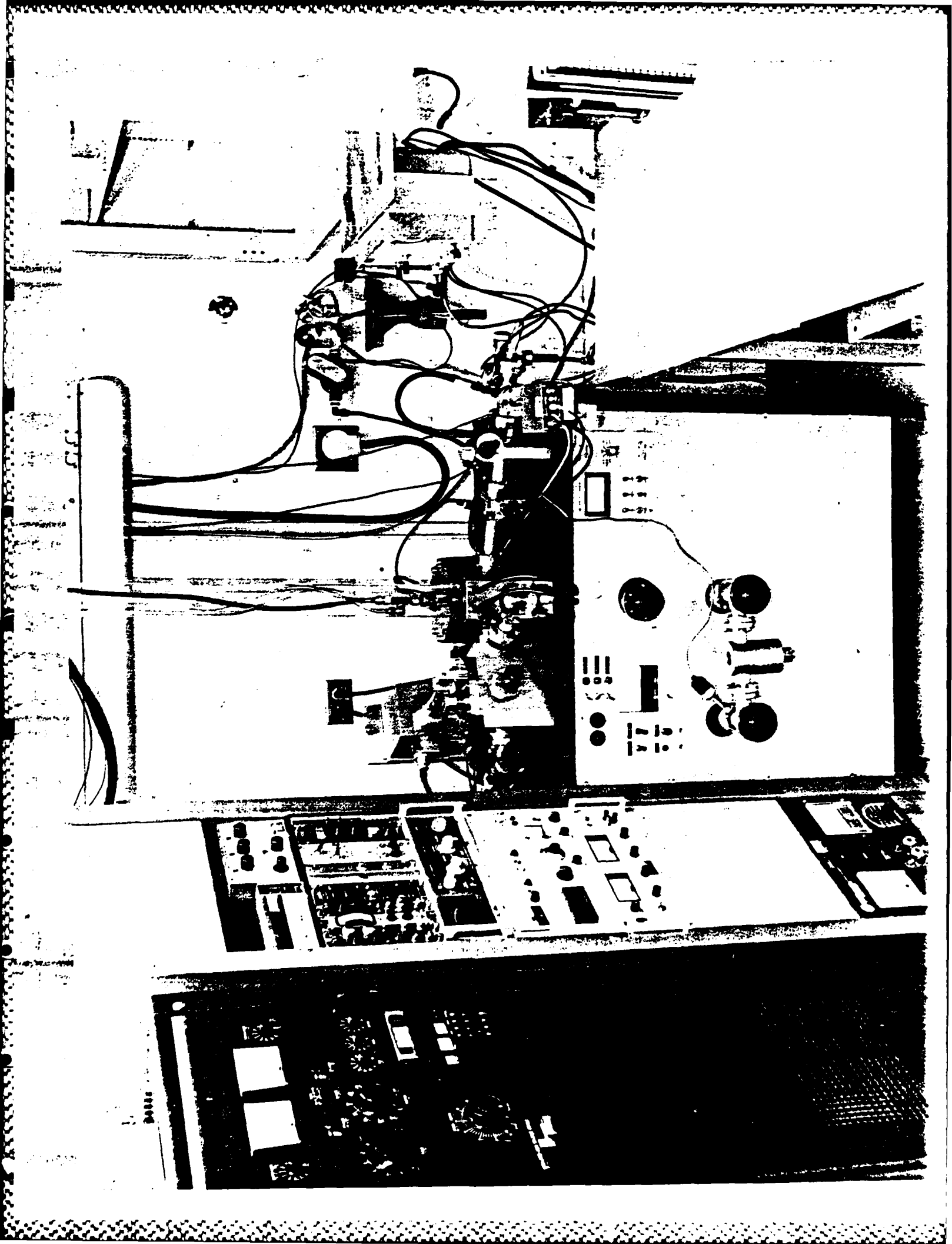

Figure 5. Clean-Bench and Dipping Tank Facility for the Construction of Molecular Multilayer Analyzers. The molecular multilayers are constructed with a specially designed tank as described here. The most successful multilayers for constructing x-ray analyzers have been by depositing insoluble fatty acids upon a very pure substrate of water to which a small concentration of a heavy, bivalent cation (such as lead or barium) has been added. The carboxyl end of this straight-chain acid molecule, $CH_3(CH_2)_nCOOH$, chemically reacts to form a salt with a monatomic layer of cations at the interface and with the CH_2 chains projecting away from the surface. This monomolecular layer is compressed by a floating barrier "piston" and is deposited upon a smooth substrate, as a glass plate, which is slowly dipped in and out of the tank surface. The molecular forces involved cause the cation monolayers to come together and form a doubly dense layer of heavy metal atoms and the ends of the CH_2 chains (CH_3 groups) to connect so that the separation between the heavy metal layers is approximately two CH_2 chain lengths.

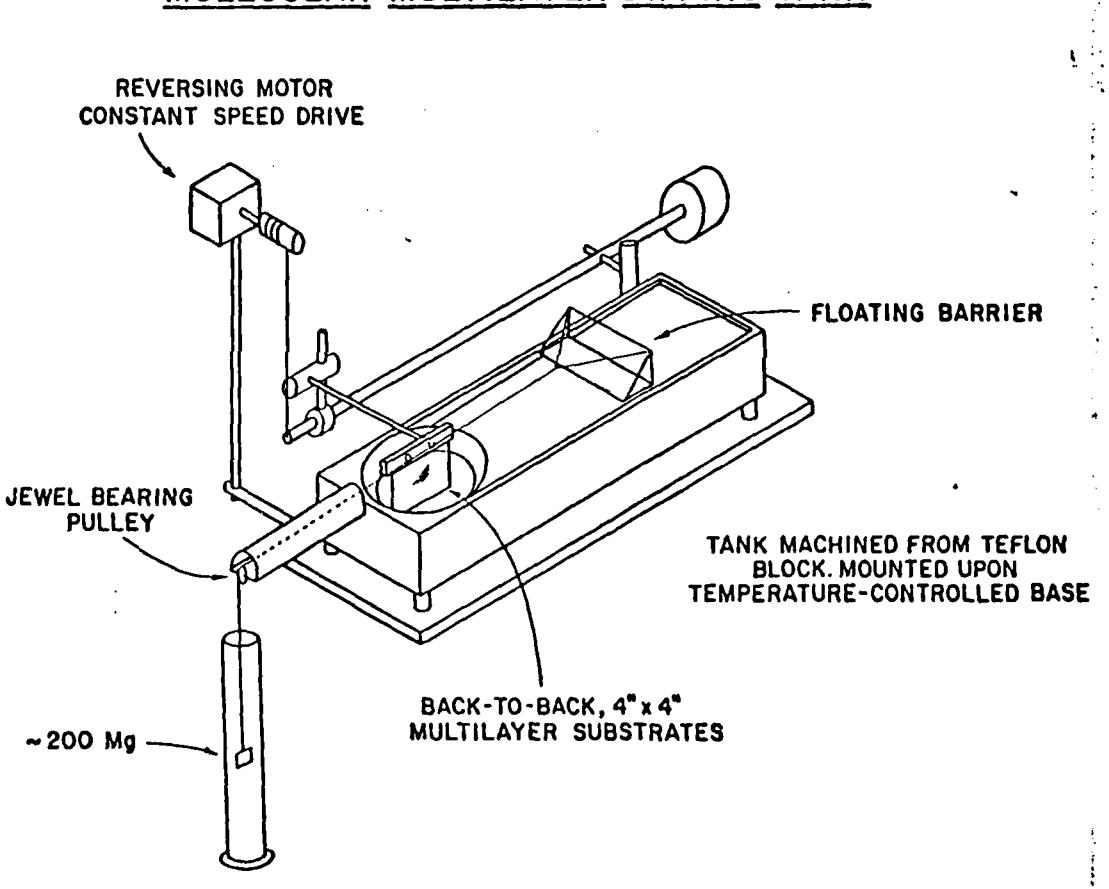

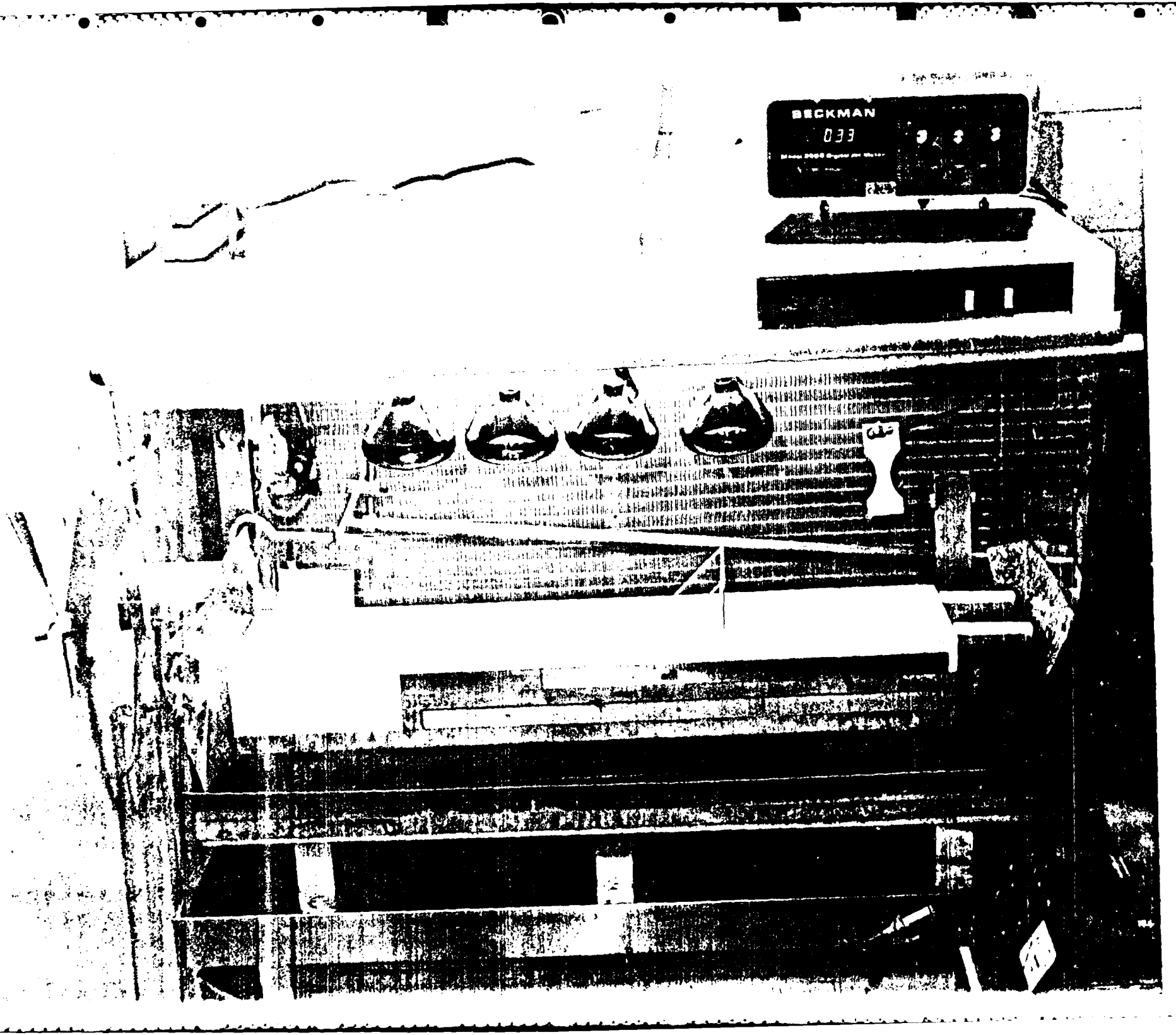
BECKMAN
033

Figure 6. The high intensity excitation source that is used in this low energy x-ray and electron spectroscopy. Typical interchangeable anodes are of copper, aluminum and graphited copper for the Cu-K, Al-K, Cu-L and C-K characteristic radiations of 8050, 1487, 930 and 277 eV, respectively. Some useful fluorescent radiation line sources that are applied in this work in the low energy region are listed here.

Some Useful Characteristic Line Sources
for Ultrasoft X-Ray Spectroscopy

Line Source	Energy (KeV)	Wavelength (Angstroms)	Line Source	Energy (KeV)	Wavelength (Angstroms)
Al-K$\alpha_{1,2}$	1.487	8.34	Ti-L$\alpha_{1,2}$	.452	27.4
Mg-K$\alpha_{1,2}$	1.254	9.89	Ti-Lℓ	.395	31.4
Na-K$\alpha_{1,2}$	1.041	11.9	N-Kα	.392	31.6
Zn-L$\alpha_{1,2}$	1.012	12.3	C-Kα	.277	44.7
Cu-L$\alpha_{1,2}$	.930	13.3	W-$N_{V,VII}$	.212	58.4
Ni-L$\alpha_{1,2}$	.852	14.6	Mo-Mζ	.193	64.4
Co-L$\alpha_{1,2}$	.776	16.0	B-Kα	.183	67.6
Fe-L$\alpha_{1,2}$	.705	17.6	Nb-Mζ	.172	72.2
F-Kα	.677	18.3	Zr-Mζ	.151	81.9
Mn-L$\alpha_{1,2}$	.637	19.4	S-Lℓ	.149	83.4
Cr-L$\alpha_{1,2}$	.573	21.6	Y-Mζ	.133	93.4
Mn-Lℓ	.556	22.3	Sr-Mζ_1	.114	109.
O-Kα	.525	23.6	Be-Kα	.109	114.

TWO-KILOWATT ULTRASOFT X-RAY SOURCE

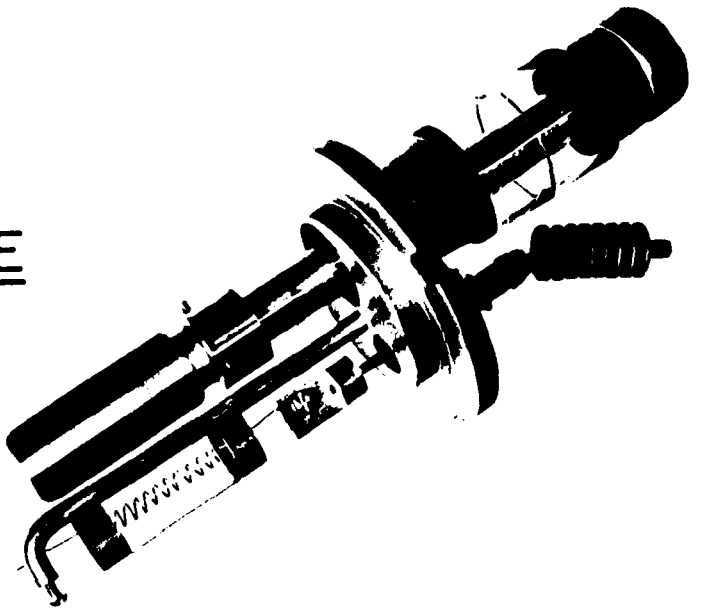

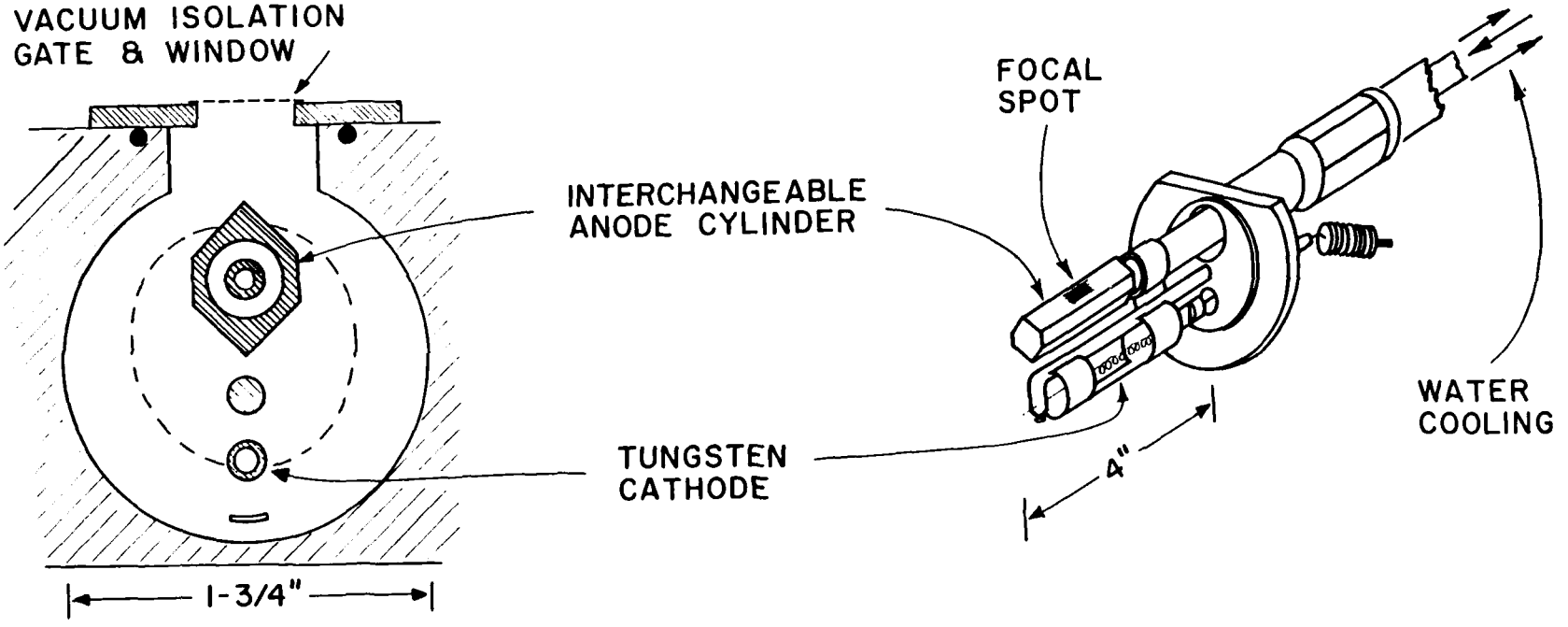

PULSED SOURCE SPECTROMETRY

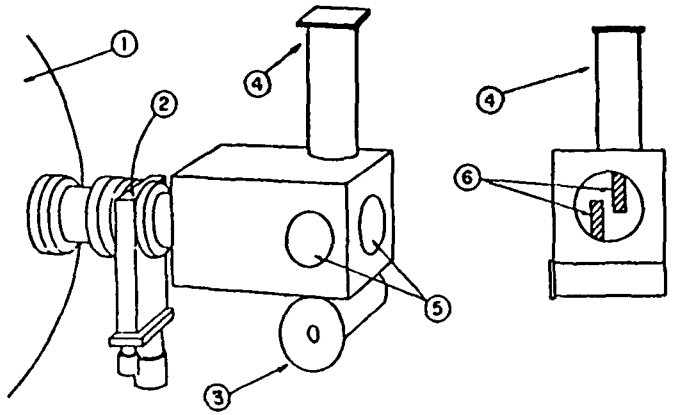

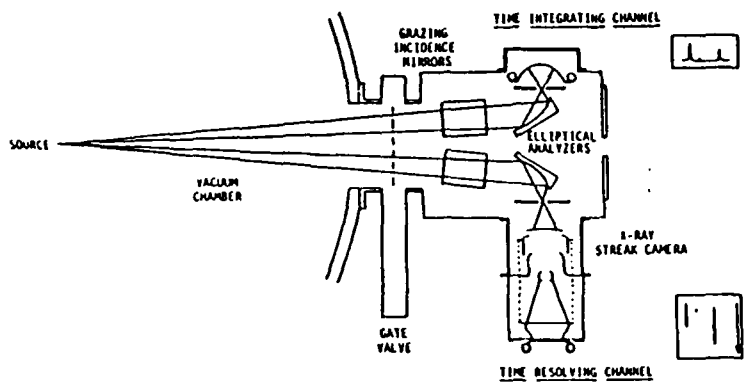

① CHAMBER
② 4"-VALVE
③ PHOTOGRAPHIC CAMERA
④ STREAK CAMERA
⑤ ALIGNMENT PORTS
⑥ ELLIPTICAL ANALYZERS

A TWO-CHANNEL, ELLIPTICAL ANALYZER SPECTROGRAPH FOR ABSOLUTE, TIME-RESOLVING/TIME-INTEGRATING SPECTROMETRY OF ICF PLASMAS IN THE 100-10,000 eV REGION

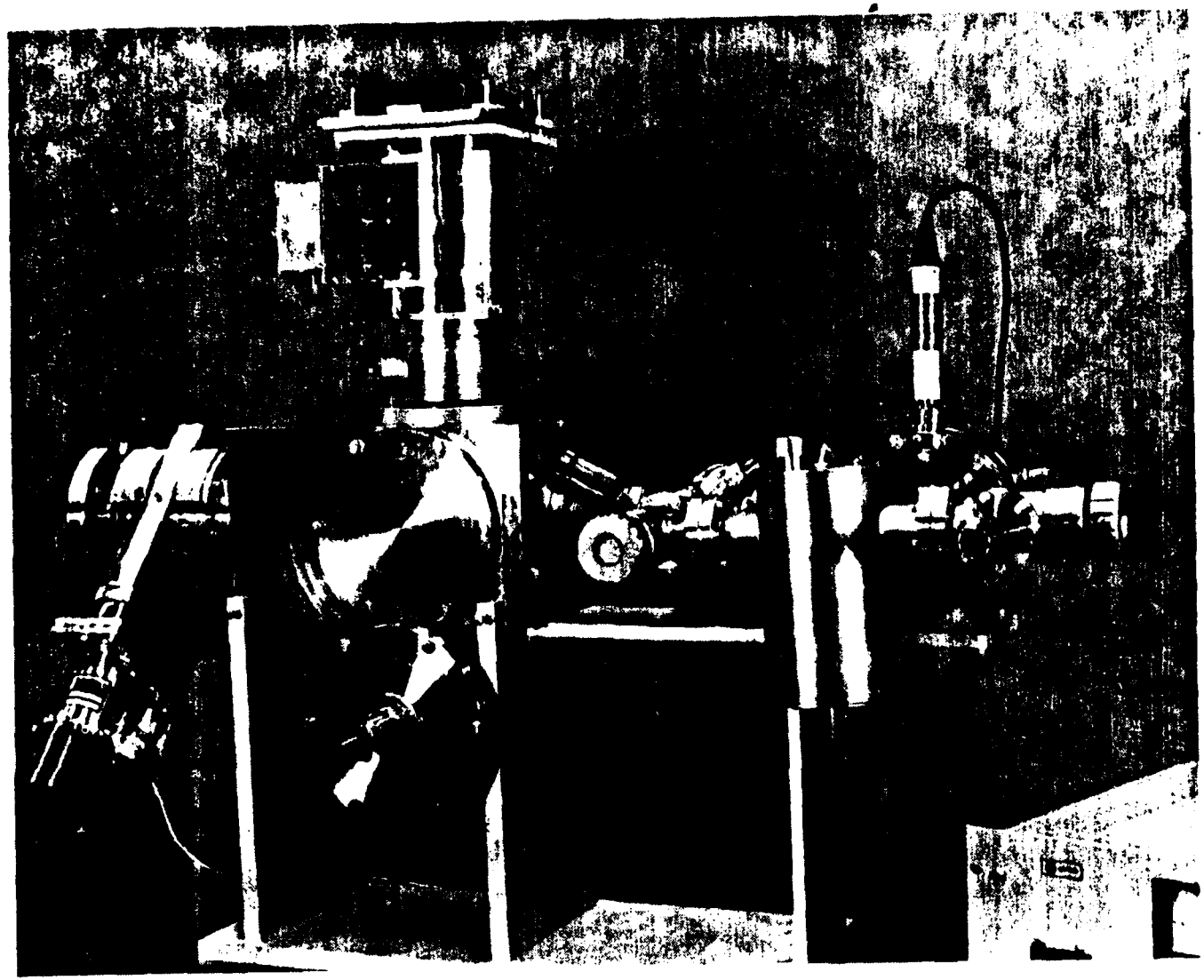

A new spectrograph system developed and calibrated for absolute spectrometry of ICF plasmas in the 100-10,000 eV region. This spectral region is analyzed with fixed elliptically curved crystals of LiF, PET and RAP, and with molecular multilayers of 2d-values in the 70-160 A range. Twin channels are utilized for simultaneous time-integrating photographic recording and for time-resolving x ray streak camera recording. Absolute calibrations of the elliptical analyzers, of the photographic film and of gold and low and high density CsI transmission photocathodes have been made using monoenergetic, DC laboratory x-ray sources. The instrument has been designed for mounting upon a 4 inch port of a one-meter diameter source chamber and includes an appendage, high vacuum, sputter ion pumping system. The final testing and application of this new spectrograph will be on the University of Rochester's LLE 24-beam Omega facility.

LOW ENERGY X-RAY AND ELECTRON ANALYSIS LABORATORY

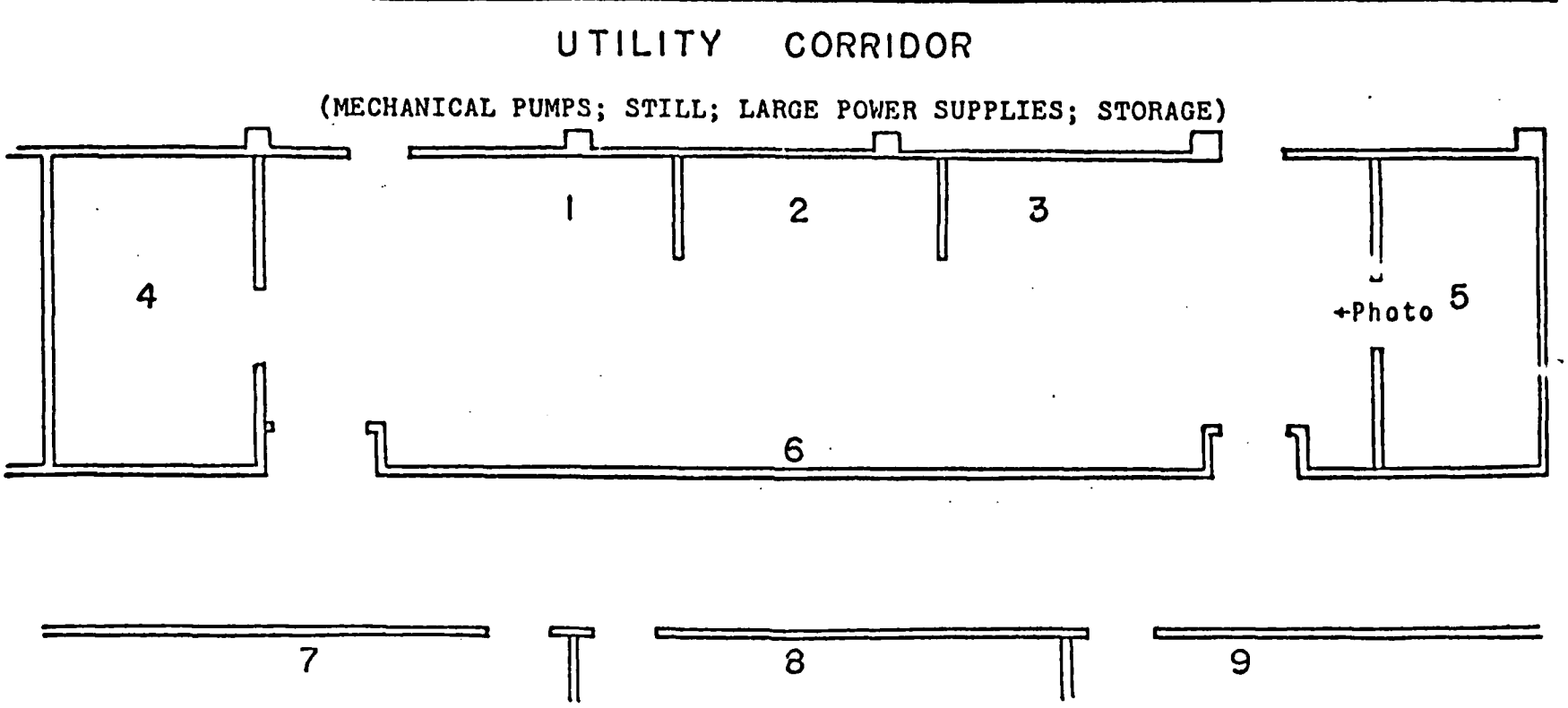

SCALE = 1/10" = 1'0"

1,2,3 - Low energy x-ray and electron spectroscopic systems

4 - Sample preparation lab and clean-bench for crystal research

5 - Data analysis lab and library

6 - Work benches and active storage

7,8,9 - Offices (Research associates, principal investigator, drafting room)

Figure 8. This low energy x-ray and electron spectroscopy laboratory (of more than 2000 square feet). Included are rooms at each end of the laboratory for sample preparation and crystal analyzer construction, and for a small computer and data analysis. Available to this laboratory are such facilities as a large IBM-370 computer system and a large, complete experimental machine shop.

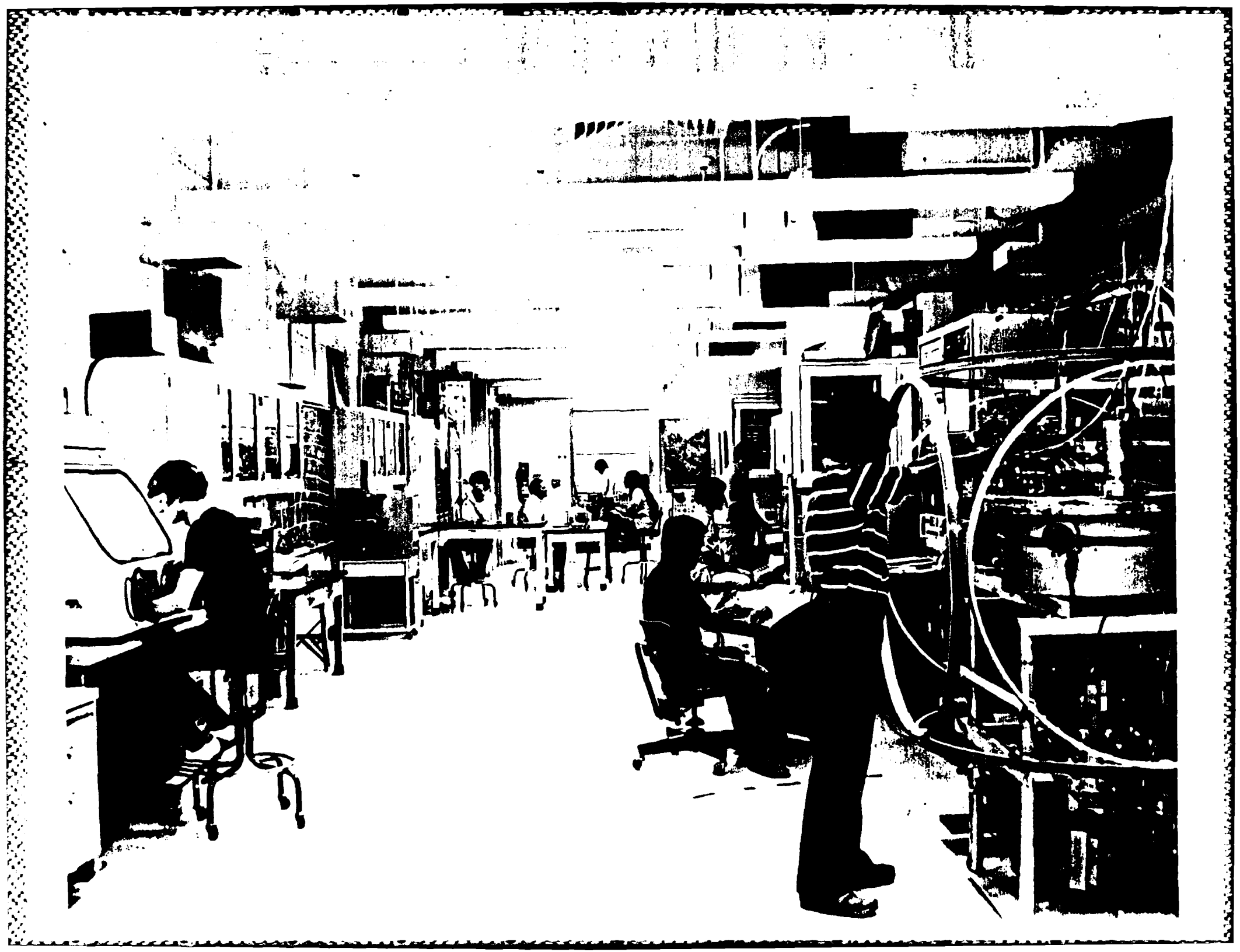

END
DATE
FILMED
JAN
1988